MODELING OF HEMODYNAMICALLY INDUCED VEIN GRAFT REMODELING

By

MINKI HWANG

A DISSERTATION PRESENTED TO THE GRADUATE SCHOOL
OF THE UNIVERSITY OF FLORIDA IN PARTIAL FULFILLMENT
OF THE REQUIREMENTS FOR THE DEGREE OF
DOCTOR OF PHILOSOPHY

UNIVERSITY OF FLORIDA

2011

© 2011 Minki Hwang

To my parents

ACKNOWLEDGMENTS

I thank my advisor Dr. Roger Tran-Son-Tay for giving me this opportunity to study and his guidance throughout this study. I thank Dr. Scott A. Berceli for his supports and helps during the entire period of my study. I thank Dr. Marc Garbey for helping me much improve the research results. I thank my committee professors Dr. Balachandar, Dr. Kim, Dr. Sarntinoranont, and Dr. Batich for their advisory on this study. I thank the lab members of Dr. Tran-Son-Tay's lab, and the members of Dr. Berceli's lab. I thank my brother and his family for their support during this study. I couldn't thank my parents enough for their love and support. My parents made me who I am today with their unbelievable love towards me and my brother.

TABLE OF CONTENTS

page

ACKNOWLEDGMENTS 4

LIST OF TABLES 7

LIST OF FIGURES 8

ABSTRACT 10

CHAPTER

1 INTRODUCTION 12

2 BACKGROUND 15

Hemodynamic Impact on Vein Graft Remodeling 15
Previous Models of Blood Vessel Remodeling 19
Modeling and Role of Leukocytes in Blood Vessel 19
Leukocyte Rolling Mechanism 22
Leukocyte Rolling Models 24
Rule-Based Simulation of Biological Systems 26

3 SINGLE-LAYER MATHEMATICAL MODEL OF VEIN GRAFT REMODELING 41

Model Development 42
Intimal Thickening in Rabbit Model 42
Predictive Model of Intimal Growth 43
Model Application 47
Focal Vein Graft Stenosis Construct 47
Simulation of Intimal Thickening around a Focal Stenosis 47
Parameter Sensitivity Analysis 52
Discussion 53

4 MULTI-LAYER MATHEMATICAL MODEL OF VEIN GRAFT REMODELING 56

Model Development 57
Remodeling Characteristics of Vein Graft Wall 57
Intima Model 58
Media Model 61
EEL Model 63
Sensitivity and Stochastic Analysis 65
Model Application 68
Simulation of Idealized Stenosis 68
Simulation of Human Vein Graft 75
Discussion 75

5 RULE-BASED MODEL OF VEIN GRAFT REMODELING 79

Determination of Probabilities of Cellular Activities 80
Probability of Smooth Muscle Cell Division 80
Probability of Smooth Muscle Cell Apoptosis 84
Probability of Extracellular Matrix Behaviors 87
Effects of Monocytes 88
Monocyte Entry Model 88
Monocyte Effects on ECM synthesis 88
Algorithm 90
1-D Algorithm 90
2-D Algorithm 90
Results 92
1-D Model Validation 92
2-D Model Validation 94
Focal Stenosis Simulation 97
Discussion 98

6 CONCLUSION 101

LIST OF REFERENCES 105

BIOGRAPHICAL SKETCH 117

LIST OF TABLES

Table page

3-1 Parameter sensitivity analysis for single-layer model 53

4-1 Parameter sensitivity analysis for multi-layer model 67

5-1 Assumptions used in the rule-based model of vein graft remodeling..... 88

LIST OF FIGURES

Figure		page
1-1	Vein bypass surgery in coronary artery and infrainguinal artery	13
2-1	Hemodynamic impact on vein graft remodeling	17
2-2	Biologic mechanism of intimal hyperplaisa	18
2-3	Schematic of computational domain for rule-based simulation of multi-cellular biological system	27
2-4	Schematic of cell behavior implementation on the lattice	28
3-1	Schematic of vein graft	42
3-2	Intimal thickenss as a function of shear stress at each measurement day.	45
3-3	Surface plots of intimal thickness and intimal thickening rate	46
3-4	Iteration procedure for simulation of intimal thickening.	48
3-5	Hemodynamic characteristics inside the focal stenosis.	50
3-6	Comparison of focal stenosis simulation results with experimental data.	51
4-1	Schematic of the cross-section of venous wall.	58
4-2	Normalized geometical variables of vein graft with respect to shear stress.	59
4-3	Normalized medial area as a function of time	61
4-4	Rate of normalized medial area change as a function of wall tension.	62
4-5	Normalized EEL radius as a function of time.	64
4-6	Surface plots of the normalized geometrical variables of vein graft.	66
4-7	Stochastic analysis of the vein graft mathematical model.	68
4-8	Schematic of stenosis simulation	69
4-9	Simulation results for intimal area around the stenosis under low flow condition	72
4-10	Simulation results for intimal area around the stenosis under high flow condition.	73

4-11 Simulation results for EEL radius and medial area under low flow condition. 74
4-12 Simulation results for human vein graft. 76
5-1 Schematic of cells undergoing cell cycles during 1 day prior to harvest. 81
5-2 % of BrdU positive cells as a function of normalized shear stress. 82
5-3 % of BrdU positive cells as a function of actual distance from endothelium 83
5-4 % of TUNEL positive cells as a function of time. 85
5-5 % of TUNEL positive cells as a function of actual distance from IEL. 86
5-6 Simulated intimal area with normalized rate of monocyte entry 89
5-7 Schematic of 1-D domain. 90
5-8 Flow chart for the rule-based simulation of vein graft remodeling 91
5-9 2-D algorithm of rule-based simulation of vein graft remodeling 92
5-10 Element redistribution algorithm for stenosis simulation. 93
5-11 1-D simulation results. 94
5-12 An example of 2-D simulation. 95
5-13 Simulation results and experimental data of intimal area and comparison of 1-D and 2-D simulations. 96
5-14 An example of focal stenosis simulation 97
5-15 Comparison between simulation result and experimental data for intimal thickening around focal stenosis 98

Abstract of Dissertation Presented to the Graduate School
of the University of Florida in Partial Fulfillment of the
Requirements for the Degree of Doctor of Philosophy

MODELING OF HEMODYNAMICALLY INDUCED VEIN GRAFT REMODELING

By

Minki Hwang

August 2011

Chair: Roger Tran-Son-Tay
Major: Mechanical Engineering

Though vein grafting, which is one of the primary treatment options for arterial occlusive disease, provides satisfactory results at an earlier stage of the treatment, the patency is limited to a few months for many patients. Early adaptation of vein graft to arterial flow environment, which precedes the later vein graft failure, has been found to be influenced by hemodynamic forces. The goal of this study is to develop mathematical and computational models of vein graft remodeling induced by hemodynamic forces, which can potentially be used as predictors of vein graft failure. This study consists of three components: single-layer mathematical model, multi-layer mathematical model, and rule-based model. The single-layer model describes intimal layer remodeling as a function of wall shear stress and time. The mathematical form is simple and predicts intimal thickening around focal stenosis, which agrees very well with experimental data. The multi-layer model describes the remodeling of three layers: intima, media, and external elastic lamina. The effect of wall tension is included as an additional hemodynamic factor. All the three layer models are based on experimental data, and the models can be applied to the simulation of idealized stenosis as well as irregular geometry of human vein graft. The rule-based model incorporates biologic mechanism

of vein graft remodeling. Rules of behaviors are applied to smooth muscle cell, monocyte, and extracellular matrix, and the wall thickening (global behavior) is observed emerging from the local interactions among the components. Monocytes have been found to have significant contribution to the wall thickening. The models developed in this study provide detailed insight into the mechanism of vein graft remodeling, and are a foundation for the future development of long-term predictor that can be used in clinical environment.

CHAPTER 1
INTRODUCTION

Every year since 1900 except 1918, cardiovascular disease (CVD) has been the leading cause of death in the United States (Rosamond et al., 2007; Roger et al., 2011) accounting for 33.6% of all deaths in the United States in 2007. One in three American adults are estimated to have 1 or more types of CVD. The CVD death rates are higher than those of cancer. There are three major CVDs: heart attack, stroke, and peripheral vascular occlusive disease (PVOD). Heart attack occurs when the coronary artery which supplies oxygen-rich blood to the heart muscle is blocked due to atherosclerotic lesion. Stroke occurs when the vasculature in the brain is blocked by atherosclerotic or blood clot originated from diseased blood vessel in other part of the body. PVOD is caused by atherosclerotic plaque in the artery resulting in blockage of the supply of blood to the organs other than heart and brain. All of these major CVDs are related to the occlusion of artery.

One of the primary treatments for the occluded arteries in heart attack and PVOD is vein bypass grafting. Autologous vein such as saphenous vein in leg is extracted and attached to the diseased artery to make the blood flow bypass the occluded region (Figure 1-1). Approximately, 400,000 coronary and 100,000 lower-extremity bypass graftings are performed annually in the United States (Jacot et al., 2004). However, the problem is that, although the vein grafting provides satisfactory results at an early stage of the treatment, the patency is limited to a few months for many patients (Fitzgibbon et al., 1996). Vein graft failure occurs in 30% to 40% of lower extremity cases at 5 years, and more than 50% of coronary grafts fail within 10 years (Jacot et al., 2004). Although

it is due to atherosclerotic lesion when vein graft failure occurs, the early remodeling of vein graft precedes the atherogenesis (Figure 1-1).

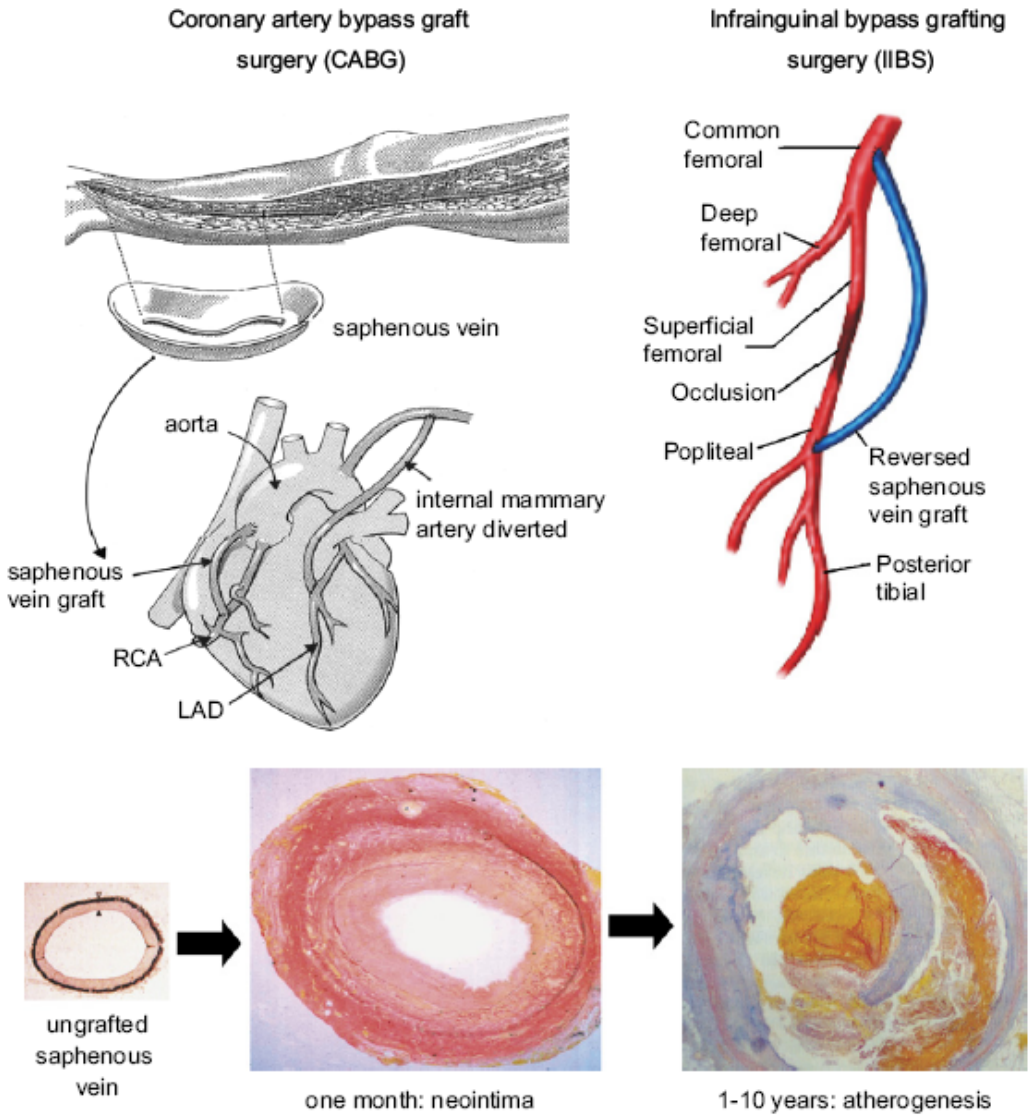

Figure 1-1. Vein bypass graft surgery in coronary artery and infrainguinal artery (Jeremy et al., 2007 with permission).

When vein graft is implanted in the arterial system, the vein graft is exposed to higher blood pressure and wall shear stress than those of the venous system. The

morphology of the implanted vein graft changes such that the vein graft wall becomes thicker and the graft diameter increases. It is believed that these early stage remodeling processes are adaptive processes to the high pressure and high shear environment of the arterial system (Dobrin et al., 1989; Fillinger et al., 1994; Zwolak et al., 1987; Galt et al., 1993). Though the biologic mechanism underlying the vein graft failure are not completely understood, early vein graft remodeling induced by hemodynamic forces such as wall shear stress stands among the primary regulators for these events (Varty et al., 1993; Mills et al., 1995).

In this dissertation, early vein graft remodeling is studied using mathematical and computational modeling approach. More specifically, mathematical and computational models of early vein graft wall remodeling are developed in order to gain insight into the exact mechanism of vein graft remodeling and to lay the foundation for developing predictors of vein graft failure.

CHAPTER 2
BACKGROUND

Hemodynamic Impact on Vein Graft Remodeling

Venous wall consists of three layers: the intima, media and adventitia. The intima is the innermost layer in direct contact with the blood flow. The intima consists of monolayer of endothelial cells though there are sometimes other components such as smooth muscle cells. The media, which is the layer between the intima and adventitia, consists of smooth muscle cells and extracellular matrix. The adventitia is the outermost layer which is in contact with surrounding tissue. Between the intima and media lies a connective tissue layer known as the internal elastic lamina (IEL), and the external elastic lamina (EEL) between the media and adventitia.

Shear stress has been recognized as one of the major hemodynamic factors which modulate vein graft remodeling. It has been found that lower shear stress increases the vein graft wall thickness. One of the earliest observations that the flow rate is related to the vein graft failure is the one by Grondin et al. (1971). They examined the vein grafts implanted into human arteries, and observed that all grafts with flow of 20ml/min or less measured at implantation became occluded after 10 to 21 days while all grafts with the implantation flow greater than 45ml/min remained open. Later, Berguer et al. (1980) hypothesized that the low shear stress was related to intimal hyperplasia in vein graft, and since then, numerous evidences which support the low shear hypothesis have been reported. Dobrin et al. (1989) separated the effects of various hemodynamic factors in canine vein graft experiment and showed that the intimal hyperplasia is best associated with low flow velocity. Galt et al. (1993) observed the inverse relationship between flow rate and intimal thickness in their rabbit vein graft

experiment. Jiang et al. (2004) observed a sevenfold greater intimal thickness 28 days after implantation when the flow rate remained 15-fold lower throughout most of the perfusion period in their rabbit bilateral vein graft experiment.

While lower shear stress increases intimal thickness, higher shear stress has been known to increase vein graft diameter. Fillinger et al. (1994) reported a linear relationship between the percent change in vein graft diameter over 12 months and initial shear stress in human saphenous vein grafts after infrainguinal bypass. Jiang et al. (2004) observed a 24% increase in lumen diameter at 28 days in the vein graft under elevated flow condition in their rabbit bilateral vein graft experiment. Owens et al. (2006) reported a positive correlation between the initial shear stress and the change in lumen diameter during the time interval of 1 month after autogenous vein implantation in human patients undergoing lower extremity bypass. The vein graft enlargement under high flow condition can be understood with regard to the Glagov phenomena (Glagov et al., 1987) which is the observation that the coronary arteries enlarge in the early stages of atherosclerosis to preserve lumen area.

Wall tension induced by blood pressure is another important hemodynamic factor in vein graft remodeling. Higher wall tension has been known to increase the vein graft wall thickness. Zwolak et al. (1987) observed that the thickening wall in rabbit jugular vein segments transplanted into the carotid artery caused the ratio of luminal radius to wall thickness to decrease to a level equal to that of normal artery. Schwartz et al. (1992) reported a linear relationship between myointimal area and wall tension in their rabbit vein graft experiment.

The effect of each hemodynamic factor on vein graft remodeling is summarized in Figure 2-1.

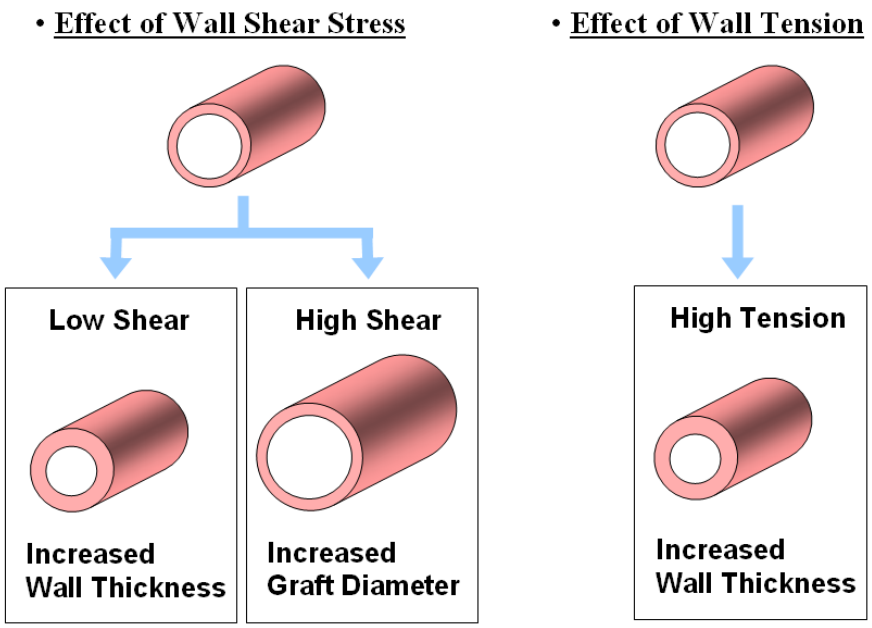

Figure 2-1. Hemodynamic impact on vein graft remodeling.

Two of the representative processes of the intimal hyperplasia in vein grafts are smooth muscle cell (SMC) proliferation and extracellular matrix (ECM) accumulation in the intima (Figure 2-2). The SMCs migrate from the media, and they proliferate before migrating from the media to the intima. One of the factors that promote the SMC proliferation in the media is the endothelial damage. Damaged endothelium produces the SMC growth-stimulating factors, and the amount of SMC proliferation-inhibiting factors which are produced from normal endothelium decreases due to the endothelial damage (Lemson et al., 2000). SMC in the media starts to migrate into the intima a few days after implantation due to degradation of ECM which normally prevents the SMC migration. The migrated SMCs proliferate in the intima and produce the ECM. Growth

factors such as TGF-β and PDGF are known to stimulate ECM production by SMC (Lemson et al., 2000).

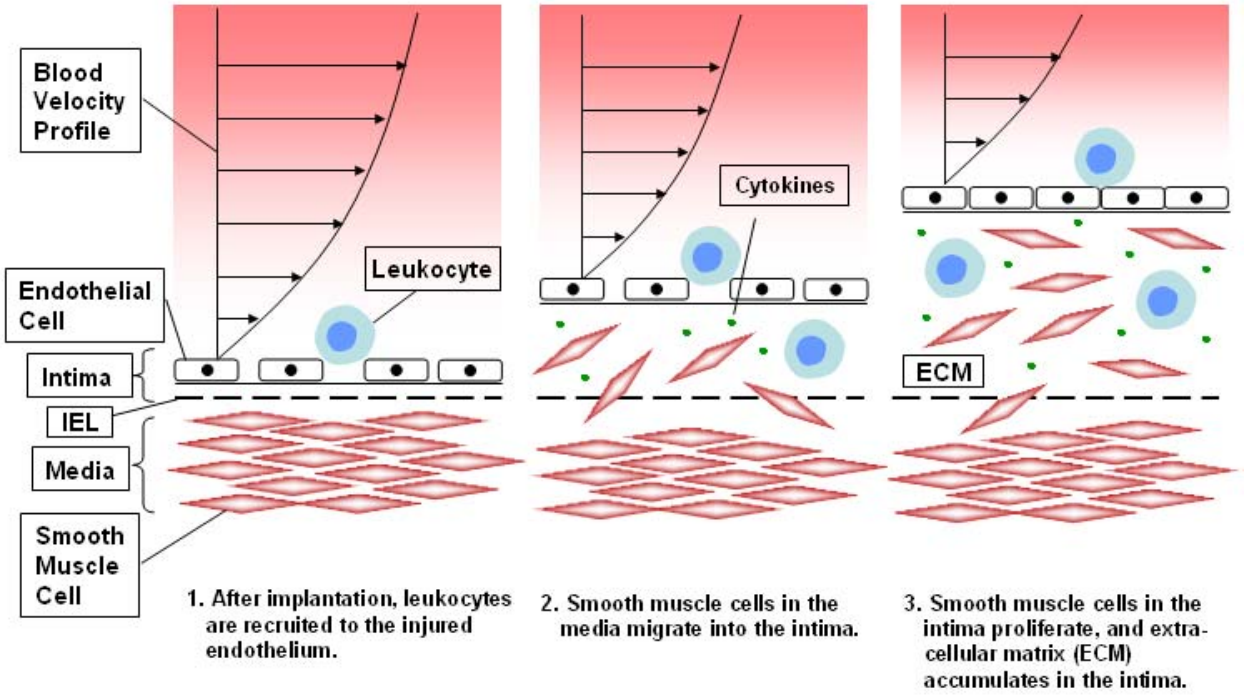

Figure 2-2. Biologic mechanism of intimal hyperplasia.

Shear stress has been known to be an important factor in the vein graft remodeling. Altered shear stress stimulates the expression of adhesion molecules and chemokines involved in vein graft wall thickening (Lemson et al., 2000). After the vein graft is implanted, leukocytes are recruited to the vein graft wall, and they release cytokines which influence the SMC proliferation and migration (Golledge, 1997). Low shear stress has been observed to promote the leukocyte entry into the vein graft wall (Walpola et al., 1995; Richter et al., 2004).

Outward remodeling in the early stage of the vein graft remodeling compensates the wall thickening resulting in the preservation of lumen area (Galt et al., 1993).

Change in shear stress induces the endothelial cells to release numerous biologic mediators related to blood vessel diameter change (Fillinger et al., 1994). Recently, Jiang et al. (Jiang et al., 2007) reported that the reorganization of adventitial myofibroblasts was the dominant histological events that limited the early outward remodeling of vein grafts in their rabbit vein graft-fistula experiment.

Previous Models of Blood Vessel Remodeling

Previous investigators have sought to develop predictive models of intimal growth in diseased arteries or in vein grafts. Among the first were Friedman et al. (1986), who developed a model of shear-dependent intimal thickening of human arterial intima based on experimental data. Because their model is based on experimental data which were measured at only one time point, they introduced the concept of a time variable based on measured intimal thickness to describe the time-dependent behavior of intimal growth. Lee and Chiu (1992) used this model to simulate the growth of intima in a curved artery. Yang et al. (2003) assumed a linear inverse relationship between the intimal growth rate and shear stress, and applied the model to the simulation of intimal growth in a rat vein graft. Unique was their use of a modified piecewise linear growth function based on their experimental data. Zohdi (2005) developed a theoretical model of blood vessel lumen reduction based on the concept of feedback control, employing a linear inverse relationship between the lumen radius changing rate and shear stress to examine the lumen reduction as a function of time.

Modeling and Role of Leukocytes in Blood Vessels

Leukocytes (white blood cells) are inflammatory cells (diameter on the order of 10μm) circulating in the blood stream. Leukocytes migrate to the inflammation sites by sensing the inflammatory signals originated at the infection sites in the tissue. When the

circulating leukocytes migrate to the inflammation sites, they go through several steps: initial capture, rolling, firm adhesion, and transendothelial migration. Leukocytes are captured from the blood stream through the binding between the selectins expressed on the leukocytes and the ligands on the surface of the endothelial cells. The captured leukocyte rolls on the surface of the endothelium under the combined effect of shear stress imposed by the blood flow and the association/dissociation between the endothelial selectins and the leukocyte ligands. When the chemokine receptors on the rolling leukocyte detect chemokines on the endothelial cells, the leukocyte integrins which were previously low affinity state undergo conformational change to become high affinity state. Through the binding between these high affinity integrins on the leukocyte and the ligands on the endothelium, the rolling leukocytes firmly adhere to the endothelium. The firm adhesion triggers the cytoskeleton diapedesis machinery leading to transendothelial migration (Shuhaiber et al., 2002).

Monocytes enter the vein graft wall as part of an inflammatory response, and the cytokines released by macrophages are known to promote the intimal hyperplasia (Hoch et al., 1999). It has been reported that the monocyte entry into the blood vessel wall is affected by the wall shear stress imposed by the blood flow. Walpola et al. (1995) decreased shear stress 73% in a rabbit carotid artery by surgical manipulation, and observed adhered monocytes in 5 days, while they did not detect any adhered monocyte when they increased the shear stress by 170%. Richter et al. (2004) observed densely adhered monocytes at the region of low shear stress and complete absence of monocytes in high shear region inside an arterial branch in their porcine model.

Leukocytes and other blood cells are differentiated from the pluripotent hematopoietic stem cell in the bone marrow. Several hundred billion leukocytes are produced daily due to the short half-life which is typically hours to days (Silverthorn, 2001). There are five types of leukocytes: lymphocytes, monocytes, neutrophils, eosinophils, and basophils. Monocytes develop into macrophages when they enter the tissue from the blood vessel. Neutrophils, monocytes, macrophages, and eosinophils are phagocytes because they engulf foreign invaders such as bacteria. Basophils, eosinophils, and neutrophils are called granulocytes because granules are observed in their cytoplasm. Neutrophils are also called polymorphonuclear leukocytes because their nucleus consists of several nuclear lobes. Neutrophils, the most abundant type of leukocytes, typically kill five to twenty bacteria during their life span of several hours to few days. On the other hand, monocytes constitute only 1 to 6% of all leukocytes in the blood, but kill about 100 bacteria during their life span of several months (Silverthorn, 2001). Lymphocytes play an important role in the acquired immune response of the body.

On the surface of the leukocytes, there are projections of plasma membrane, called microvilli. There are 500 to 10,000 microvilli on a leukocyte surface (Knutton et al. 1975). The length of the microvilli ranges from 50 to 3500 nm (Bruehl et al. 1996), and the surface area of the tip of a microvillus is approximately 0.01 μm^2 (Bongrand and Bell 1984). At the tip of the microvilli, there are various adhesion molecules which mediate cell to cell interactions. The microvillus elongates when force is exerted. At small force, the microvillus stretches like an elastic spring, and the spring constant has been measured to be 43 pN/μm in case of neutrophil microvilli (Shao et al. 1998). The

leukocyte plasma membrane has numerous wrinkles and folds which accommodate surface area increase when the leukocyte deforms from its initial spherical shape. The surface area increases more than 100% when the leukocyte spreads on the endothelium before extravasation (Dewitt and Hallett 2007).

Among the adhesion molecules on the surface of the leukocytes and endothelial cells, selectin and integrin play critical roles in the leukocyte recruitment to inflammation sites. Selectins are transmembrane molecules composed of N-terminal extracellular domain, epidermal growth factor, consensus repeats, transmembrane domain, and cytoplasmic tail. L-selectin is expressed on leukocytes and binds to the ligands on endothelial cells. P-selectin is expressed on endothelium and platelets, and binds to PSGL-1 on leukocyte. E-selectin is expressed on endothelial cells and binds to ligands on leukocytes. Integrins are heterodimeric glycoproteins which are subdivided according to their subunits. Integrins are also transmembrane molecules composed of extracellular domain and cytoplasmic tail which is linked to the cytoskeleton of the cell. VLA-4 integrin on leukocyte binds to VCAM-1 ligand on endothelium upon activated by chemotactic agents.

Leukocyte Rolling Mechanism

Leukocyte rolling before transendothelial migration in the inflammatory response is a movement coordinated by fluid shear and binding between adhesion molecules on the leukocyte and endothelium. When the bonds at the trailing edge of the contact area dissociate, the leukocyte rotates forward due to the fluid force, and the probability of bond association at the leading edge increases. Leukocyte rolling is mediated mostly by

selectins, and different rolling velocities have been observed on different types of selectins (Jung et al. 1996).

It has been observed that the rolling velocity increases as fluid shear stress increases. Lawrence and Springer (1991) reproduced rolling of neutrophils on artificial lipid bilayers containing purified CD62 in vitro, and observed that the rolling velocity increased with increasing shear stress. They also observed that the rolling velocity increased with decreasing selectin density. Alon et al. (1995) reported that the rolling velocity of blood T lymphocytes increased when shear stress was increased in a parallel flow chamber assay. Dong and Lei (2000) observed that rolling velocities of HL-60 cells which express comparable levels of PSGL-1 (P-selectin ligand) as most human leukocytes increased on a surface with P-selectin adsorbed as wall shear stress increased in their in vitro side-view flow assay.

An interesting phenomenon in the leukocyte rolling is the stop-and-go motion. The leukocytes frequently stop for some time as they roll on the ligands, and it presumably results from the fact that the binding between the adhesion molecules is stochastic in nature. Goetz et al. (1994) measured the instantaneous velocity of bovine neutrophils interacting with lipopolysaccharide-stimulated bovine aortic endothelium at various shear stresses, and confirmed that the neutrophils translated with a nonconstant velocity. The population average variance in the instantaneous velocity was at least 2 orders of magnitude higher than the theoretical variance generated from experimental error. Smith et al. (1999) obtained the dissociation constants (k_{off}) for P-, E-, L-selectin from the pause times in the neutrophil rolling in their parallel plate flow chamber. The elasticity of the microvilli on the surface of the leukocyte also has a role in the leukocyte

rolling. Park et al. (2002) compared the rolling characteristics of PSGL-1 coated microbead and neutrophil, and reported that the dissociation rates for the PSGL-1 microbeads were briefer than those of neutrophils. They also observed the elongated microvilli at the rear of the rolling neutrophils using scanning electron microscope. Fluid shear affects the number of tethered and rolling leukocytes. Finger et al. (1996) reported that the number of tethered and rolling neutrophils on E-selectin and P-selectin decreased as the shear stress increased. However, they observed that, in case of L-selectin, the number of tethered and rolling neutrophils increased as the shear stress increased up to around 1 dynes/cm^2, and then the number decreased with increasing shear stress over about 1 dynes/cm^2. Later, Lawrence et al. (1997) reported that the threshold shear exists for E-selectin and P-selectin as well. Dwir et al. (2003) identified short-duration (4 to 20 ms) tethers of L-selectin below 0.3 dynes/cm^2 of shear stress, and postulated that shear-mediated multivalent tether is required for the L-selectin tethers to become stabilized. An interesting observation was made by Chen and Springer (2001) that the tether formation is related to shear rate rather than to shear stress. They showed that the tether frequency of neutrophils to P-selectin reached the maximum value at the shear rate of ~100 s^{-1} regardless of viscosity.

Leukocyte Rolling Model

Hammer and Apte (1992) modeled the leukocyte as a rigid sphere with microvilli on the leukocyte surface. They used the bond model described in the previous section for the reaction between the adhesion molecules on the tip of the microvilli and on the surface on which the leukocyte is rolling. The hydrodynamic force was calculated based on Stokes' solution (Goldman et al. 1967). Their model enabled them to examine the

effects of microvilli density on cell surface, receptor density on microvillus tip, the stiffness of the receptor-ligand bond, and the magnitude of the hydrodynamic force. The simulation results showed the velocity fluctuation which is one of the characteristics of leukocyte rolling.

N'Dri et al. (2003) simulated the rolling of deformable compound drop model which has nucleus inside the cell. They solved the Navier-Stokes equations to simulate the flow field, and used immersed boundary technique (Peskin, 1977) to incorporate the effect of the cell in the simulation. The Eulerian-Lagrangian technique (Shyy et al. 1999, 2001) was used to track the moving interfaces between the outer flow and the cell, and between the cytoplasm and nucleus. They simulated the association and dissociation of the adhesion molecules on the leukocyte and the surface using the bond model described in the previous section. They found that the presence of nucleus inside the cell increases the bond life time, and decreases the cell rolling velocity. They also found that a bigger cell rolls faster, and causes bond lifetime decrease, possibly due to the fact that a larger cell experiences greater hydrodynamic force from the blood stream.

Jadhav et al. (2005) extended the model of N'Dri et al. (2002) to 3-dimesional model. They modeled the cell as an elastic capsule, and used the immersed boundary method to simulate the motion of the capsule in a shear flow. The nucleus was not included in the cell model. They simulated the forward and reverse reactions between the adhesion molecules on the leukocyte and the surface based on the probabilities of each reaction (Hammer and Apte 1992). They showed the rolling velocity fluctuation for 0.7 seconds at 200 s^{-1} of shear rate. They observed that higher membrane stiffness

made the cell roll faster, and the number of bonds decreased with increasing membrane stiffness. Bond lifetime also decreased with increasing membrane stiffness.

Pappu and Bagchi (2008) examined a similar model as that of Jadhav et al. (2005). They showed the forward movement of the contact area between the cell and the surface, and the displacement of the cell as a function of time for up to 3 seconds, which showed the stop-and-go motion. They observed a sideway motion during the rolling due to discrete nature of microvilli distribution. They also found that most of the adhesion force is sustained by only 1 to 3 tethered microvilli in the rear-most part of a cell.

Tang et al. (2007) developed an in silico model of leukocyte rolling, activation, and adhesion. They modeled the leukocyte as having rectangular contact area which is discretized such that each element has adhesion molecules. The surface on which the leukocyte rolls is also discretized and adhesion molecules are contained in the elements. The bindings between the adhesion molecules were simulated using the probabilities of bond formation/dissociation. They applied a fluid force which affects the dissociation of the bonds, and when all the bonds have been dissociated at the rear row of the contact area, the leukocyte rolls forward. Their simulation results of rolling behavior agreed well with in vitro experimental data, and the transition from rolling to adhesion was also simulated.

Rule-Based Simulation of Biological Systems

Introduction

Modeling multi-cellular biological systems (MCBS) poses challenges in that the global system behaviors result from individual cell behavior and the interactions among

the cells. Cells are live creatures which differentiate, proliferate, move, and die, and these behaviors of living cells constitute the dynamics of MCBS. Moreover, these cell behaviors are influenced by the environmental factors such as extracellular matrix, chemicals, and forces. Modeling MCBS requires incorporating these complex interactions among the individual cells and the environment (Figure 2-3).

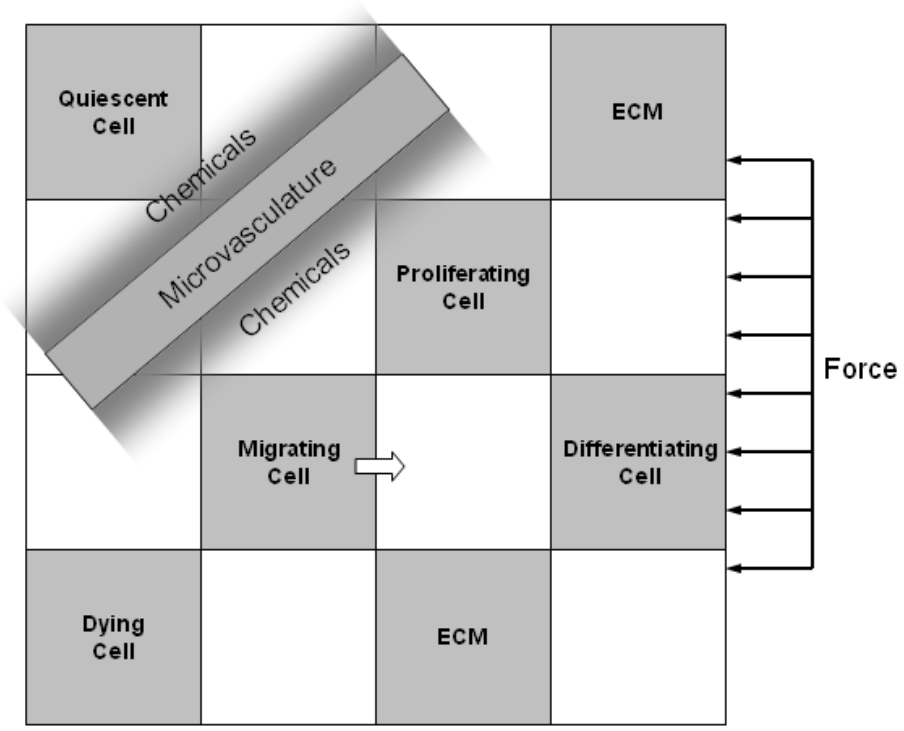

Figure 2-3. Schematic of computational domain for rule-based simulation of multi-cellular biological system.

Modeling approaches for MCBS can be grouped into two categories: continuum models and cell-based models (Byrne and Drasdo, 2009). Continuum models usually take the form of partial differential equations (PDE). One of the advantages of the PDE models is that the model equations provide insight into the relationship among the components in the system. PDE can be used for modeling all levels of biological systems from molecular to organ levels. However, the continuum models do not catch

the discrete nature of MCBS consisting of individual cells, and become cumbersome when modeling complex process involving many variables. On the other hand, the cell-based models such as cellular automata (CA) and agent-based (or individual-based) models (ABM) simulate each individual cell behavior and interactions among them enabling the observation of the emergent system behavior (Figure 2-4). Hybrid models combine these two approaches taking the advantages of each method (Gerlee and Anderson, 2008; Guo et al., 2008).

This review focuses on the cell-based models of MCBS, and especially, the technical aspect of the rule-based simulation method for MCBS is reviewed. How to implement the cell behaviors and their interactions with other cells and with the environment into the computational domain is discussed, and application examples from recent publications are introduced.

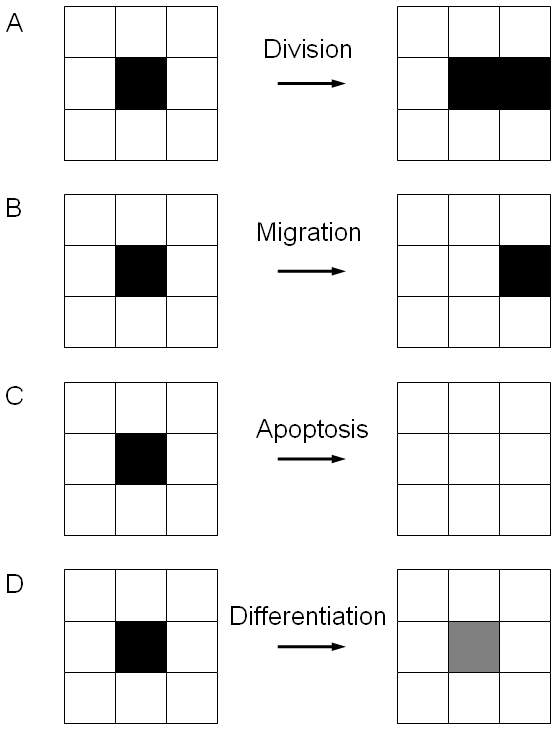

Figure 2-4. Schematic of cell behavior implementation on the lattice.

Cellular Automata and Agent-Based Modeling

CA and ABM are two of the widely used methodologies for rule-based simulation of MCBS (Alber et al., 2003; Chavali et al., 2008; Deutsch and Dormann, 2005; Ermentrout and Edelstein-Keshet, 1993; Thorne et al., 2007; Thorne et al., 2007). Both methods are believed to have originated from an idea by John von Neumann in the 1940s (Gilbert, 2008; Wolfram, 2002). Later, John von Neumann with the help of Stanislaw Ulam introduced the concept of CA (Deutsch and Dormann, 2005; Neumann, 1966; Wolfram, 2002), and ABM also started to be established by other researchers thereafter (Gilbert, 2008). Traditional CA is defined by the following components: a regular discrete lattice, a finite set of cell states, a finite set of neighboring cells, and rules for the transition of cell states (Deutsch and Dormann, 2005). In real-life application of CA, the traditional definition is considered too restrictive, and there have been many relaxations such as non-uniform grid, asynchronous update of the cell states, and extension of the cell neighborhood (O'Sullivan, 2001). ABM is defined in a similar way. ABM is a computational method in which decision-making agents interact with the environment following a set of rules (Bonabeau, 2002; Gilbert, 2008). CA and ABM are similar in that the behaviors of cells or agents are governed by the rules in their neighborhood or environment, and generate global behavior of the system emergent from the local interactions. CA, however, seems more mathematical in its formulation. Mathematical rigorousness of the CA can be seen in the graph-CA proposed by O'Sullivan (2001), a new CA introduced to accommodate non-uniform grid whereas the traditional CA is defined on uniform grid. Although the relationship between CA and ABM is not obvious, some researchers think of ABM encompassing CA (Galle

et al., 2009; Zhang et al., 2009) possibly due to the more general definition of ABM (Bonabeau, 2002). Both CA and ABM have been widely used in the modeling of a variety of systems such as social, economic, and biological systems (Bonabeau, 2002; Gilbert, 2008; Wolfram, 2002). Detailed modeling techniques of these methods applied to MCBS are discussed in the following sections.

Lattice

Rule-based simulations are usually performed on a lattice system. Cells and other components occupy some of the grid elements and can move from one element to another (Figure 2-3). Regular, irregular, or lattice-free approach can be used, and each of these grid systems is discussed in this section.

In the case of regular lattice, the distance between two adjacent elements remain constant over the entire simulation domain, and hence the grid-dependency of the simulation results can be minimized. The lattice can be triangular, square, or hexagonal (Deutsch and Dormann, 2005; Kim et al., 2009). Engelberg et al. (2008) reported that, in their simulation of tumor spheroid growth, square grid required a higher order implementation of discrete diffusion compared with hexagonal grid, and generated artifacts that are not present with the hexagonal grid. The size of individual lattice element can be made to be comparable to that of the biological cell (Gerlee and Anderson, 2007; Mallet and De Pillis, 2006), or can be any value (Grant et al., 2006; Simpson et al., 2007). One biological cell (Cheng et al., 2006; Simpson et al., 2007) or multiple cells (Kansal et al., 2000; Piotrowska and Angus, 2009; Ferreira et al., 2002) can occupy one lattice element. Piotrowska and Angus (2009) reported that assigning many biological cells to one lattice site can reduce the total number of lattice sites for a

given number of biological cells, and hence the computational time, and provides the flexibility in positioning the newly created cells from cell divisions.

Cellular Potts model is a type of CA in which one biological cell occupies more than one lattice sites (Alber et al., 2003; Engelberg et al., 2011). This model enables the incorporation of the shape change of each cell into the simulation. Jiang et al. (2005) simulated an avascular tumor growth using an extended large-Q Potts model. “Large-Q” means that the number of possible cell states is comparable to that of the connected subdomains of different cell types (Alber et al., 2003). Robertson et al. (2007) segmented one biological cell into nine sub-compartments enabling different portions of a cell to respond to different stimuli. These sub-compartments can also incorporate cell polarity and sense the spatial gradient of the environment across the cell.

Kansal et al. (2000) used an irregular lattice for CA simulation of brain tumor growth. They used Voronoi tessellation to generate the lattice, and each resulting automaton cell takes the form of polyhedra in three-dimensional space. They also used varying lattice density with higher density at the center to allow the tumor to grow to a large size during the simulation. Due to their varying size of the elements, the number of real cells contained in the automaton cells ranged from roughly 100 to 10^6 depending on the size of the automaton cell (Kansal et al., 2000). Gevertz and Torquato (2006) adopted a similar irregular lattice to investigate the effects of vasculature on early brain tumor growth.

In the case of lattice-free models, cells can be at any location in the computational domain. The positions of the cells are usually determined by solving equations of motion incorporating the forces acting on the cells (Galle et al., 2005; Galle

et al., 2009; Schaller and Meyer-Hermann, 2007). Rheological properties of the cells also can be included in the simulation (Palsson, 2008). Galle et al. (2005; 2009) simulated multi-cellular systems using lattice-free models incorporating contact-dependent regulation mechanisms. Schaller and Meyer-Hermann (2007) simulated steady-state flow equilibrium of skin using an off-lattice agent-based model.

Cell Behavior

Division, migration, apoptosis, necrosis, and differentiation are among the cell behaviors that are commonly modeled in the rule-based simulations of MCBS. The rules for these behaviors are dependent upon specific biological applications. Some of the rules found in recent publications are discussed in this section.

Two of the important decisions regarding the cell division are determination of the division probability and where to position the two daughter cells. For the cell division probability, cells can be programmed to divide after cell cycle time (Cheng et al., 2006; Grabe and Neuber, 2005; Piotrowska and Angus, 2009). Experimentally obtained cell cycle time can be applied (Cheng et al., 2006; Piotrowska and Angus, 2009; Walker et al., 2004). Each cell can be assigned different cell cycle time based on a normal distribution (Cheng et al., 2006; Piotrowska and Angus, 2009), and in that case, the daughter cells can inherit the cell cycle time of the parent cell (Piotrowska and Angus, 2009). When incremental time step Δt is used for time dependent simulation, the probability of cell division can be applied such that $P_d = \Delta t / t_c$ where P_d is the cell division probability at the time step and t_c is the cell cycle time (Schaller and Meyer-Hermann, 2007). The cell division probability can also be calculated based on other parameters such as local nutrient concentration (Ferreira et al., 2002).

Cell cycle can also be modeled. In their model for the epidermis, Schaller and Meyer-Hermann (2007) incorporated a cell cycle in which cells can enter different phases depending on the local environment. Walker and coworkers (2004) modeled a cell cycle in their simulation of epithelial cells. Jiang et al. (2005) used a simplified protein regulatory network to model the transition between different phases of the cell cycle in their simulation of avascular tumor growth.

Regarding where to position the two daughter cells, one of the common rules is to position them randomly at the adjacent vacant sites (Checa and Prendergast, 2009; Cheng et al., 2006; Gerlee and Anderson, 2007). Contact inhibition is a commonly used rule which prevents cell division when all the adjacent sites are already filled (Bartha and Rieger, 2006; Checa and Prendergast, 2009; Piotrowska and Angus, 2009). Depending on specific application, the daughter cells can be placed away from each other with a site between them (Simpson et al., 2007) or always adjacent to each other (Perez and Prendergast, 2007). Pérez and Prendergast (2007) assigned different probabilities at different available sites in their anisotropic mitosis model. Piotrowska and Angus (2009) applied a probabilistic overlay to determine the location for the daughter cells to avoid morphological artifact in their simulation of *in vitro* multicellular spheroid tumour growth. In their simulation of three-dimensional brain tumor growth, Kansal et al. (2000) used the intercellular mechanical stress algorithm in which a daughter cell pushes an adjacent cell outward until the cell at the tumor edge fills the adjacent empty space. Ferreira et al. (2002) enabled the cancer cells to pile up in a given lattice site in their simulation of avascular tumor growth. If the dividing cancer cell was inside the tumor, the daughter cell piled up at the site, and if the cell is on the tumor

border, the daughter cell replaces the normal or necrotic cell at the nearest neighboring site (Ferreira et al., 2002).

In the case of cellular Potts model in which one biological cell occupies more than one lattice sites, half of the lattice sites in the parent cell can become a new cell (Alber et al., 2003; Jiang et al., 2005). In the case of lattice-free models, the orientation of cell division can be determined by the direction of the total force the dividing cell experiences (Galle et al., 2005). Galle et al. (2005) included the effect of the substrate in the determination of the cell division orientation in their simulation of the growth of epithelial cell populations *in vitro*.

Cell growth can be modeled between the cell divisions in the models such as cellular Potts model or lattice-free model both of which can accommodate cell shape change. In their Potts model of avascular tumor growth, Jiang et al. (2005) set a target volume which each cell tries to reach, and reaching the target volume is a condition for cell division. Galle et al. (2005) modeled the cell growth such that the cell doubles its mass and volume during the interphase in their simulation of the growth of epithelial cell populations. When a cell is compressed by its neighbor cells and the resulting cell volume is less than a threshold value, the growth is inhibited (Galle et al., 2005).

For random movement of cell, new location of the cell can be selected randomly from one of the neighboring sites (Checa and Prendergast, 2009; Gerlee and Anderson, 2007; Perez and Predergast, 2007). The migration, however, can occur several times for each proliferation step because the time scales of the migration and the proliferation are different (Checa and Prendergast, 2009; Perez and Predergast, 2007). Contact inhibition is commonly used as in the case of cell division such that the cell cannot move

if all the neighboring sites are occupied (Checa and Prendergast, 2009; Gerlee and Anderson, 2007; Perez and Prendergast, 2007). Cheng et al. (2006) developed a tissue growth model in which cell migration is modeled as a persistent random walk. Each cell moves in one direction for a certain period of time until it changes its direction and continues to move. After the cell cycle time, the cell stops to divide. The two daughter cells resume their persistent random movements. When the two cells collide, they stop for some time and start moving again (Cheng et al., 2006). For directed movement of cell, Deisboeck and coworkers (Mansury and Deisboeck, 2003; Zhang et al., 2007) chose the best location for migration among the neighboring sites based on the amount of nutrients, levels of toxicity, and mechanical confinement in their tumor model . In their simulation of cell movement in the prostate epithelium, Lao and Kamei (2008) tested different movement behaviors of transit amplifying/intermediate cells and luminal cells in the prostate duct, and compared with experimental data.

In their model of avascular tumor growth, Ferreira et al. (2002) used a probability of migration which increases with the number of tumor cells in the element. This probability also increases with the level of nutrient. In a similar model by Mallet and De Pillis (2006) for tumor-immune system interactions, immune cells move randomly until they encounter a tumor cell. In the case study of their hybrid agent-based model for microbiological systems, Guo et al. (2008) modeled the chemotactic displacement of cells such that it is proportional to the difference in newly bounded receptors at the front and rear of the cell. Robertson et al. (2007) modeled the cell migration based on the relative concentrations of fibronectin, integrin, and cadherin in their simulation of *Xenopus laevis* morphogenesis.

In the case of lattice-free models, the movements of the cells are usually computed from the equations of motion which incorporate the forces acting on the cells (Galle et al., 2009; Schaller and Meyer-Hermann, 2007).

When apoptosis occurs, cells are usually removed from the lattice, and the site can remain vacant until it is filled with other cells (Galvao et al., 2008). In their simulation of tissue differentiation, Checa and Prendergast (2009) implemented apoptosis to the cells differentiated by a type of stimulus when the stimulus changed to other type. In the model of chronic chagasic cardiomyopathy after stem cell transplantation by Galvão el al.(2008), the apoptosis of inflammatory cell occurs if there is at least one bone marrow stem cell in the neighborhood of the inflammatory cell. In their simulation of the growth of epithelial cell populations *in vitro*, Galle et al. (Galle et al., 2005; Galler et al., 2009) made the cell undergo anoikis when the contact area to the substrate is smaller than a threshold value.

One of the common ways to model necrosis is to make it occur when local nutrient concentration is below a threshold value (Jiang et al., 2005; Piotrowska and Angus, 2009). In case of tumor growth simulations, the necrotic cells usually do not vanish from the lattice but are added to the necrotic material inside the tumor (Dormann and Deutsch, 2002; Jiang et al., 2005).

When a cell differentiates into other cell, the type of the cell in the lattice site can simply be changed. Checa and Prendergast (2009) made a portion of the mesenchymal stem cells differentiate into fibroblasts, chondrocytes, or osteoblasts depending on the level of mechanical stimulus and local vascularity when the cells have reached the maturation age. Grant et al. (2006) determined whether a cell would make a transition to

a more differentiated form based on the arrangement of cell, matrix, and free space around the cell in the hexagonal grid system in their simulation of *in vitro* epithelial cell morphogenesis. They also included the de-differentiation of the cell in their simulation.

Environment

Cell behaviors are influenced by their interaction with the environment. Gerlee and Anderson (2007) linked the environmental factors to the cell behaviors using a response network in their model of tumor growth. They consider the environmental factors such as neighbors, oxygen concentration, glucose concentration, and hydrogen ion concentration, and the cell behaviors such as proliferation, quiescence, apoptosis, metabolism, and movement. The cellular responses to those environmental factors are determined through the response network that each cell is equipped with (Gerlee and Anderson, 2007). In this section, modeling of extracellular matrix (ECM), chemicals, microvasculature, and forces are reviewed. Chemical concentrations and forces are usually computed in a different spatial scale from that of the cell, and this information from different spatial scale is projected to the cellular level for the cells to react to those factors.

Extracellular matrix (ECM) can be placed in the lattice sites which are available for cells as well (Checa and Prendergast, 2009; Grant et al., 2006). Checa and Prendergast (2009) let their lattice sites available for either cell or ECM in their simulation of tissue differentiation. They made the cells synthesize ECM after cell division so that the number of cells and matrix production can be in a proportional relation. Grant et al. (2006) made the cells produce matrix depending on the arrangement of the surrounding elements in their simulation of *in vitro* epithelial cell

morphogenesis. When matrix is generated by a cell, the cell moves to a neighboring site, and the resulting vacant site is filled with the produced matrix. Robertson et al. (2007) enabled each pixel to have different amount of fibronectin, and affect the cell behavior.

One of the popular ways to determine the concentrations of the chemicals such as nutrients is solving the reaction-diffusion partial differential equations (Jiang et al., 2005; Ferreira et al., 2002). Finite difference method can be used for the computation of the equations (Gerlee and Anderson, 2007; Guo et al., 2008), and the grid system which cells occupy can be used for the numerical computation of the reaction-diffusion equations as well (Gerlee and Anderson, 2007; Mallet and De Pillis, 2006). Mallet and De Pillis (2006) gained sufficient accuracy in nutrient concentrations when they used the same grid system for cells and for the reaction-diffusion equations for nutrients in their simulation of tumor-immune system interactions. Their equations are based on the ones used by Ferreira et al.(2002), and for the boundary conditions, they assumed that the nutrients are constantly supplied from the blood vessels located at the top and bottom sides of the computational domain. Palsson (2008) used a regular 3-D grid for the calculation of cAMP concentrations while letting the cells unrestricted to the grid points in his 3-D model of multicellular systems. As a result, the cAMP concentrations are interpolated between the cells and the grid system where the cAMP concentrations are calculated.

Incorporating microvasculature in the model provides the source for nutrients. In their modeling of the effects of vasculature evolution on early brain tumor growth, Gervertz and Torquato (2006) modeled the microvasculature evolution on a triangular

lattice overlaid on top of the lattice for cells. The interaction between the microvasculature and the cells were simulated such that the interaction is mediated by the key proteins involved in the vessel growth and regression. The concentrations of the proteins were obtained from the numerical solution of the reaction-diffusion equations. Checa and Prendergast (2009) modeled each capillary as a sequence of endothelial cells in their model for tissue differentiation. The growth of the vascular network on a regular lattice was simulated following their random walk model. High oxygen concentration was assumed within a distance from any blood vessel.

Peirce and coworkers (Bailey et al., 2007; Bailey et al., 2009) modeled the microvasculature consisting of endothelial cells and smooth muscle cells based on the confocal microscopy image of mouse muscle, and simulated circulating inflammatory cell trafficking (Bailey et al., 2007) and adipose-derived stromal cell trafficking during ischemia (Bailey et al., 2009). Qutub and Popel (2009) simulated capillary sprouting by applying local rules to the individual endothelial cells.

In their model for tissue differentiation, Checa and Prendergast (2009) incorporated the interaction between mechanical stimuli and the cell behavior in the tissue. The mechanical stimuli affect the differentiation of precursor cells and angiogenesis, and in turn, the mechanical properties of the tissue change due to the resulting change of the tissue composition. The mechanical stimuli were calculated from finite element analysis. Ausk et al. (2006) simulated the real-time signaling induced by mechanical stimuli in osteocytic networks. Bailey et al. (2007; 2009) used the pressure differential calculated from network flow model to drive leukocyte movement in their microvasculature model. In lattice-free models, the forces that the cell experiences

usually determine the direction and magnitude of the cell displacement (Galle et al., 2009; Schaller and Meyer-Hermann, 2007).

CHAPTER 3
SINGLE-LAYER MATHEMATICAL MODEL OF VEIN GRAFT REMODELING

Transposition of a vein segment into the arterial system where flow rate and intraluminal pressure are higher than those of venous system makes the vein segment experience increased wall shear stress and intramural wall tension. These forces act together with the biologic injury response to modulate the morphologic changes of the implanted vein graft (Dobrin et al., 1989; Fillinger et al., 1994; Galt et al., 1993; Zwolak et al., 1987). Because of the complexity of the remodeling process, there is a need for a mathematical model to better understand the role of the various factors involved. Toward that goal, a mathematical model is developed in this chapter that will account for the effect of wall shear stress. Because the intima is the wall layer that is directly exposed to blood flow, the change of its thickness will be monitored as a function of time and shear stress, and the model will be derived for that layer.

Reduced shear forces lead to accelerated intimal hyperplasia development and reduction in lumen size, while increased shear retards intimal thickening and leads to an expansion in vein graft diameter. A quantitative model of these conceptualized relationships between shear and hyperplasia will help gain insight into the dynamics of the remodeling process. To develop and validate a mathematical model relating the dynamic changes in intimal thickening to the imposed shear stress during early vein graft adaptation, a set of experimental data obtained from the vascular biology laboratory (Dr. Scott A. Berceli) at the University of Florda is used. The experimental data are from a bilateral rabbit carotid vein graft model which was developed and validated in the vascular biology laboratory (Jiang et al., 2004) This model induces a 10-fold difference in flow rate between the right and left vein grafts (Figure 3-1).

Morphology data obtained from grafts exposed to these high and low shear conditions were used to create the data matrix (shear stress, implantation time, graft diameter and intimal thickness) for the model development. Performance of the model and its utility in non-linear geometries are tested by applying the model to the complex flow environment of a focal stenosis in a rabbit vein graft.

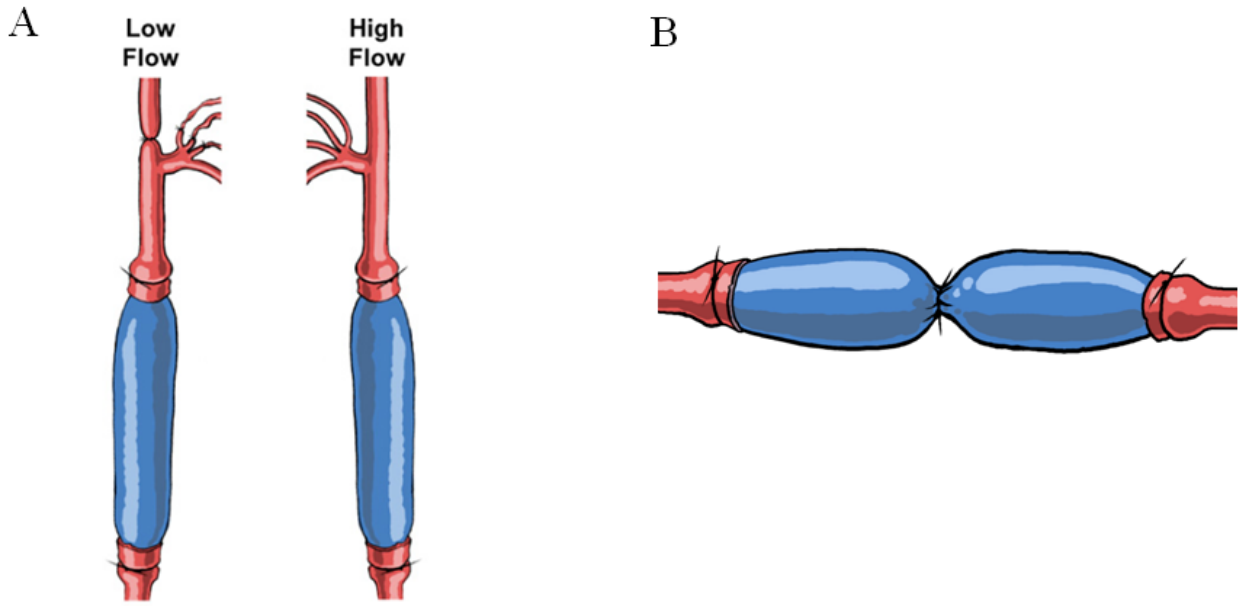

Figure 3-1. Schematic of vein grafts. A. Schematic of bilateral vein graft. B. Schematic of focal stenosis.

Model Development

Intimal Thickening in Rabbit Model

Data used in the development of the model were obtained from the work by Jiang et al. (2004). A brief description of the experiment is provided here. Thirty-four New Zealand White male rabbits (3.0-3.5 kg) underwent bilateral carotid vein grafting, and differential flow conditions were created by distal branch ligation as described previously (Fernandez et al., 2004; Jiang et al., 2004). An anastomotic cuff technique was used to

implant bilateral external jugular vein segments into the common carotid arteries. A flow differential between grafts was created by ligating the internal carotid artery and three of the four primary branches of the external carotid artery, resulting in an approximate 10-fold difference in mean flow rates.

At 1 (n=8), 3 (n=7), 7 (n=8), 14 (n=5), and 28 (n=6) days after implantation, dynamic flow rates (Transonic Systems, model T106, probe 2SB) were recorded, and the vein grafts were harvested for morphometric analysis. In the parentheses above, n represents the number of experiments performed. External vein graft radius was measured using a video camera (Sony, model DXC-151A) attached to a dissecting microscope. Formalin-fixed graft segments (n=34) were embedded in paraffin and 5 μm histologic cross sections stained with Masson's trichrome and van Gieson's elastin stains. Digitized images were collected and analyzed (Zeiss Imaging, AxioVision v4.4) to measure cross-sectional area of each layer of the graft wall. The *in vivo* radius of each layer was then calculated from the measured cross-sectional areas using the measured external vein graft radius. It was assumed that the vein graft was originally in a cylindrical shape and the area of each layer was conserved. The shear stress, τ, was calculated from the measured flow rate and assuming a Poiseuille flow ($\tau = 4 \cdot \mu \cdot Q/\pi \cdot r^3$; where μ is the blood viscosity (0.035 poise), Q is the mean flow rate, and r is the lumen radius).

Predictive Model of Intimal Growth

The intimal thickness data obtained from the bilateral vein graft experiment as a function of time and shear stress are shown in Figure 3-2. At Day 1 and 3, minimal intimal thickening is identified beyond the single layer of endothelium and basement

membrane that characterizes the normal venous architecture. Intimal growth is identified at Day 7, 14 and 28, and is consistent with previous experimental observations (Meyerson et al., 2001; Schwartz et al., 1992; Zwolak et al., 1987). The data show an inverse relationship with the imposed shear. As a consequence, the intimal thickness is assumed to be of the form:

$$h = h_0 + \frac{R_{lumen}[1 - e^{-A(t-t^*)}]}{1 + B\tau^C} \quad , \quad t \geq t^* \qquad (3\text{-}1)$$

where h_0 is the intimal thickness at implantation, R_{lumen} is the initial lumen radius, τ is shear stress, t is time, t* is the time when the onset of intima thickness change occurs, and A, B and C are constants to be determined from experimental data. The units used for length, shear stress and time are μm, dynes/cm^2 and day, respectively. An important feature of this model is the use of a decaying exponential term to describe the initial burst and then the gradual reduction in the rate of intimal growth as a function of time. Noting a period of quiescence prior to the start of active growth, a latency period (t*) is incorporated to model this behavior. Because a direct inverse shear-dependent relationship will lead to an infinite intimal thickness at zero shear stress, a form $(1+B\tau^C)$ is used. At infinite time and zero shear stress, the maximum inward growth is bounded by the value of the initial lumen radius, which corresponds to a complete occlusion of the vessel. Coefficient A is a measure of the rapidity at which intimal growth reaches steady state. Coefficients B and C represent the proportionality and power characteristics to the shear stress term, respectively.

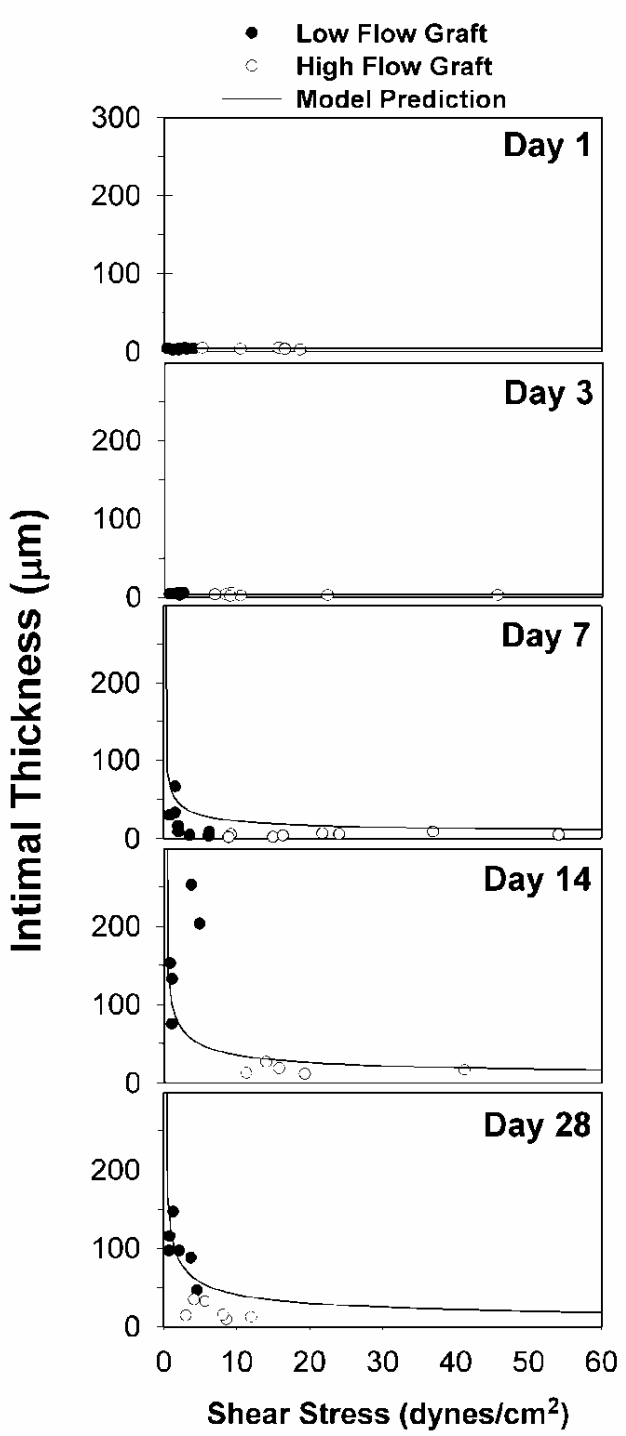

Figure 3-2. Intimal thickness as a function of shear stress at each measurement day. Measured intimal thickness data for both low (filled circle) and high (open circle) flow conditions are shown. Solid curves represent model curves. Experimental data are from Jiang et al. (2004).

Equation 3-1 is used to fit all the intimal thickness data points from Day 1 to Day 28 (Figure 3-2). The coefficients A, B and C are obtained by minimizing the sum of the squared differences between the data and the fitted values, using the nonlinear regression function in MATLAB (Version 7.0, The MathWorks Inc.). They are found to be equal to 0.170 ± 0.221, 10.9 ± 5.05, and 0.523 ± 0.351, with the associated 95% confidence intervals, respectively. From the experimental morphology data, no response to shear is seen in the intimal thickness before 3 days so t* was assigned a value of 3 days. The initial lumen radius, R_{lumen}, and intimal thickness, h_o, are found from specimens collected at the time of vein graft implantation to have an average value of 1402 μm and 4 μm, respectively. Figure 3-3A shows a surface plot of the intimal thickness as a function of shear stress and time as predicted by Equation (3-1). It is found that 77% of the experimental data points are located between the upper and lower bounds of the 95% confidence interval of the model surface.

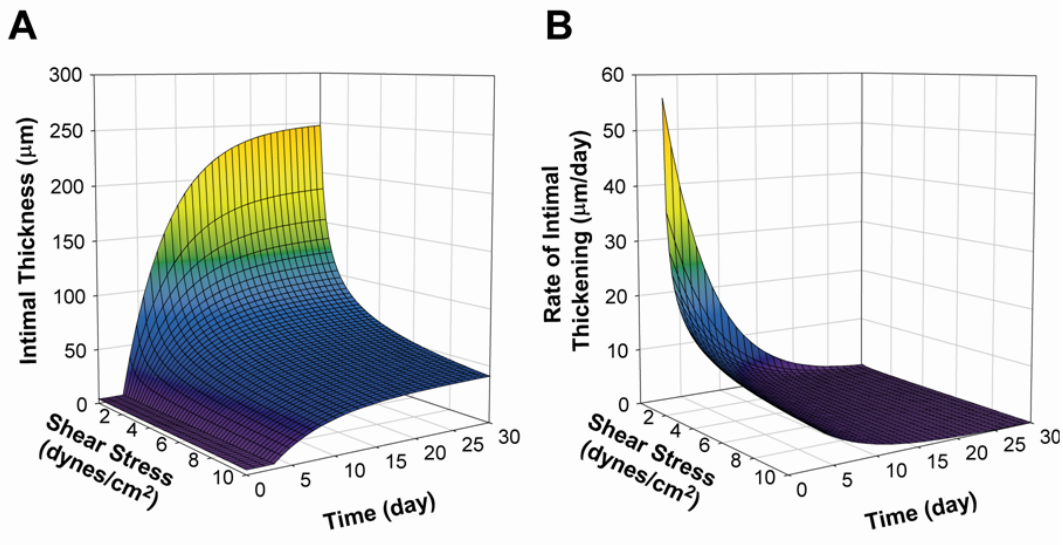

Figure 3-3. Surface plots of intimal thickness (A) and intimal thickening rate (B).

The dynamic nature of the intimal growth in response to shear stress can be further explored through differentiation of Equation (3-1):

$$\frac{dh}{dt} = \frac{R_{lumen} A e^{-A(t-t^*)}}{1 + B\tau^C}, \qquad t \geq t^* \qquad (3\text{-}2)$$

Figure 3-3B provides a surface plot of the rate of change of the intimal thickness as a function of time and shear. A rapid intimal growth is seen under low shear conditions during the first week following implantation. A significant drop in the rate of growth as time progresses or when the shear stress increases is also observed.

Model Application

Focal Vein Graft Stenosis Construct

In order to assess the intimal growth model, it is applied to a rabbit focal vein graft stenosis construct. Bilateral carotid interposition vein grafts with partial distal branch ligation were performed by the members of the vascular biology laboratory (Dr. Scott A. Berceli) as described in Model Development Section. Prior to restoration of flow, a 3.0 French (1.0 mm) polyethylene mandrel is placed external to the graft, and a Mid-graft focal stenosis is created by placement of a single 8-0 silk ligature, resulting in an approximate 80% stenosis of the lumen cross-sectional area. Flow measurement and video morphometry are recorded at the time of implantation (day 0) and 28 days later. At 28 days following implantation, vein grafts are surgically exposed and perfusion fixed with 10% buffered formalin at 80 mm Hg. Grafts are paraffin embedded and longitudinally sectioned at a thickness of 5 μm. Every tenth section is collected, stained with Mason's trichrome, and analyzed for morphology.

Simulation of Intimal Thickening around a Focal Stenosis

Due to the complex geometry around the focal stenosis, the shear stress along the length of the graft is determined numerically using a commercially available finite element analysis software package ADINA (Version 8.3, ADINA R&D Inc.). Calculations of the local shear stress and estimation of graft remodeling are performed in an iterative fashion where the shape of the wall is tracked as a function of time, as described in Figure 3-4.

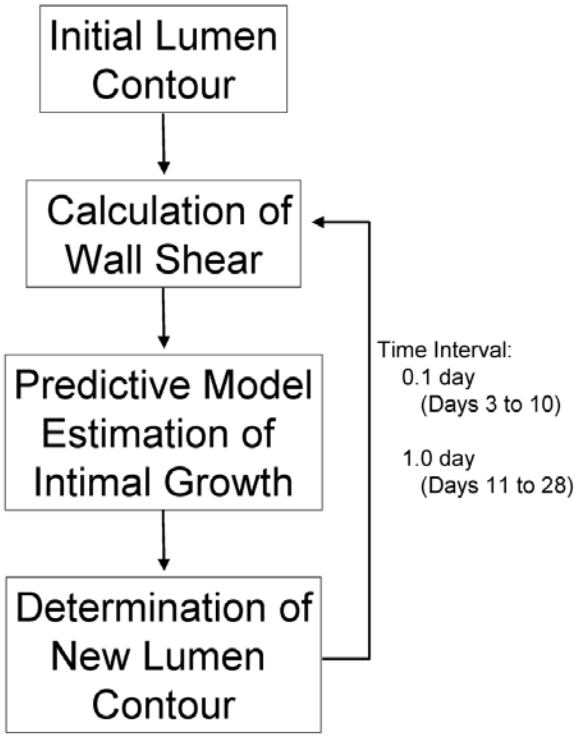

Figure 3-4. Iteration procedure for simulation of intimal thickening.

The profile of the radius of the internal elastic lamina along the axial direction is reconstructed using a smoothing spline algorithm (MATLAB) through the measured data points. The radius of the internal elastic lamina at Day 28 is assumed to be the lumen radius at Day 0 where the intimal thickness is negligible. Though there must be some degree of diameter change, it is assumed that the diameter change is minimal due to

the ligature at the focal stenosis. The wall shear stress along the length of the graft is obtained from the steady state axisymmetric computation of blood flow in the vessel using ADINA. Blood is assumed to be Newtonian, and incompressible, and a no slip boundary condition is applied at the lumen wall. The computational domain is constructed such that the total axial length from the inlet to outlet is 20 times the inlet diameter with the focal stenosis located in the middle. The length of the graft from proximal to distal cuffs is approximately 3cm. As a first order approximation, the effect of the cuffs is neglected. Although the cuffs are going to affect the flow environment and model coefficient values used, they should not have an effect on the general method presented here. Based on the experimental measurements of the flow rate and lumen radius at the time of implantation, a parabolic velocity profile with a center velocity of 16.2 cm/s and 4.7 cm/s, for high and low flow grafts respectively, is applied at the inlet at time zero. The center velocities are calculated by assuming a Poiseuille flow (u_{center} = $2Q/\pi r^2$, where Q is flow rate and r is lumen radius.). The values of the calculated wall shear stress are entered into Equation (3-2) to estimate the intimal growth and determine a new lumen contour. This updated graft geometry is then used to calculate the new wall shear stress. With the most dynamic changes in graft geometry occurring early following implantation, a time step interval of 0.1 day is used from Day 3 to Day 10, followed by use of a 1 day interval between Day 10 and Day 28. As defined in the model (Equation (3-1)), it is assumed that no change in intimal thickness occurs prior to Day 3, i.e., $t^* = 3$.

Figure 3-5 shows the pathlines and wall shear stress profiles at Day 28 for stenotic grafts exposed to low and high flow conditions. It also shows the shear stress

gradient along the vein graft. Peak values in shear and gradient are observed at the focal stenosis, and recirculation zones just downstream to them. That zone of recirculation is getting larger as the shear is increased.

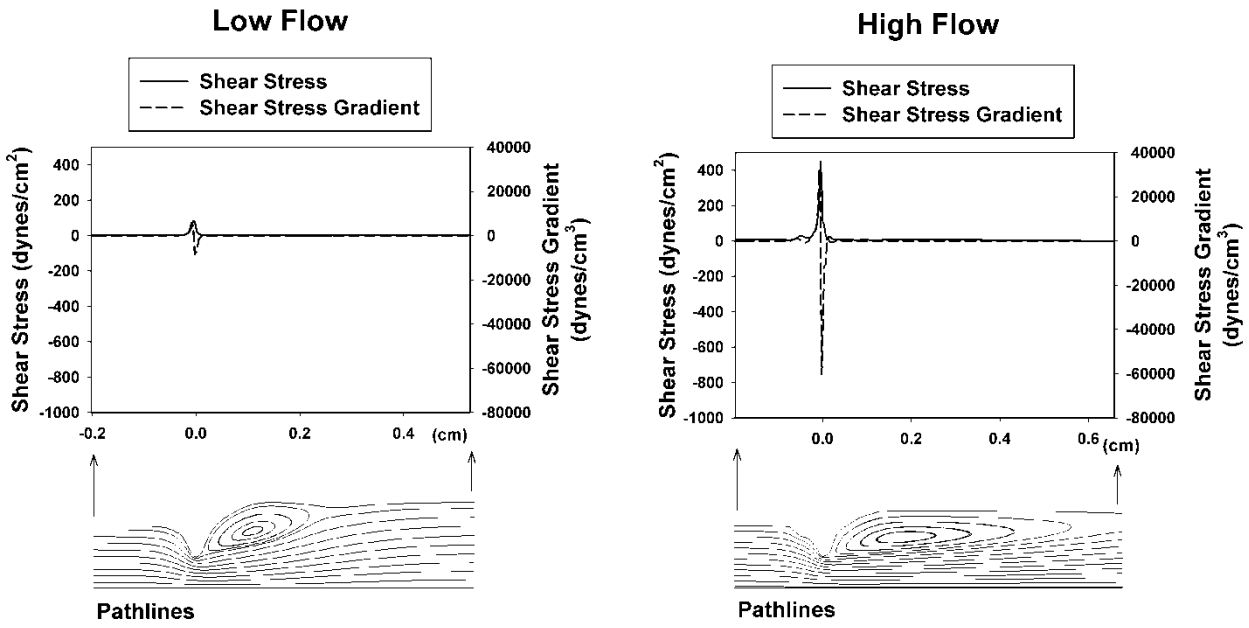

Figure 3-5. Hemodynamic characteristics inside the focal stenosis at Day 28.

The corresponding experimentally measured and predicted graft geometries at Day 28 for each flow simulation are provided in Figure 3-6. Figure 3-6A provides a schematic of the focal stenosis experiment. It also shows histology images at two different locations, including the one at the center of the stenosis. The empirical model predicts enhanced intimal growth in the area around the constriction (Figures 3-6B and 3-6C). This is observed experimentally for both flow conditions, but is most dramatic under low flow.

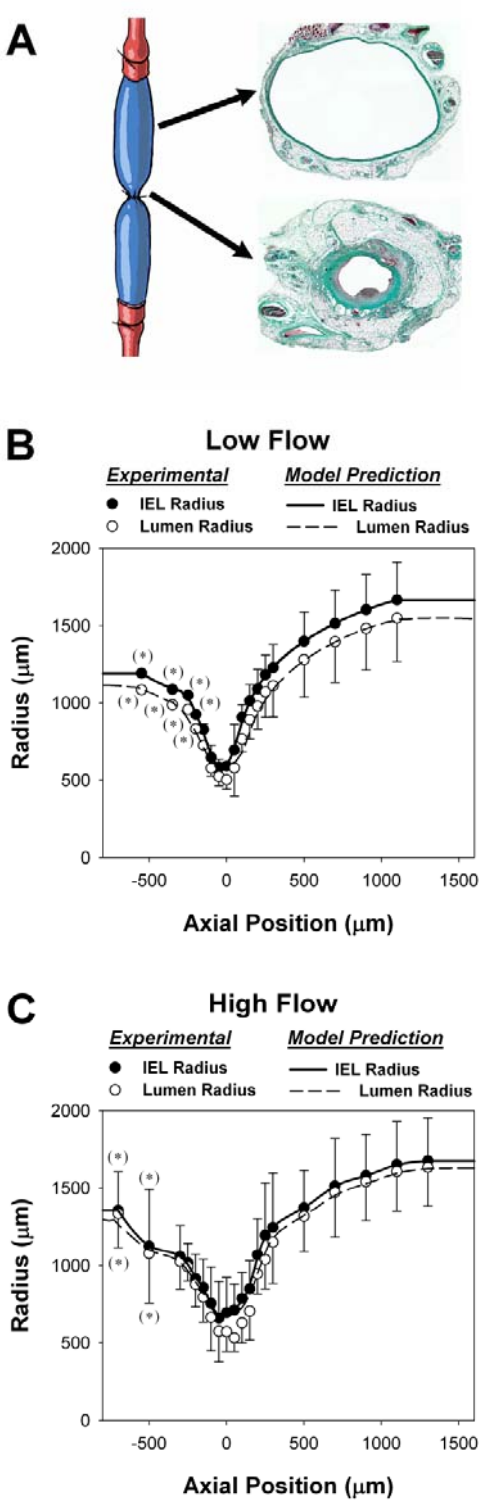

Figure 3-6. Comparison of focal stenosis simulation results with experimental data. Schematic of focal stenosis experiment (A). Measured and simulated morphology data for low (B) and high (C) flow conditions. Experimental data are from the vascular biology laboratory (Dr. Scott A. Berceli).

Of particular importance in validating the presented approach is the relative fidelity between predictive and experimental intimal growth at various locations along the graft. The low flow graft data (Figure 3-6B) generally demonstrate a good agreement between the experimental and predictive results, with a modest trend towards over-estimation of the magnitude of intimal thickening in the downstream region. In the high flow graft case (Figure 3-6C), reasonable agreements proximal and distal to the stenosis are observed. However, marked difference near the stenosis is seen. Significant intimal thickening is experimentally observed in this high shear region, a site where the model suggests a limited hyperplasia response. This is not too surprising since the model takes into consideration only the effect of shear stress.

Parameter Sensitivity Analysis

To examine the sensitivity of the simulated intimal growth data within the focal stenosis construct to the empirical parameters in Equation (3-2), low flow data at day 28 are used. Equation (3-2) is used because it reflects the rate of change of the thickness. It is more practical than Equation (3-1) since it does not depend on the knowledge of an initial thickness value. Each coefficient (A, B, and C) is varied ±10%, and its effect on the simulation is analyzed. For axial positions ranging from -500 μm to 1500 μm with respect to the center of the stenosis, Table 3-1 shows the percent change of intimal growth associated with the variation of each coefficient. It is found that coefficient A has a limited influence on the value of the intimal thickness due to the exponential growth and rapid rise to steady state at Day 28. Coefficient B has the greatest overall effect, with average intimal thickness changes of 8.5% and 10.3% following a 10% increase and decrease, respectively. Coefficient C amplifies any local shear stress changes, and

provides the largest increase in intimal thickness (24.1%) at 0.06mm upstream to the stenosis when C is decreased by 10%.

Table 3-1. Parameter Sensitivity Analysis

	% Change of each coefficient in Eq. (3-2)	% Change of intimal growth (Mean±SD)
Coefficient A	+10	0.5±0.05
	-10	0.8±0.07
Coefficient B	+10	8.5±0.6
	-10	10.3±0.9
Coefficient C	+10	3.6±4.0
	-10	3.9±4.8

Discussion

In this chapter, a mathematical model of vein graft intimal hyperplasia has been developed based on experimental data obtained from a rabbit vein graft construct exposed to a wide range of physiologic shear stresses. It is understood that shear stress is not the only factor leading to intimal hyperplasia. Intimal hyperplasia is a very complex process involving a large number of biologic and hemodynamic factors. Nevertheless, a general approach has been developed to model vessel thickening due to shear. Additional factors can be included following a similar approach in order to get a more comprehensive vessel remodeling model.

The model utilizes a nonlinear inverse relationship between the intimal thickening rate and shear stress, which is consistent with the experimental data of our group (Fernandez et al., 2004) and others (Meyerson et al., 2001; Schwartz et al., 1992). It successfully describes the time-dependent behavior of early vein graft remodeling (Zwolak et al., 1987). Zhang et al. (2002) found that the neointimal hyperplasia develops rapidly, and stabilizes by about 4 weeks postoperatively in a

murine vein graft model. Zou et al. (1998) observed increasing intimal thickness up to 16 weeks in a mouse model, with the rate of thickening decreasing after 4 weeks.

The present study confirms that the rate of change of intimal thickness depends not only on shear stress, but also on time. Also unique to the model is the use of a time delay prior to the initiation of the hyperplasia response. From the experimental data, this time delay is found to be 3 days. For other clinical conditions or diseases, this time delay is expected to be different. This time delay is not known a priori and needs to be determined experimentally or treated in the model as a variable. While the underlying mechanisms for this time delay may include multiple factors, it appears to be related to the development of microvasculature growth from the surrounding tissue (Westerband et al., 2001). For example, it has been reported that the smooth muscle cell migration from media to intima starts 4 days after injury (Lemson et al., 2000). Also critical may be the initial disequilibrium between cell proliferation and cell death, with several investigations confirming an early burst of apoptosis following vein graft implantation (Jiang et al., 2007; Westerband et al., 2001). As such, the incorporation of biologically-defined parameters into the predictive model may provide a critical insight into the remodeling process.

Among the strength of the current model is the use of an initial experimental construct to define the model parameters, and application of the model to the simulation of a second, independent experimental construct, the focal stenosis geometry. The secondary analysis revealed a difference between experimental data and model predictions at the throat of the stenosis where shear stress is higher (Figure 3-6C). It suggests that the elevations in shear do not universally yield reductions in the rate of

intimal growth, instead suggesting elevated shear leads to enhancement of the hyperplasia response. It is not clear either if it is shear stress or its gradient that is responsible for this enhanced intimal thickening at the maximum constriction (Figure 3-5).

Also a limitation of the current model is the focus on intimal growth as the dominant mechanisms for changes in lumen geometry. Work by our group (Jiang et al., 2007) and others (Glagov et al., 1987; Korshunov and Berk, 2004; Owens et al., 2006) have established the early process of outward remodeling is critical in maintaining lumen patency. The shear stress data used in this study (Figure 3-2) also show that there was outward remodeling at Day 28 in the high flow construct case. Experimental constructs designed specifically to evaluate outward remodeling and incorporation to our predictive model could be a future direction of this work.

The process of early adaptation of vein graft to arterial environment also involves medial thickening, though it has been reported that the medial thickening has little or no relation to shear stress, and correlates more with circumferential strain (Dobrin et al., 1989; Fernandez et al., 2004; Galt et al., 1993). It is evident that other factors than shear (e.g. tension and biological environment) need to be taken into account in order to fully describe the thickening process.

CHAPTER 4
MULTI-LAYER MATHEMATICAL MODEL OF VEIN GRAFT REMODELING

Though the relationship between wall shear stress and the remodeling of vein graft intimal layer is described in the previous chapter, the lumen reduction in vein graft adaptation is the result of the combination of multiple layers remodeling. Also, as described in chapter 2, wall tension as well as wall shear stress is another important hemodynamic factor influencing vein graft remodeling. Although numerous experimental evidences relating hemodynamic forces to vascular remodeling have been reported, a comprehensive mathematical model describing the relationship among the wall shear stress, wall tension, and the remodeling of each individual wall layer of vein graft is lacking.

One of the characteristics of vein graft implantation is the injury that occurs due to the altered hemodynamic environment the vein graft experiences. In response to the damage, repair events such as leukocyte recruitment, re-endothelialization, smooth muscle cell proliferation, and matrix deposition occur in a time frame ranging from hours to months. The imposed hemodynamics has different effects on vein graft adaptation depending on the time frame. This temporal dependence between the local hemodynamic environment and the response of the vascular wall is frequently lacking from models that have been developed to quantitatively examine the morphologic changes of vein graft.

In this chapter, a multi-layer mathematical model which describes time-dependent behaviors of multiple layers of vein graft is developed based on experimental data from the well-characterized rabbit model. Founded on the model developed in the previous chapter, which focused on the influence of shear stress on intimal adaptation,

the current model examines the changes in intimal and medial areas and the radius of external elastic lamina (EEL). Also unique in the current model is the integration of a logistic relationship between independent and dependent variables to describe the early acceleration and later reduction in the rate of adaptation. The detailed understanding of the temporal changes in vein graft morphology that can be extracted from the current model is critical in identifying the dominant contributors to vein graft failure and developing strategies to improve their longevity.

Model Development

Remodeling Characteristics of Vein Graft Wall

Experimental data of rabbit bilateral vein graft construct used in the model development were obtained from the vascular biology laboratory (Dr. Scott A. Berceli), as described in Chapter 3 (Jiang et al., 2004; Jiang et al., 2009).

In the previous chapter, the mathematical model of intimal layer remodeling (Tran-Son-Tay et al., 2008) was based on experimental data up to 28 days. In the present development, to accommodate additional wall layers and additional data at 3 month and 6 month time point, a logistic model is used to describe the time-dependent adaptation of the intimal area, medial area, and EEL radius (Figure 4-1). The experimental data of wall thickening (Figures 4-2, 4-3, 4-5) show an initial accelerated growth and then damping once the wall thickness has reached a critical value, which is the hallmark of most growth models. The S-shaped behavior parallels the population growth of smooth muscle cells. For that reason, a logistic model, which is a common and one of the simplest models of population growth, is used to describe the observed S-shaped behavior. A logistic model with the following general form was used (Britton, 2003):

$$\frac{dN}{dt} = aN\left(1 - \frac{N}{b}\right) \tag{4-1}$$

where N is the variable of interest, t is time, and a and b are constants representing the growth rate and carrying capacity of N, respectively.

The logistic relationship was appropriately modified to model the time-dependent changes in intimal area, medial area, and EEL radius. To minimize the influence of inherent variations in initial vein geometries, each outcome variable was normalized to the corresponding value at the time of implantation. The exception is intimal area, which was normalized with respect to the medial area due to the inherent inaccuracies in measuring the cross-sectional area of this single-cell layer.

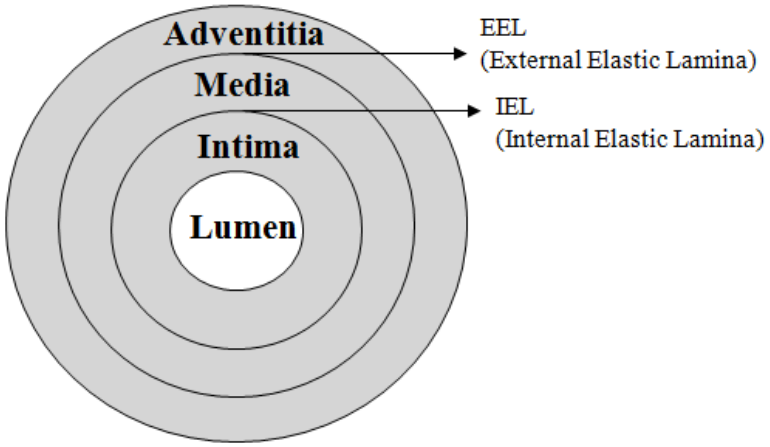

Figure 4-1. Schematic of the cross-section of venous wall.

Intima Model

Experimental data detailing the effect of shear stress and implantation time on the normalized intimal area is shown in Figure 4-2.

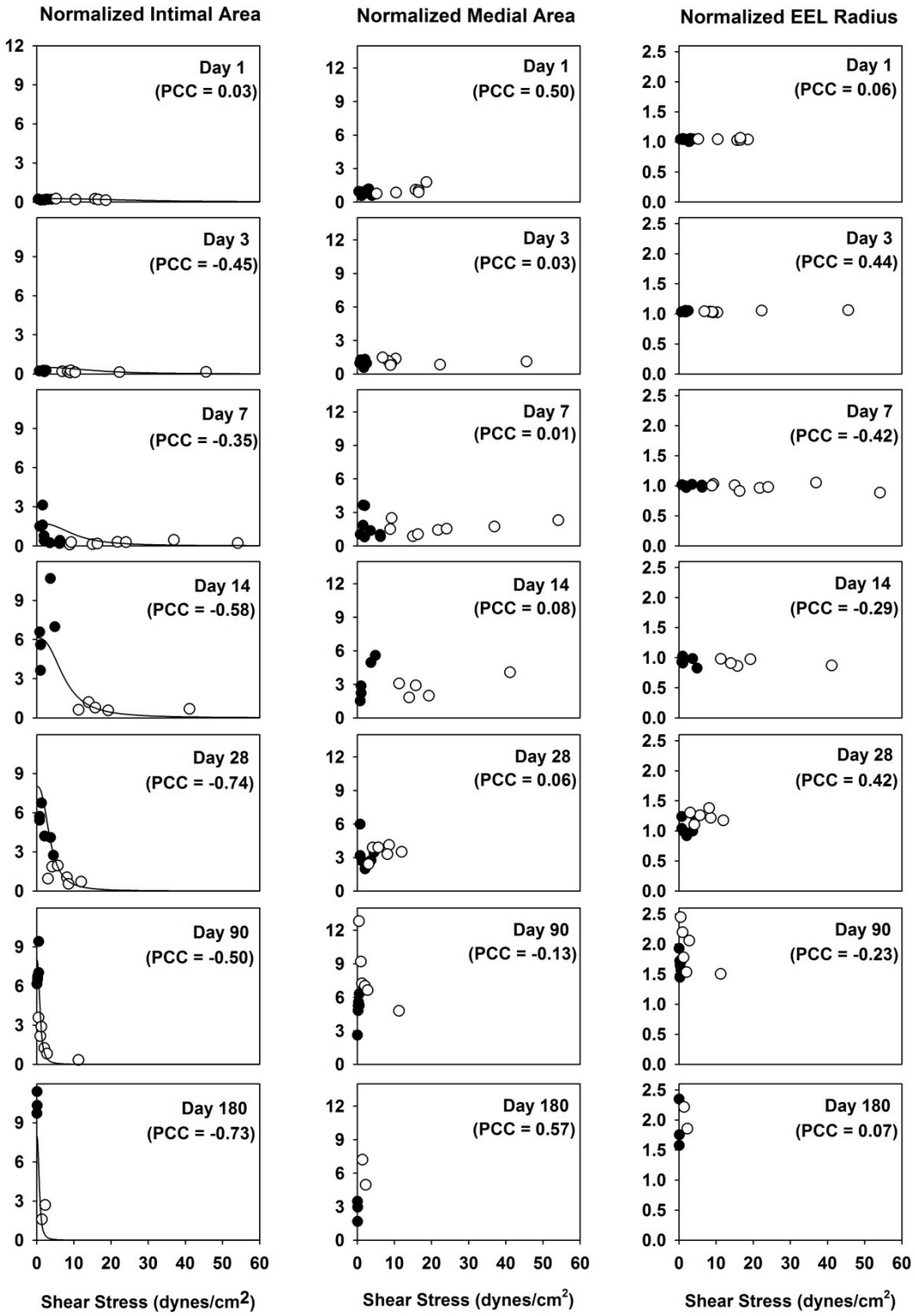

Figure 4-2. Normalized intimal area, medial area, and EEL radius with respect to shear stress at each time point. Experimental data are from Jiang et al. (2004).

Consistent with the finding of other investigators (Meyerson et al., 2001; Schwartz et al., 1992), an inverse relationship between the intimal area and shear stress is observed. Due to outward remodeling of the graft and an increase in lumen diameter, a reduction in shear stress is initially observed at 28 days after implantation and continues throughout the 180 day observation period. To incorporate these characteristics, the logistic model for the growth of the intima is as follows.

$$\frac{\partial A_I^*(\mathbf{x},t)}{\partial t} = a_I A_I^*(\mathbf{x},t)\left(1-\frac{A_I^*(\mathbf{x},t)}{b_i'}\right), \text{ with } \quad b_i' = \frac{b_I}{1+c_I(D_I\tau(\mathbf{x},t))^{d_I}} \qquad (4\text{-}2)$$

where A_I^* is the normalized intimal area, τ is the shear stress, $D_I=(R/R_0)^3$, R is the lumen radius at time t, R_0 is lumen radius at implantation, **x** is a position vector, and a_I, b_I, c_I, and d_I are constants. The coefficient a_I represents the slope of the rate of intimal area growth. The coefficient b_I provides the limit of intimal area growth for the shear stress. The exponents c_I and d_I represent the dependence on the shear stress. Note that b_i' represents the upper limit that can be obtained by the intimal area, and incorporates the inverse relationship with shear stress that was previously described. Integration of Equation (4-2) yields:

$$A_I^*(\mathbf{x},t) = \frac{b_i' A_{I0}^*(\mathbf{x})e^{a_I t}}{b_i' - A_{I0}^*(\mathbf{x}) + A_{I0}^*(\mathbf{x})e^{a_I t}} \qquad (4\text{-}3)$$

The coefficients a_I, b_I, c_I, and d_I were obtained through non-linear regression (MATLAB v7.7, The MathWorks Inc., Natick, MA) against the experimental data (Figure 4-2) and were found to be 0.35±0.06, 8.0±0.9, 0.013±0.035, and 2.6±1.4 with 95% confidence intervals, respectively. A_{10}^* is the normalized intimal area at implantation and

was experimentally measured to be 0.186. The units used for shear stress and time are dynes/cm^2 and day, respectively.

Wall thickness depends on both cell proliferation and vein graft diameter change while wall area changes only by cell proliferation. By using wall area as the modeling variable, the effects of cell proliferation and graft diameter change can be separated.

Media Model

Experimentally measured medial areas, normalized to the medial area at the time of implantation, are illustrated in Figures 4-2 and 4-3.

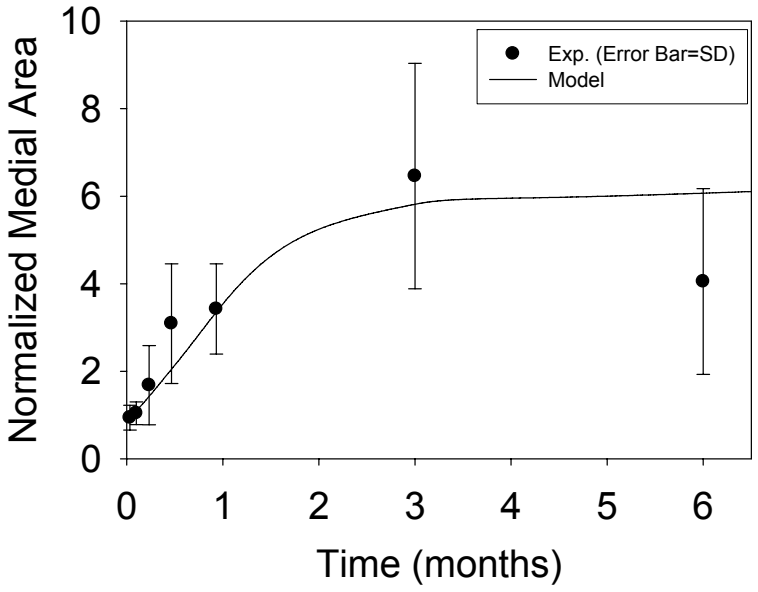

Figure 4-3. Normalized medial area as a function of time. Experimental data are from Jiang et al. (2004).

Unlike the notable influence of shear stress on intimal hyperplasia, the process of medial thickening appears independent of the imposed wall shear stress. Instead, previous investigators have shown intramural wall tension to have an important dependence on medial thickening (Schwartz et al., 1992; Zwolak et al., 1987). Although the experimental design was not developed to directly evaluate the influence of wall

tension on vascular remodeling, examination of our data supports a positive correlation between the rate of medial hypertrophy and the imposed wall tension (Figure 4-4).

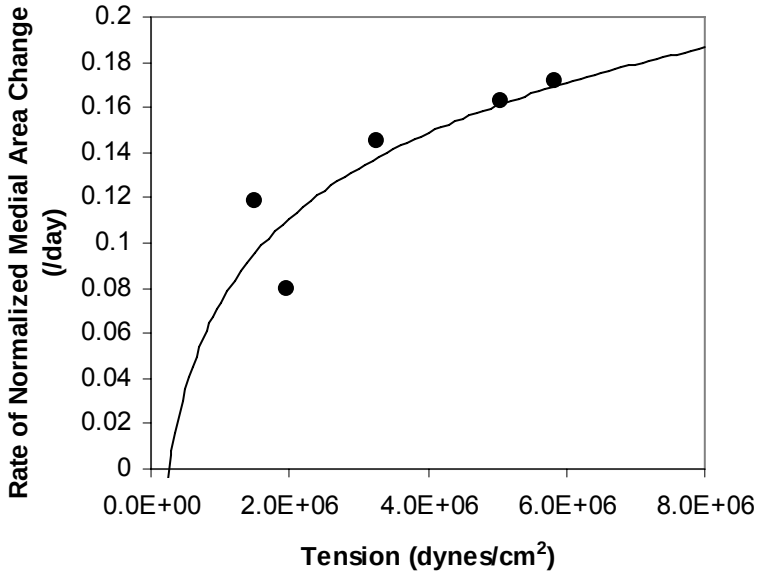

Figure 4-4. Rate of normalized medial area change as a function of wall tension. Experimental data are from Jiang et al. (2004).

Using this as a starting point, a linear correlation is assumed between the rate of medial area growth and wall tension, modifying the logistic model as follows.

$$\frac{\partial A_M^*(\mathbf{x},t)}{\partial t} = a_M A_M^*(\mathbf{x},t)\left(\left(D_M T(\mathbf{x},t)\right)^{c_M} - b_M A_M^*(\mathbf{x},t)\right) \qquad (4\text{-}4)$$

where A_M^* is the normalized medial area, D_M=R_0/R, R is the lumen radius at time t, R_0 is the lumen radius at implantation, T is the circumferential wall tensile stress, **x** is a position vector, and a_M, b_M, and c_M are constants.

The coefficient a_M represents the slope of the rate of medial area growth. The coefficient b_M gives the limit of medial area growth for the wall tensile stress. The exponent c_M is a function of the tensile stress.

In order to obtain the coefficients in Equation (4-4), the rate of change of the normalized medial area (dA^*_M/dt) is needed. The equation $A^*_M = A - Be^{Ct}$ (t is time, and A, B, and C are constants) is fitted to the experimental data in Figure 4-3 to obtain the rate of change ($dA^*_M/dt = -BCe^{Ct}$). Knowing that rate, the values for a_M, b_M, and c_M in Equation (4-4) are obtained through a non-linear regression of the logistic model using the experimental data for A^*_M, dA^*_M/dt, D_M, and T, where the wall tension stress is calculated from the relation T=PR/h (T: tension per unit area, P: blood pressure, R:lumen radius, and h: medial thickness). Using this approach, the coefficients a_M, b_M, and c_M in Equation (4-4) were found to be 0.014±0.175, 0.79±8.33, and 0.30±2.03 with 95% confidence intervals, respectively. The units used for blood pressure and time are 10^4 dynes/cm^2 and day, respectively. Figure 4-3 shows the model curve obtained by numerically integrating Equation (4-4).

EEL Model

EEL radii were determined experimentally over a 6 month period and are shown in Figures 4-2 and 4-5. Similar to our observations related to adaptation of the media, changes in the graft radius were relatively independent of wall shear stress (Figure 4-2). Hence, the logistic model for the normalized EEL radius (R^*_{EEL}) utilizes time as the only dependent variable and is provided by the following expression

$$\frac{\partial R^*_{EEL}(\mathbf{x},t)}{\partial t} = a_E\left(R^*_{EEL}(\mathbf{x},t)-1\right)\left(1-\frac{R^*_{EEL}(\mathbf{x},t)}{b_E}\right) \tag{4-5}$$

where t is time, **x** is a position vector, and a_E and b_E are constants. The coefficient a_E represents the slope of the rate of EEL radius increase. The coefficient b_E is the limit of EEL radius increase.

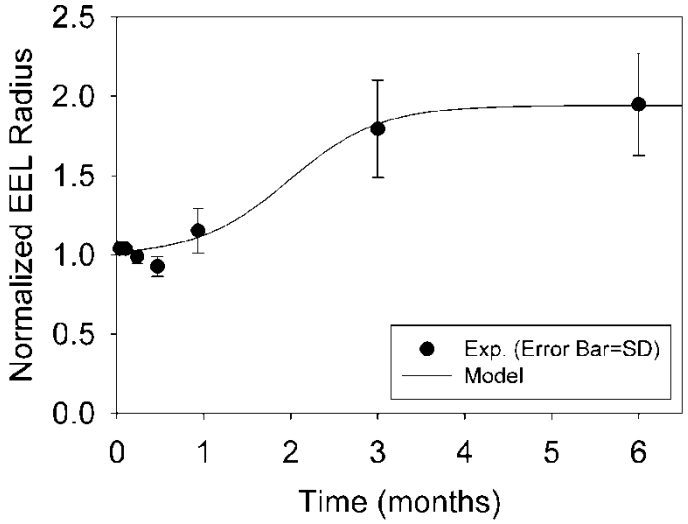

Figure 4-5. Normalized EEL radius as a function of time. Experimental data are from Jiang et al. (2004)

The analytical solution to Equation (4-5) is

$$R^*_{EEL}(\mathbf{x},t) = \frac{b_E - R^*_{EEL0}(\mathbf{x}) + b_E\left(R^*_{EEL0}(\mathbf{x})-1\right)e^{\frac{a_E(b_E-1)}{b_E}t}}{b_E - R^*_{EEL0}(\mathbf{x}) + \left(R^*_{EEL0}(\mathbf{x})-1\right)e^{\frac{a_E(b_E-1)}{b_E}t}} \tag{4-6}$$

and the coefficients a_E, b_E, and R^*_{EEL0} are found to be 0.133±0.092 and 1.94±0.19, and 1.02±0.04 with 95% confidence intervals, respectively, through nonlinear regression using the shear-averaged experimental data in Figure 4-5. Note that coefficients a_E

and b_E are proportionality constants and they define the maximum limit of R^*_{EEL}. The unit used for time is day. The model curve describing the normalized EEL radius as a function of time is shown in Figure 4-5.

Figure 4-2 shows that there is no consistent correlation between WSS and EEL remodeling. This is somewhat surprising considering that it has been suspected that vein graft expands to reduce the WSS imposed by faster arterial flow. Wall tension does not seem to be the driving force of EEL remodeling either. EEL expansion tends to increase lumen radius which increases wall tension. EEL remodeling seems to be related to the biologic environment of the arterial system which is represented by time dependent terms in the model equation.

Figure 4-6 shows the surface plots of the normalized EEL radius as a function of time, the normalized intimal area inversely related to shear stress, and the normalized medial area positively related to tension and reaching plateau after about 3 months.

Sensitivity and Stochastic Analysis

To examine the effects of the variation of each coefficient on the calculation of the change of the area or radius in Equations (4-2), (4-4), and (4-5), each coefficient was varied 100% and -50%, and the model predictions at 6 months were obtained (Table 4-1). In the intima model (Equation (4-2)), b_I has the greatest impact where the % change of the coefficient was directly reflected on the model prediction. The other coefficients have minimal impacts. In the media model (Equation (4-4)), the coefficients b_M and c_M have the greatest impacts on the model prediction. In the EEL model (Equation (4-5)), b_E has direct impact. However, for all the coefficients, the % change of the model prediction was within the range of the % change of the coefficient.

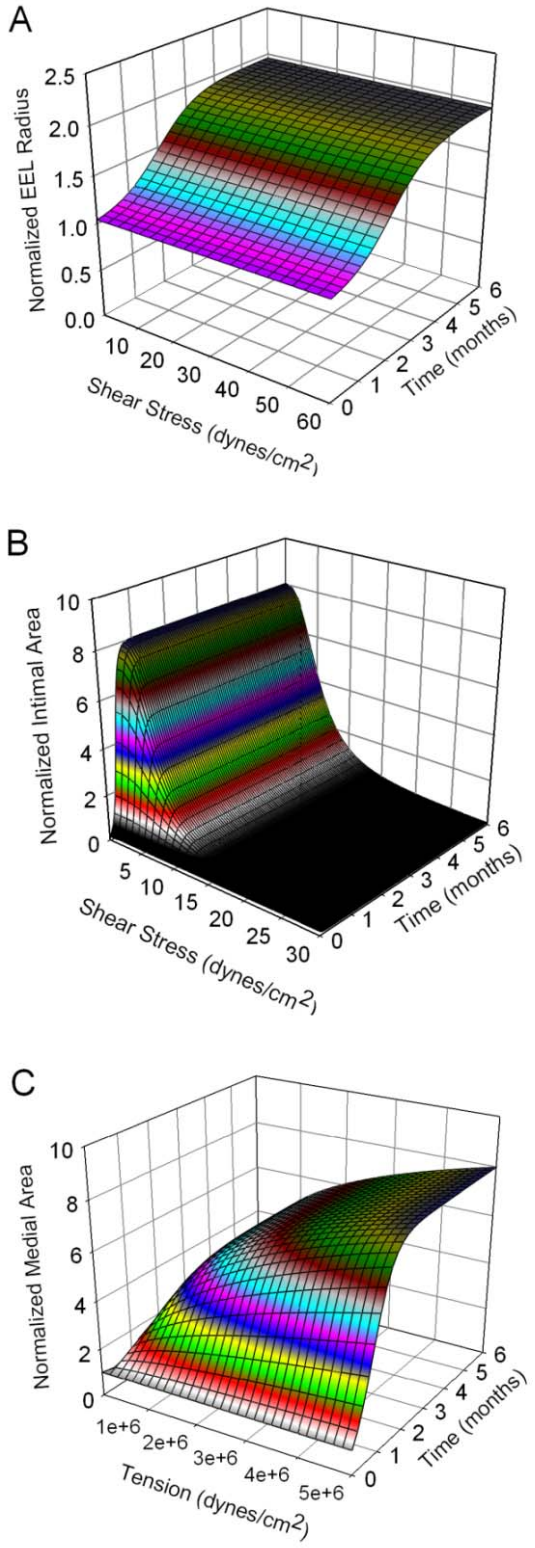

Figure 4-6. Surface plots of normalized EEL radius (A), normalized intimal area (B), and normalized medial area (C).

Table 4-1. Parameter Sensitivity Analysis

Coefficient	% Change of Coefficient	% Change of Model Prediction at 6 months
a_I	100	0
	-50	0
b_I	100	100
	-50	-50
c_I	100	-6
	-50	4
d_I	100	-24
	-50	4
a_M	100	0
	-50	0
b_M	100	80
	-50	-44
c_M	100	102
	-50	-36
a_E	100	0
	-50	-6
b_E	100	100
	-50	-48

In order to examine the robustness of the model to variations in the experimental data, a stochastic analysis was performed. Using the mean and standard deviation (SD) of the experimental data at each time point, 10^4 sets of new data (consisting of intima, media, and EEL) were generated assuming a normal distribution at each data point. In the absence of a standard deviation for the shear- and time-dependent intimal area experimental data (Figure 4-2), these values were assumed to have a coefficient of variation (CV) equal to that of the medial area (CV=0.39). Using the experimentally measured flow rate, blood pressure and initial vein graft geometry, Equations (4-2), (4-4), and (4-5) were used to update the vein graft geometry at every 0.5 day. Because each experimental data point represents an individual rabbit, separate simulations were

performed for each harvest day using the average of the initial conditions for that specific day. To parallel the experimental design, simulations were performed separately for the low and high flow groups of the vein grafts. Figure 4-7 shows both experimental data and model predictions for these stochastic simulations.

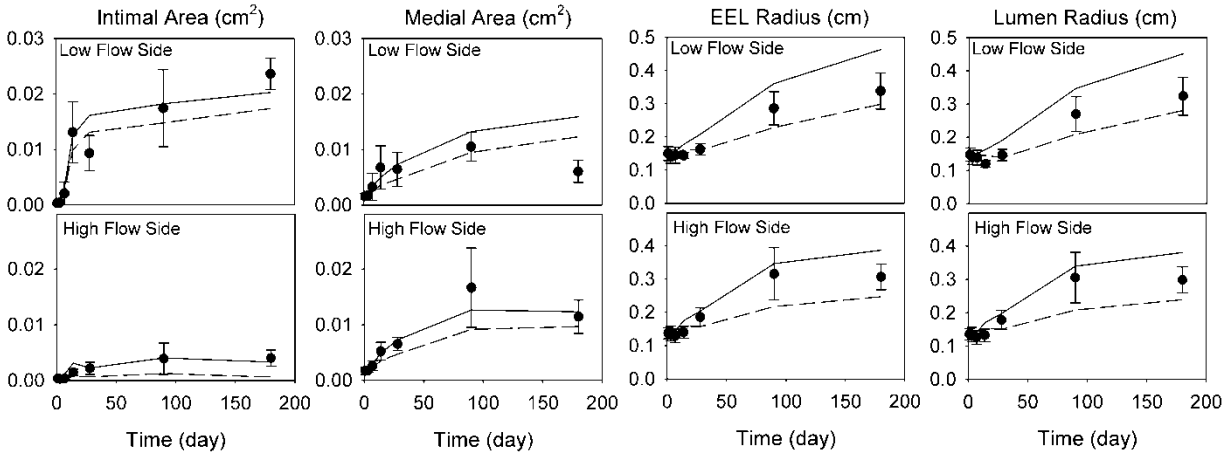

Figure 4-7. Stochastic analysis of the vein graft mathematical model. Experimental data are from Jiang et al. (2004).

In the cases of the EEL and lumen radii, the mean values of the experimental data are located within one standard deviation of the model predictions after 28 days. In the cases of the intima and media, some increased deviations at the 6 month time point are observed. However, for all the data points, the SDs of the model predictions are comparable to those of the experimental data, confirming the robustness of the model.

Model Application

Simulation of Idealized Stenosis

The model described in the previous sections is now applied to the simulation of wall remodeling in an idealized stenosis to test the applicability of the model. Figure 4-8 shows a schematic of the stenosis geometry and the equations describing dynamic

remodeling within each layer of the vein graft wall. A smooth geometry within the throat region was modeled using a sinusoidal curve.

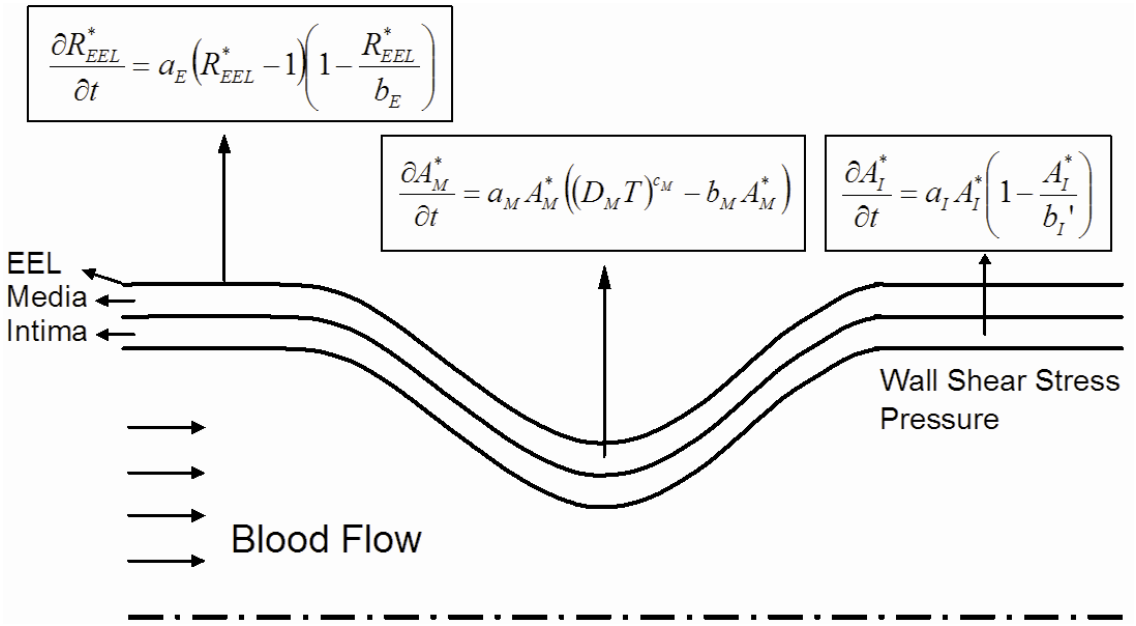

Figure 4-8. Schematic of stenosis simulation.

The initial wall shear stress was estimated using the ADINA finite element analysis software package (Version 8.5, ADINA R&D Inc., Watertown, MA), assuming axial symmetry, a Newtonian fluid, and a non-slip boundary condition at the wall. Supported by our histological examination of the developing intima, which demonstrates a disorganized extracellular matrix structure, we have assumed this layer to be a non-load bearing structure in the analysis schema, and the resulting wall tension is determined by the relationship T=PR/h (T: tensile stress, P: blood pressure, R:lumen radius, and h: medial thickness). Using wall shear and tension as input parameters for Equations (4-2), (4-4), and (4-5), a new wall geometry (i.e. intimal and medial thickness and EEL radius) was determined. Updated wall geometries were determined at 1 day

intervals for the duration of the simulation as follows. At the time interval, t_i, the geometry of the vessel, WSS and pressure were computed using the mesh and values generated at t_{i-1}. This coupling between computational fluid dynamics (CFD) and growth model is in line with the one used by Figueroa et al. (2009). In order to evaluate the influence of the 1 day time interval on the numerical integration of Equations (4-2), (4-4), and (4-5), an analytical solution to these equations was obtained. Comparison between the forward Euler time integration using a 1 day interval and the analytic solutions demonstrated a less than 0.002% difference for all expressions at Day 180, using shear and tension values in the physiologic range. Analyses were performed assuming an initial 50%, 70%, and 80% stenosis (diameter) subjected to low and high flow conditions. To parallel our experimental rabbit vein graft model, the initial inlet lumen radius was set to 1.5 mm. Inlet parabolic profiles with a centerline velocity of 2.45 cm/s and 12.6 cm/s were used for the low and high flow conditions, respectively. The total axial length of the geometry was set to be equal to 80 times the inlet diameter to ensure no reverse flow at the exit.

Figure 4-9 shows the intimal area along the graft at 1 week, 2 weeks, 3 weeks, and 6 months after implantation under low flow conditions. Intimal thickening is observed along the graft except in the region of the stenosis, where shear stress is maximal. The intimal area increases rapidly and reaches an asymptote at about 1 month after implantation. In association with an initial 50% stenosis (Figure 4-9A), a localized increase in intimal thickening is observed between axial positions 0.1 and 0.3 cm and corresponds to the flow separation and reattachment distal to the stenosis. In association with the 70% and 80% stenoses (Figures 4-9B and 4-9C), the site of flow

reattachment is located at 1.1 and 1.5 cm, respectively, leading to a broad region of recirculation and a mild increase in intimal area in these regions.

Figure 4-10 shows the intimal area along the graft under high flow conditions. Within regions of uniform/unidirectional flow, proximal and distal to the stenosis, high flow conditions result in a reduction in intimal thickening. In contrast to the low flow simulations, the marked reductions in shear distal to the stenosis lead to a marked augmentation in intimal area in this region. Notable are the 70% and 80% high flow simulations where the reduced shear within the region of flow separation has shifted distally, resulting in enhanced intimal thickening that is several centimeters distal to the site of maximum stenosis.

Figure 4-11 illustrates the change in the EEL radius and medial area associated with a 50% stenosis exposed to low flow conditions. A uniform increase in both graft radius and medial area is observed proximal and distal to the stenosis.

In contrast to the effect on intimal thickening, the perturbations in the flow patterns induced by the stenosis have a limited effect on these geometric parameters. The patterns of graft expansion and medial growth associated with 70% and 80% stenoses demonstrated a similar asymptotic behavior and were not notably influenced by the magnitude of the flow (data not shown).

One of the limitations of the stenosis study is that the shear stress was obtained from steady flow simulations. However, it is expected that under pulsatile flow the recirculation zone behind the stenosis would oscillate, which would result in different prediction of wall thickening in those regions. Thus, the intimal thickening around the reattachment point shown in Figure 4-10 could be an over-prediction.

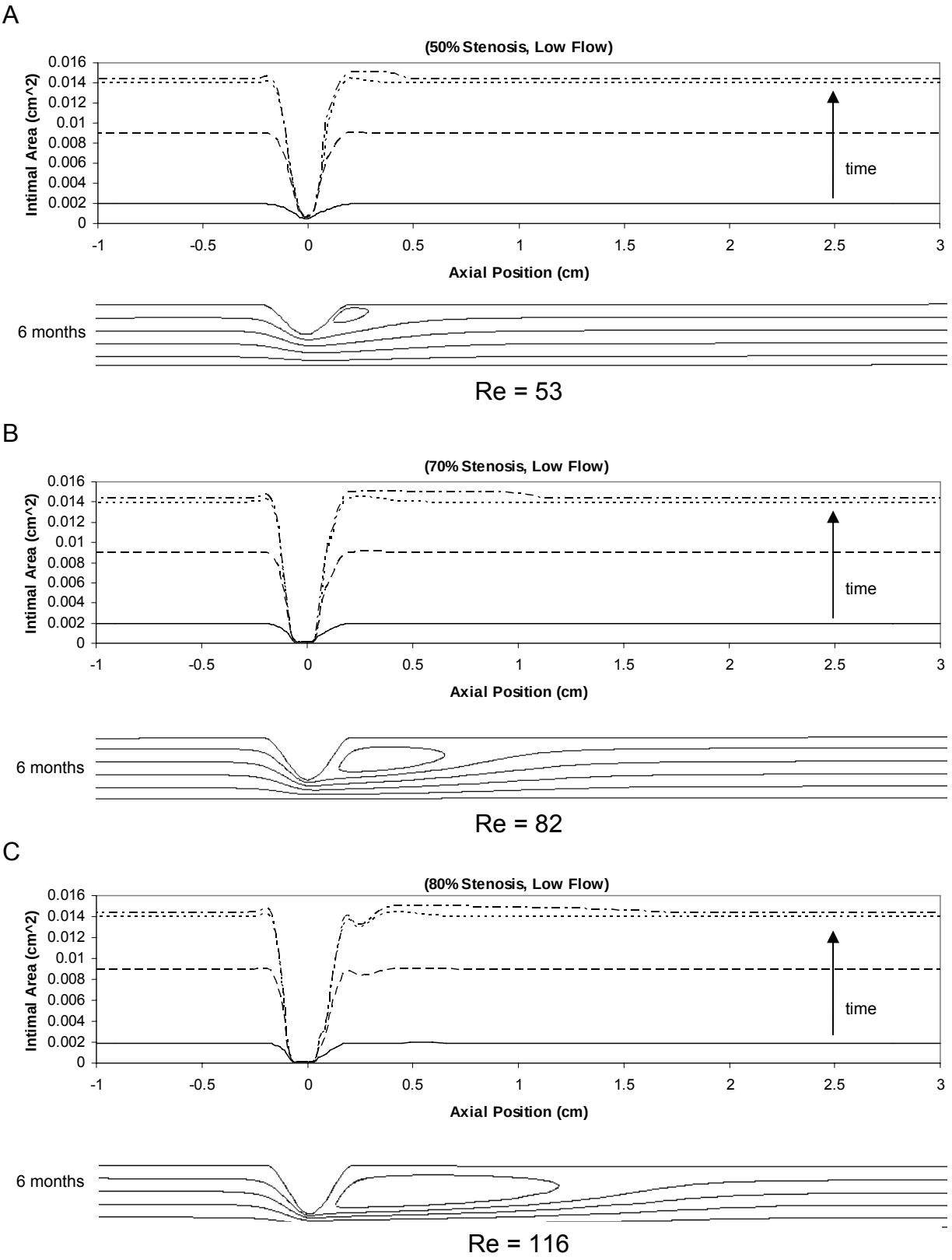

Figure 4-9. Simulation results for intimal area around the stenosis of 50% (A), 70% (B), 80% (C) reduction in stenosis (diameter) under low flow condition.

A

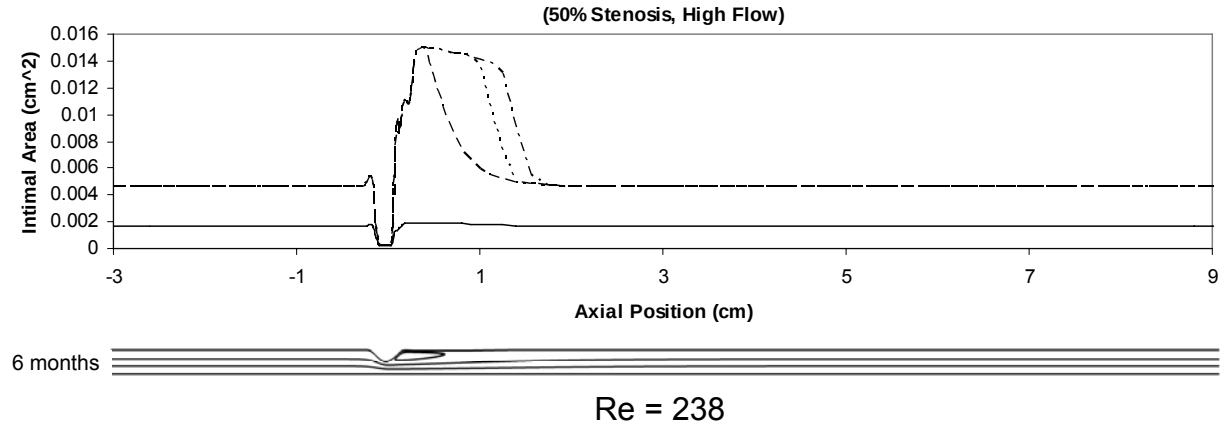

Re = 238

B

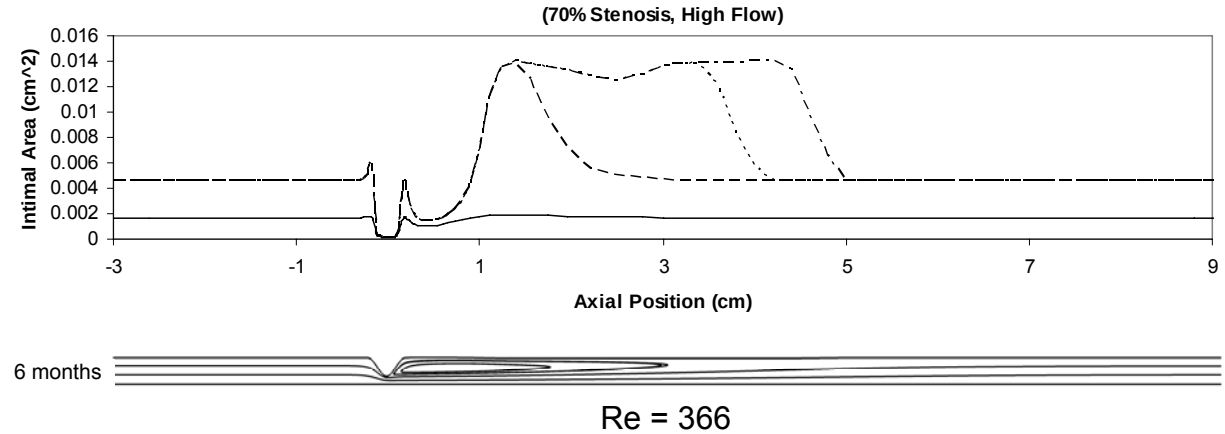

Re = 366

C

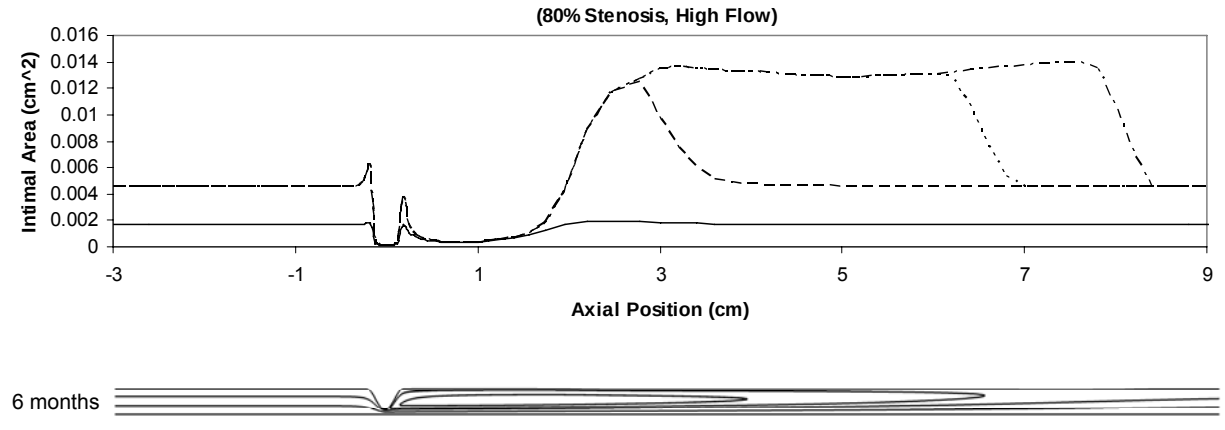

Re = 528

Figure 4-10. Simulation results for intimal area around the stenosis for 50% (A), 70% (B), 80% (C) reduction in stenosis (diameter) under high flow condition.

A

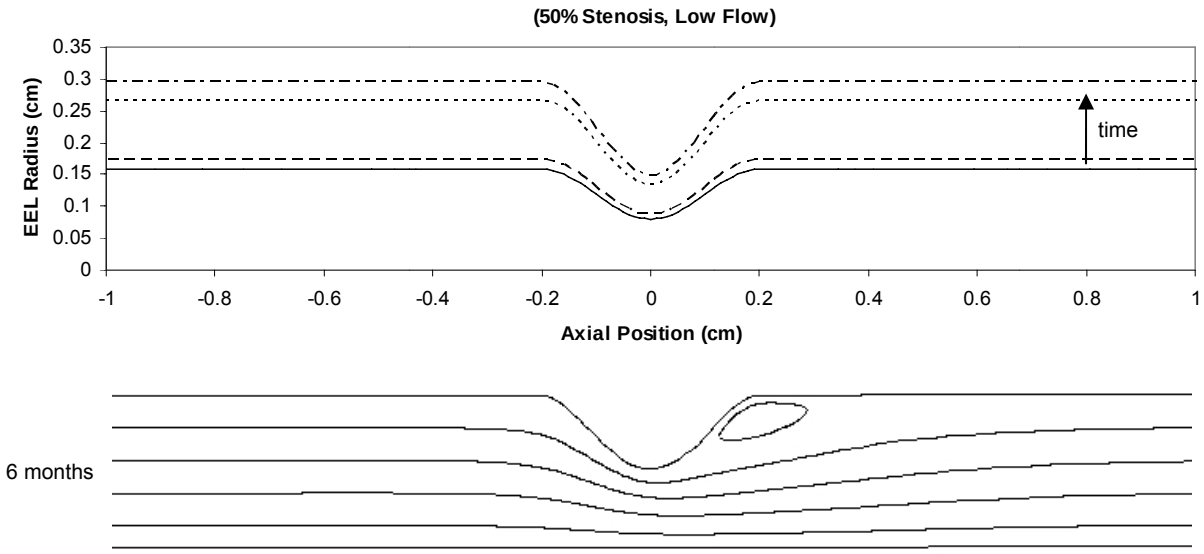

Re = 53

B

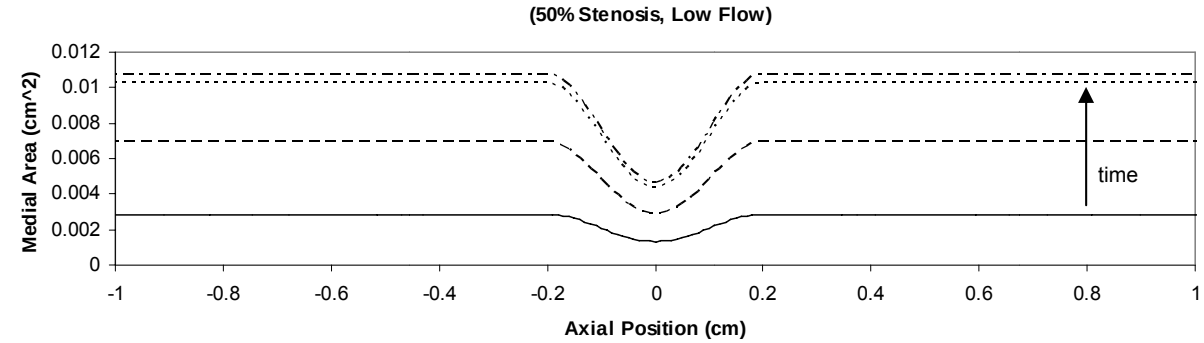

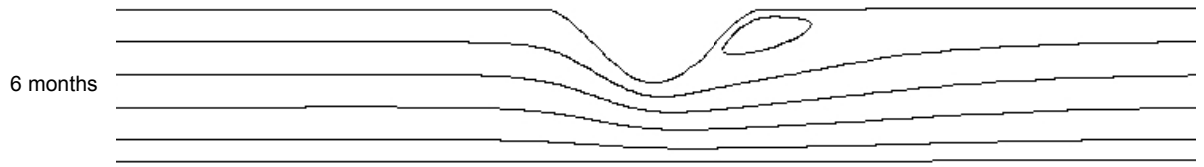

Re = 53

Figure 4-11. Simulation results for EEL radius (A) and medial area (B) for 50% stenosis under low flow condition.

Simulation of Human Vein Graft

The present mathematical model was applied to the simulation of human vein graft remodeling, encompassing the geometric complexities which are inherent in these conduits. Figure 4-12A illustrates a 14 cm segment of human saphenous vein whose structure was extracted from a computer tomographic (CT) image obtain several days after implantation. An approach similar to that described above for the idealized stenosis was used to simulate the human vein graft wall remodeling. Assuming a blood flow rate of 100 cm/sec and an intraluminal pressure of 1.3×10^4 Pa, the resulting wall shear and tension served as the input parameters for Equations (4-2), (4-4) and (4-5) to determine the interval change in intimal area, medial area, and EEL radius. Alternately calculating the local hemodynamics and graft geometry at 1 day intervals yielded a temporal understanding of vein graft remodeling through the initial 6 months following implantation.

Figure 4-12B shows the intimal area, medial area, and EEL radius along the graft at 1 week, 1 month, 3 months, and 6 months. The remodeling patterns observed in the human vein graft approximate those observed in the idealized stenosis, with intimal thickening that was minimal within the throat of the stenosis and reached a plateau at about 1 month. Medial thickening is also minimal within the stenosis, with a growth rate that decreases with time.

Discussion

There have been experimental evidences that relate each individual hemodynamic factor to the remodeling of each wall layer of the vein graft, and a set of mathematical equations which define these relationships has been developed in this chapter. Novel in the present approach is the development of a comprehensive

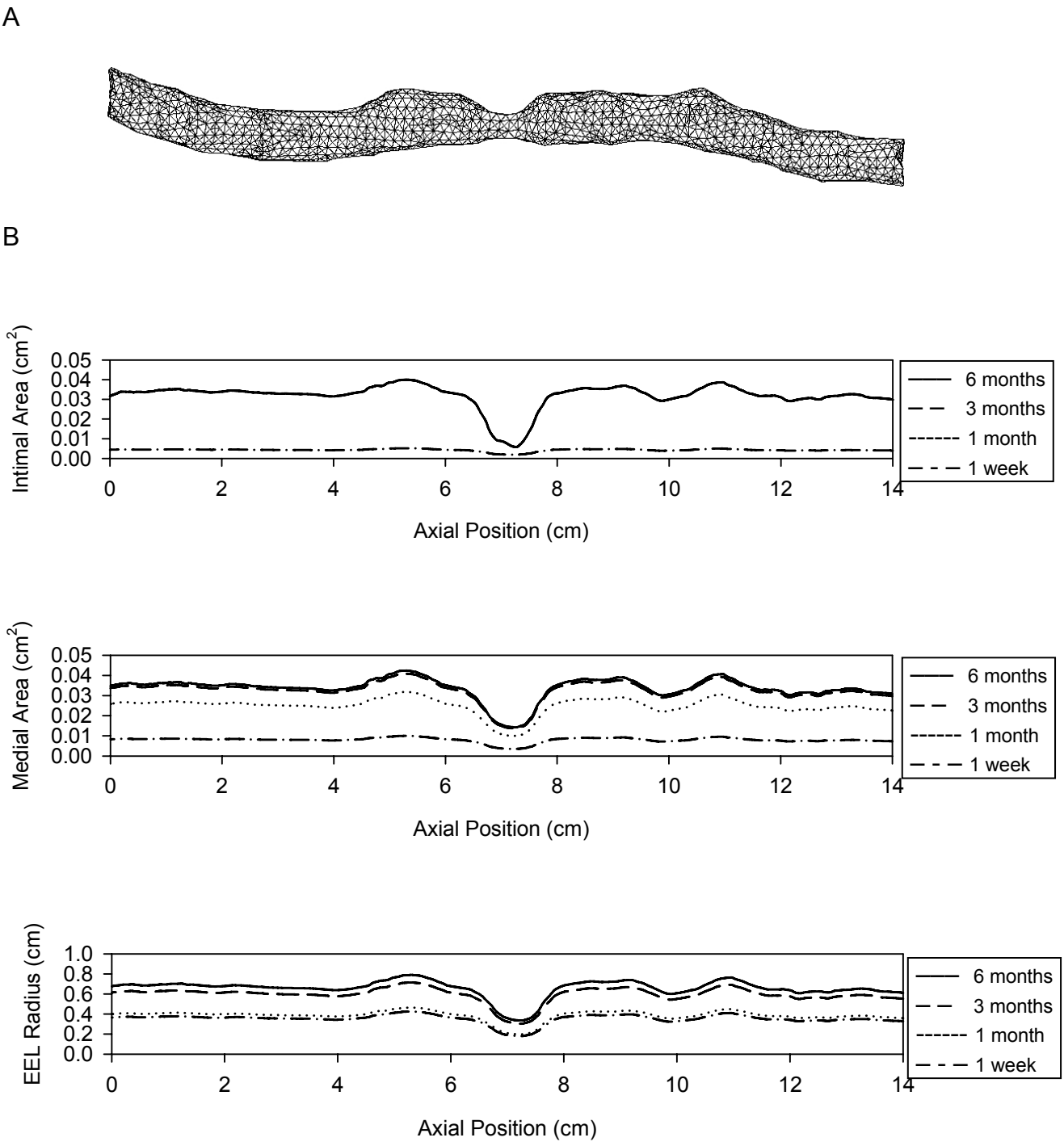

Figure 4-12. Simulation results for human vein graft. A. Vein graft geometry and mesh at implantation. B. Simulation results at different time points.

mathematical model that includes three layers for vein graft remodeling, in contrast to the less physiological single layer models previously described in the literature (Budu-

Grajdeanu et al., 2008; Friedman et al., 1986; Tran-Son-Tay et al., 2008; Zohdi, 2005). Also unique to the current formulation is the use of a logistic model as the base expression. As a simple equation that describes the S-shaped behavior observed in the experimental data (Figures 4-2, 4-3, and 4-5), this approach has been used by many researchers for modeling cell population growth (Britton, 2003; Fujikawa et al., 2004; Goudar et al., 2005), but is novel in its application to soft tissue remodeling.

In the formulation of the model, changes in intimal and medial cross-sectional area are related to wall shear stress and wall tension, respectively, and EEL radius change is a function of time only. There have been reports that vein graft dilation is dependent on shear stress. Fillinger et al. (1994) and Owens et al. (2006) observed a positive correlation between initial shear stress and percent change in lumen diameter in human vein grafts data. However, the observed shear dependence of lumen size does not depend only on graft dilation but also on wall thickening. Therefore, EEL radius is chosen as a measure of graft dilation to separate the effect of wall thickening. Moreover, Galt et al. (1993), in their rabbit vein graft experiments, observed no significant change in lumen radius of vein grafts exposed to normal and low flow for 4 weeks. In contrast, intimal-medial thickening was significantly more pronounced in the low flow case, suggesting a more prominent increase in EEL radius in those grafts exposed to low flow conditions. In the present experimental data, any significant dependence of EEL radius on the shear stress was not observed.

Wall tension has been recognized as one of the hemodynamic factors that has a notable impact on the thickening of the vein graft wall (Schwartz et al., 1992; Zwolak et al., 1987). In the present model, wall tension affects the medial layer, and the intima is

regulated by shear stress. The experimental data (Figure 4-2) show a significant difference in the initial intimal area change rates (up to 14 days) between low and high flow vein grafts, even though the experiments were started under comparable wall tension for both flow groups. The effect of the wall tension on the intima is minimal because the intimal area did not increase much in the high flow vein grafts throughout the 6 month period. The intima model describes an inverse relationship between shear stress and intimal growth rate, which has been observed by many researchers (Jiang el al., 2004; Meyerson et al., 2001; Schwartz et al., 1992). Another characteristic of the intima model is that it can predict the regression of the intima. Morinaga et al. (1987) reported that the thickened intima in a vein graft exposed to low flow regressed when the vein graft is exposed to higher flow rate in their canine vein graft experiment. In Equation (4-2), the rate becomes negative when the shear stress is increased such that the $b_i^{'}$ is less than A_I^*.

It is understood that hemodynamic forces are not the only factors that regulate vein graft remodeling. Incorporation of the biologic environment of the arterial system is needed in order to provide a more realistic description of the vein graft behavior. The current model describes vein graft adaptation in the earlier time frame after surgery. Eventually, some vein grafts will become stable after the adaptation and some unstable leading to vein graft failure. The reason why some vein grafts are stable and some are unstable is currently unknown. In addition, the mechanism of vein graft failure seems to be different from that of early adaptation. The ultimate goal of this modeling effort is to develop a model that can predict unstable remodeling leading to vein graft failure, so that the model can be used as a predictor of vein graft failure.

CHAPTER 5
RULE-BASED MODEL OF VEIN GRAFT REMODELING

In the previous chapters, mathematical models which show the relationship between hemodynamic forces and vein graft wall remodeling have been developed. While mathematical models are relatively simple and show the relationship among the variables explicitly, biological mechanisms are often implicitly included in the model. The mathematical models in the previous chapters deal with geometrical variables of vein graft remodeling while biological mechanisms are behind the geometrical change. On the other hand, rule-based modeling approach (Hwang et al., 2009) utilizes the biologic knowledge accumulated in the literature over the past decades, converts them to rules, and applies the rules to computational domain to simulate biological phenomena. In the computational domain, the elements can be molecules, cells, organs, or even a group of people.

As described in chapter 2, cell level mechanism of vein graft intimal hyperplasia is mostly smooth muscle cell (SMC) proliferation and extracellular matrix (ECM) deposition. About 60% to 80% of the volume of intimal hyperplasia is occupied by ECM, and SMC takes up about 20% to 40% of the volume (Kohler et al., 1991; Kraiss et al., 1991; Zwolak et al., 1987; Lemson et al., 2000). SMC apoptosis and ECM degradation are also involved in the change of the intimal layer (Berceli et al., 2002). The SMC and ECM are reorganized when exposed to arterial flow, and the reorganization is responsible for the change of graft diameter (Berceli et al., 2009).

The response of vein graft to hemodynamic forces can be thought of as the sum of the responses of SMCs to the hemodynamic forces. SMC has been found to respond to hemodynamic forces (Sumpo et al., 1988a; 1988b). Tissue/organ level vein graft wall

remodeling results from the cell level activities of SMC and ECM, and thus, the rule-based simulation approach is suited for this type of simulation (Boyle et al., 2010). In this chapter, rule-based simulation of hemodynamically induced vein graft remodeling is presented. SMC and ECM are two components which occupy the grid elements of rectangular grid system. At each time step, the probabilities of behaviors are applied to SMC and ECM elements to determine the next states of the elements. Those probabilities were obtained based on experimental data. The simulation is first run on 1-dimensional (1-D) domain to test the feasibility of the model. 2-dimensional (2-D) algorithm is then developed and validated against experimental data. The 2-D model is applied to focal stenosis simulation and compared with experimental data.

Determination of Probabilities of Cellular Activities

Probability of Smooth Muscle Cell Division

Cell division probability was determined based on BrdU (Bromodeoxyuridine) experimental data obtained from the vascular biology laboratory (Dr. Scott A. Berceli). BrdU is a synthetic nucleoside which can substitute thymidine when DNA is duplicated. In the BrdU experiment, BrdU was injected into vein graft 1 day prior to harvest. It is assumed in this study that BrdU is available for the first 2 hours considering that the half-life of BrdU is on the order of hours (Phuphanich and Levin, 1985).

Figure 5-1 shows a diagram of BrdU injection and cells getting stained. At harvest, the % of BrdU positive cells is determined with respect to the total number of cells at harvest. However, during the 1 day from the BrdU injection to vein graft harvest, the total number of cells changes because some cells divide during the 1 day. Under the assumption that the BrdU is available during the first 2 hours after the BrdU injection, the % of BrdU positive cells with respect to the total number of cells at the time

of BrdU injection would be a more accurate representation of the % of cells dividing. Another thing to note is that BrdU is incorporated into DNA during S-phase of cell cycle. It is assumed that the cell cycle time is 24 hours, and G1, S, and G2/M phases each takes up one-third of the cell cycle time (Yamamoto et al., 2000). All the factors discussed above put together and based on Figure 5-1, the space averaged probability of cell division during 1 hour period can be written as follows.

$$\bar{P}_{division}(\tau^*, t) = \frac{1.2BU}{100-1.2BU} \cdot \frac{1}{T_B} \quad (5\text{-}1)$$

where BU is the % of BrdU positive cells, and $\bar{P}$ is space averaged probability of cell division at 1 day prior to the day when BU is measured, and T_B is the time duration (hours) between BrdU injection and tissue harvest, which is 24 hours in the experiment.

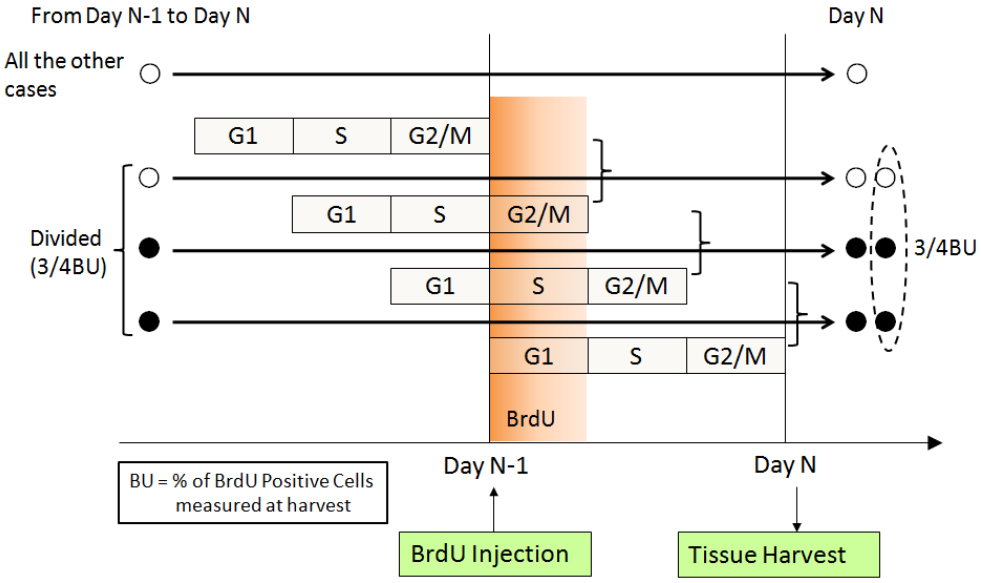

Figure 5-1. Schematic of cells undergoing cell cycles during 1 day prior to harvest.

Figure 5-2 shows % of BrdU positive cells measured at harvest. Shear stress is normalized with respect to the pre-ligation shear stress which was measured to be 10 dynes/cm^2. The following function is fitted to the experimental data.

$$BU = \frac{A}{e^{Bt+\tau^*}} \quad (5\text{-}2)$$

where t is time (day), τ* is normalized shear stress, and the coefficients A and B are found to be 44, 0.16. Figure 5-2 shows the model curve with the experimental data.

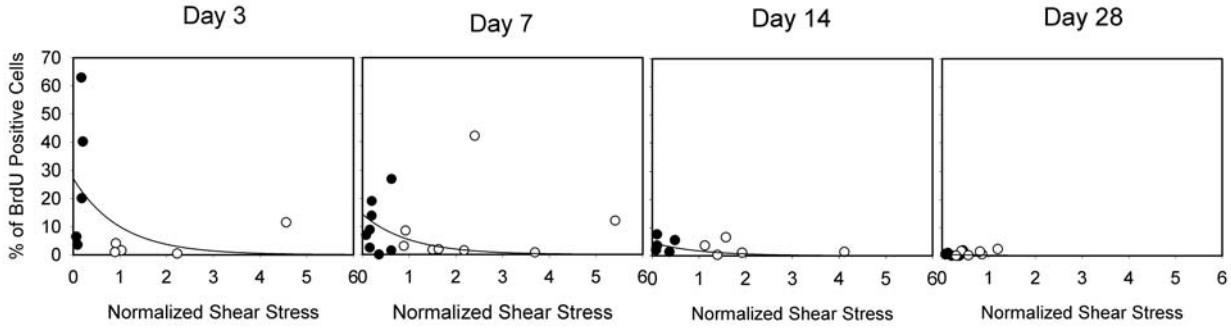

Figure 5-2. % BrdU positive cells as a function of normalized shear stress at different time points. Experimental data are from the vascular biology laboratory (Dr. Scott A. Berceli).

Figure 5-3 shows % of BrdU positive cells as a function of distance from endothelium. The data are shown for two different flow conditions. Assuming that the probability of cell division is proportional to the concentration of the molecules released from endothelium and that the concentration of the molecules decreases exponentially, the following form is fitted to the data in Figure 5-3.

$$\text{(Spatial distribution of cell proliferation)} = De^{-Ex} \quad (5\text{-}3)$$

where x is distance from endothelium.

When the Equation (5-3) is fitted to each of the six different data sets (Figure 5-3) for different flow conditions, coefficient E was found to be 27.3±9.4 (mean±SD) mm^{-1}.

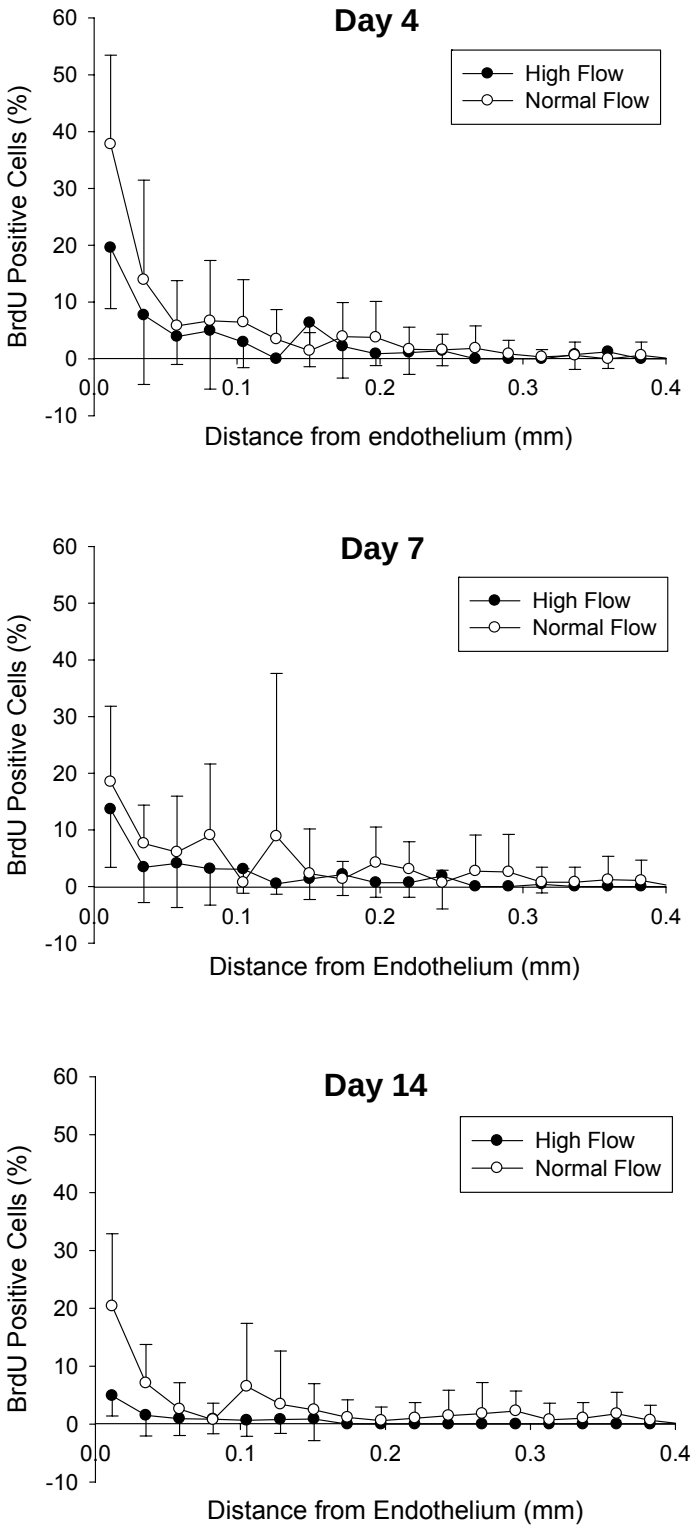

Figure 5-3. % BrdU positive cells as a function of actual distance from endothelium (From Berceli et al. (2002)).

Then, the final form of cell division probability can be written as follows.

$$P_{division}(\tau^*, t, x) = \frac{1.2BU}{100-1.2BU} \cdot \frac{D^* e^{-27.3x}}{T_B} \quad (5\text{-}4)$$

where τ* is normalized shear stress, t is time, x is distance from endothelium, and D* is a constant. The constant D* in Equation (5-4) is determined at each time step such that the integration of Equation (5-4) over the intimal thickness equals the space averaged probability multiplied by intimal thickness.

$$D^* = \frac{IT}{\int_0^{IT} e^{-27.3x} dx} = \frac{27.3IT}{(1-e^{-27.3IT})} \quad (5\text{-}5)$$

where IT is intimal thickness (mm).

Probability of Smooth Muscle Cell Apoptosis

Probability of cell apoptosis is obtained based on TUNEL (Terminal deoxynucleotidyl transferase dUTP Nick End Labeling) experimental data obtained from the vascular biology laboratory (Dr. Scott A. Berceli). It is assumed that dead cells remain in the tissue for 24 hours before getting removed. Then, TUNEL stained cells at harvest died between 1 day prior to harvest and the day of harvest. Using the same correction used in the cell division probability for the total number of cells, the space averaged probability of cell apoptosis for 1 hour can be written as follows.

$$\bar{P}_{apoptosis}(\tau^*, t) = \frac{TL}{100-1.2BU} \cdot \frac{1}{T_D} \quad (5\text{-}6)$$

where TL is the % of TUNEL positive cells, and $\bar{P}$ is space averaged probability of apoptosis at 1 day prior to the day when TL is measured, and T_D is time duration (hours) dead cells remain in the tissue before getting removed. T_D is assumed in this study to be 24 hours.

Figure 5-4 shows the % of TUNEL positive cells in the same experiment where the BrdU data were obtained. In the Figure 5-4, the low and high flow data are graphed together because the data show no dependence on shear stress.

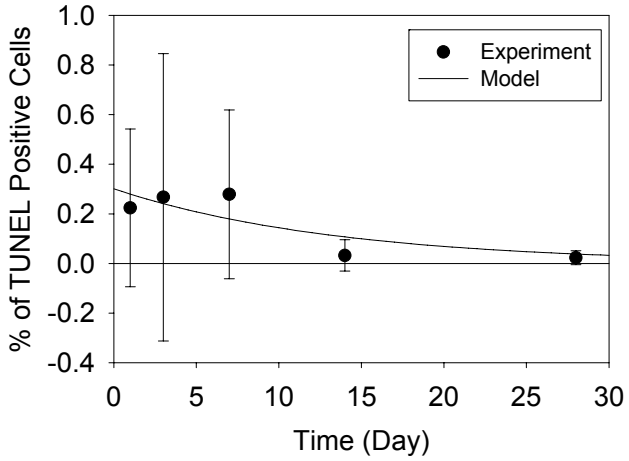

Figure 5-4. % of TUNEL positive cells as a function of time. Experimental data are from the vascular biology laboratory (Dr. Scott A. Berceli).

The following exponential form is fitted to the data in Figure 5-4.

$$TL=Fe^{-Gt} \quad (5\text{-}7)$$

where the coefficients F and G are found to be 0.301 and 0.0739. Figure 5-4 shows the model curve with the experimental data.

Figure 5-5 shows the % of TUNEL positive cells as a function of distance from internal elastic lamina (IEL).

To determine the spatial distribution of apoptosis, the same procedure used for cell proliferation is used for apoptosis as well, and the following exponential form is fitted to the data (Figure 5-5).

$$\text{(Spatial distribution of cell apoptosis)} = He^{-I\hat{x}} \quad (5\text{-}8)$$

where $\hat{x}$ is distance from IEL.

When the Equation (5-8) is fitted to each of the six different data sets (Figure 5-5) according to different flow and time conditions, the coefficient I was found to be 6.7±1.9 (mean±SD) mm^{-1}.

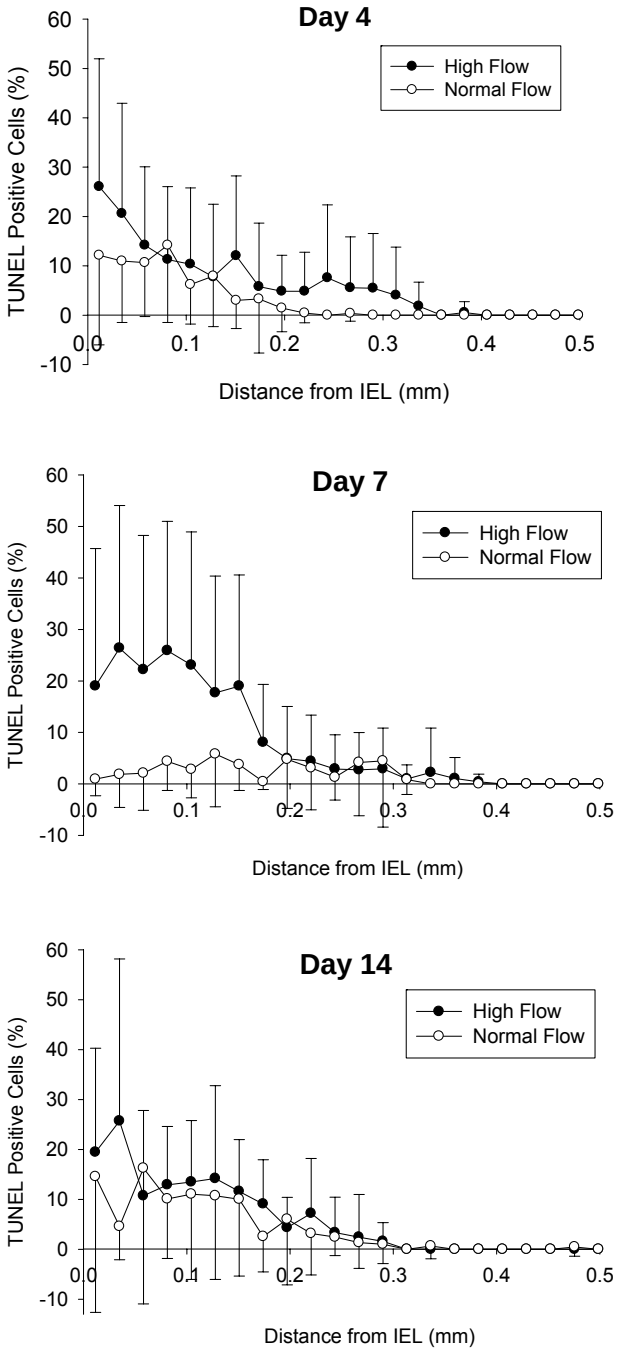

Figure 5-5. % of TUNEL positive cells as a function of actual distance from IEL (From Berceli et al. (2002)).

Then, the final form of cell apoptosis probability can be written as follows.

$$P_{apoptosis}(\tau^*, t, \hat{x}) = \frac{TL}{100-3/4BU} \cdot \frac{H^* e^{-6.7\hat{x}}}{T_D} \quad (5\text{-}9)$$

where τ* is normalized shear stress, t is time, $\hat{x}$ is distance from IEL, and H* is a constant.

The constant H* in Equation (5-9) is determined at each time step such that the integration of Equation (5-9) over the intimal thickness equals the space averaged probability multiplied by intimal thickness.

$$H^* = \frac{IT}{\int_0^{IT} e^{-6.7\hat{x}} d\hat{x}} = \frac{6.7IT}{(1-e^{-6.7IT})} \quad (5\text{-}10)$$

where IT is intimal thickness (mm).

Probability of Extracellular Matrix Behaviors

It has been reported that the volume % of SMC in vein graft intima ranges from about 20% to 40% regardless of intimal thickness (Kohler et al., 1991; Kraiss et al., 1991; Zwolak et al., 1987). In this study, total of 4 ECM elements are produced from each SMC division. Each of the two daughter cells produce one matrix element after 24 hours from the cell division, and one more matrix element after another 24 hours. Sometimes, there is the case where one or both of the daughter cells undergo cell division before producing total of 4 matrix elements. From the one-dimensional simulation which will be described later in this chapter, the volume % of SMC at Day 28 resulted in 27%. Since SMC division probability is higher near the lumen compared to the one away from the lumen, there is higher chance of SMC undergoing cell division before producing total of 4 matrix elements, which would result in higher volume % of

SMC near the lumen. When a cell undergoes apoptosis, 4 matrix elements nearest to the cell are removed from the computational domain.

Table 5-1 summarizes the assumptions used in this study.

Table 5-1. Assumptions used in the model.

Category	Assumptions
BrdU	BrdU is available for the first 2 hours.
Cell Cycle	Cell cycle time is 24 hours. G1, S, and G2/M phases each takes up one-third of the cell cycle time.
Cell Size	Cell size is 7μm×7μm. Initial volume ratio of cell to matrix is set to be 1:3.
Dead Cells	Dead cells remain in the tissue for 24 hours before getting removed.
Matrix Production	Each of the two new daughter cell elements produces two matrix elements with 24 hours time interval.

Effects of Monocytes

Monocyte Entry Model

Based on the data in Jiang et al. (2009b), the same model form used in the BrdU model (Equation (5-2)) is adopted for the model of the net rate of monocyte entry into vein graft wall.

$$\text{(Net rate of monocyte entry)} = \frac{A}{e^{Bt+\tau^*}} \qquad (5\text{-}11)$$

where t is time, τ* is normalized shear stress, and A and B are constants. B is set to be the same value (0.16) used in the BrdU model. When A is set to be 175/(mm^2·hour), the volume occupation of monocyte in the intima is simulated to be about 5%, which is consistent with the values found in the literature (Lemson et al., 2000). Each monocyte that has entered the computational domain is placed at a random position.

Monocyte Effects on ECM Synthesis

Hoch et al. (1999) showed that macrophage depletion suppresses intimal hyperplasia in vein graft. However, they observed that there was no significant change in the total number of cells, implying decreased synthesis of extracellular matrix. As a first approximation, the effects of macrophages can be incorporated into the model via the amount of matrix created as follows.

$$N_m = [2\bar{M}] \qquad (5\text{-}12)$$

where N_m is the number of matrix elements generated by each of the 2 new daughter cells, $\bar{M}$ is normalized monocyte entry rate, and [ ] denotes the rounding to the nearest integer. The normalization is with respect to the monocyte entry rate calculated from the model shown above. The two matrix elements from each of the two new daughter cells are produced with time interval of 24 hours.

Figure 5-6 shows the simulated intimal area as a function of the normalized monocyte entry rate at shear stress of 1.8 dynes/cm^2, where a positive correlation is observed.

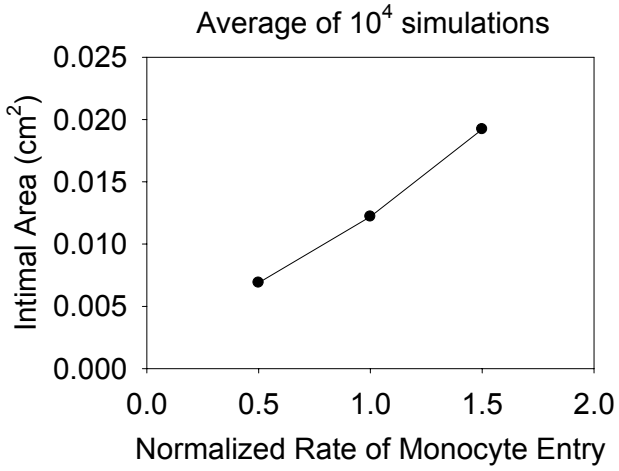

Figure 5-6. Simulated intimal area with normalized rate of monocyte entry.

Algorithm

1-Dimensional Algorithm

To test the feasibility of the model including the probabilities of cellular activities, the simulation was performed on 1-D domain, which is simpler than 2-D simulation. 1-D domain is a stack of elements in one line where each element is occupied by either SMC or ECM (Figure 5-7). The size of cell was chosen to be 7μm×7μm. When a cell is divided, the new cell is placed either on the right side or on the left side of the cell with equal probability. When a new cell is placed, the new cell pushes all the elements on the luminal side to make room for itself. The same procedure is performed when a new ECM element is produced by SMC element. When a cell dies, the empty space is filled by the elements on the luminal side by shifting themselves to fill the empty space. Figure 5-8 shows the flow chart of the general algorithm.

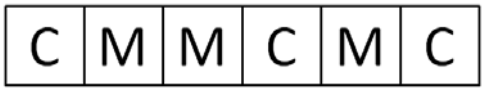

Figure 5-7. Schematic of 1-dimensional domain. (C: Cell element, M: Matrix element)

2-Dimensional Algorithm

In 2-D domain, when a new cell or matrix element is produced, it is placed at one of the 4 adjacent spaces pushing the existing element in the luminal direction (Figure 5-9A). The new cell or matrix does not push the adjacent elements in the direction normal to the luminal direction, because the increase of the length of vein graft in the longitudinal direction is not observed experimentally. Also, the new element does not push the adjacent element in the opposite direction to the luminal direction because

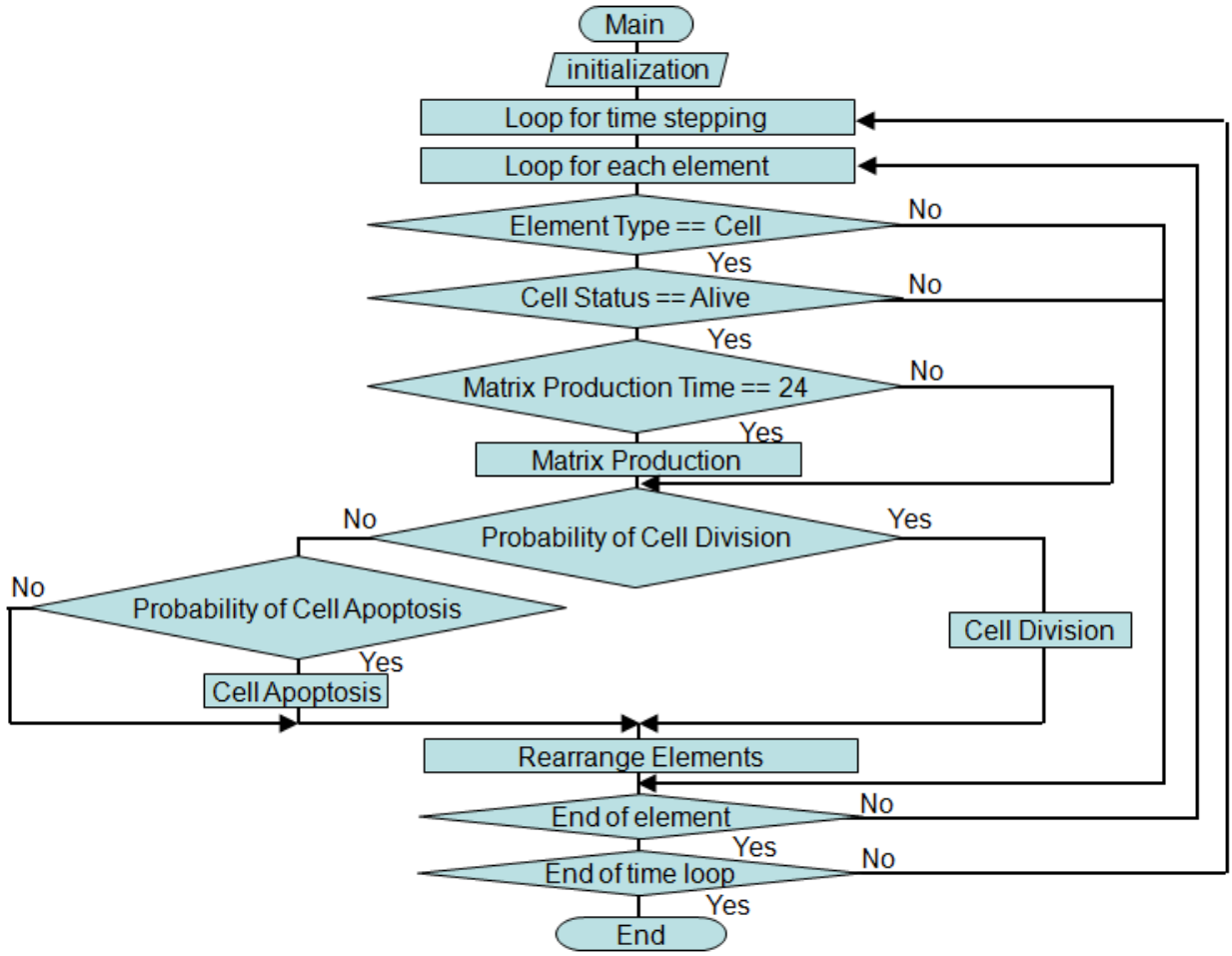

Figure 5-8. Flow chart for the rule-base simulation of vein graft remodeling.

the surrounding tissue is assumed to prevent such movement. Also not observed experimentally is excessive protrusion of the wall into the lumen. To prevent the excessive protrusion, a redistribution algorithm is applied as shown in Figure 5-9B. When there is more than 2 elements difference between adjacent columns, the last element in the longer column moves to the shorter column.

In computational domain for a more arbitrary geometry such as focal stenosis, the redistribution algorithm is a little different (Figure 5-10). For all the elements facing

lumen, the empty spaces around the element is examined, and if there is an empty space closer to the IEL, then the element is moved to the empty space.

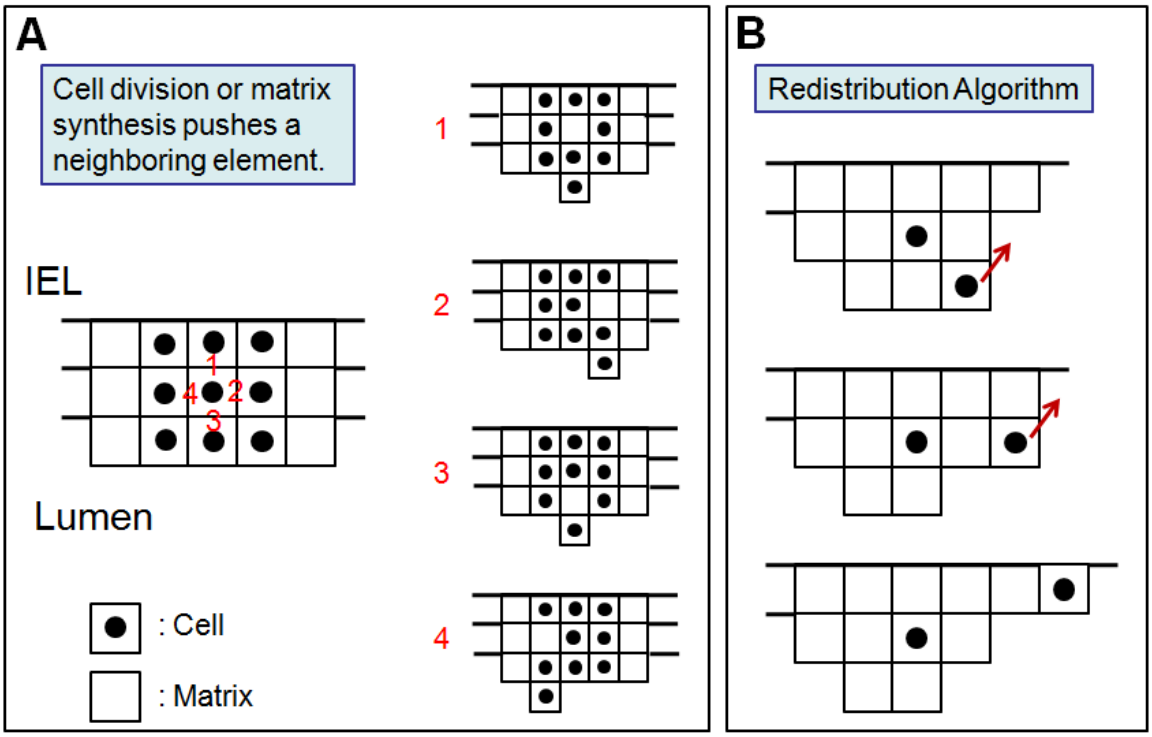

Figure 5-9. 2-D algorithm of rule-based simulation of vein graft remodeling. A. New element placement algorithm. B. Element redistribution algorithm.

Results

1-D Model Validation

Initial volume ratio of cell to matrix is set to be 1:3. This ratio determines the initial number of cells, which affects the simulation results. Figure 5-11A shows an example of the change of the number of elements with time in a single simulation, which shows the stochastic nature of the simulation. Figure 5-11B shows the location of the divided cells in a single simulation. Most of the cells divided near the lumen as expected from Equation (5-3).

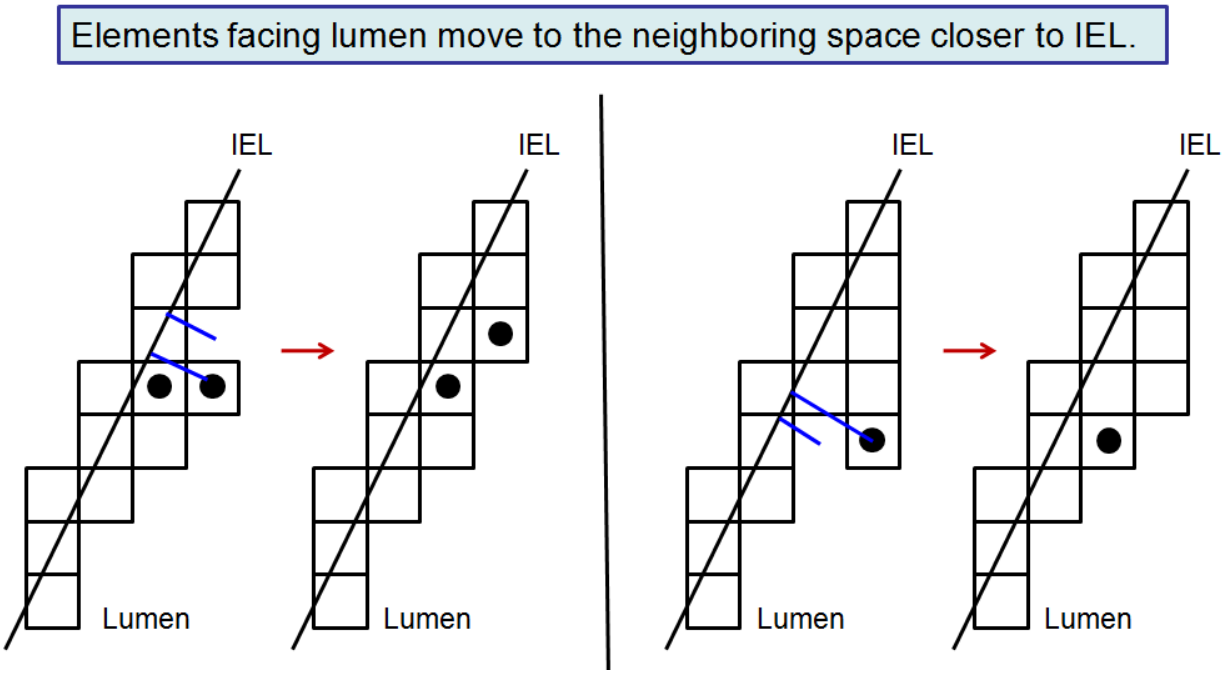

Figure 5-10. Element redistribution algorithm for stenosis simulation.

Figures 5-11C and 5-11D show the comparison between experimental data and simulation results for intimal area in radial cross-section for low (shear stress=1.8 dynes/cm2) and high (shear stress=14 dynes/cm2) flows, respectively. The intimal area in 2-D cross-section was calculated from the 1-D simulation by multiplying the 1-D intimal area by the initial number of cells in 2-D domain. The initial number of cells in 2-D domain was calculated by dividing the initial number of all the elements by 4 because 1 out of 4 elements is cell element. The simulation curves are the average of 10^4 runs, and agree well with experimental data though the simulation tends to underestimate the intimal area for low flow case. The standard deviation is 2.2 and 0.65 times the average value at Day 28 for low and high flows, respectively.

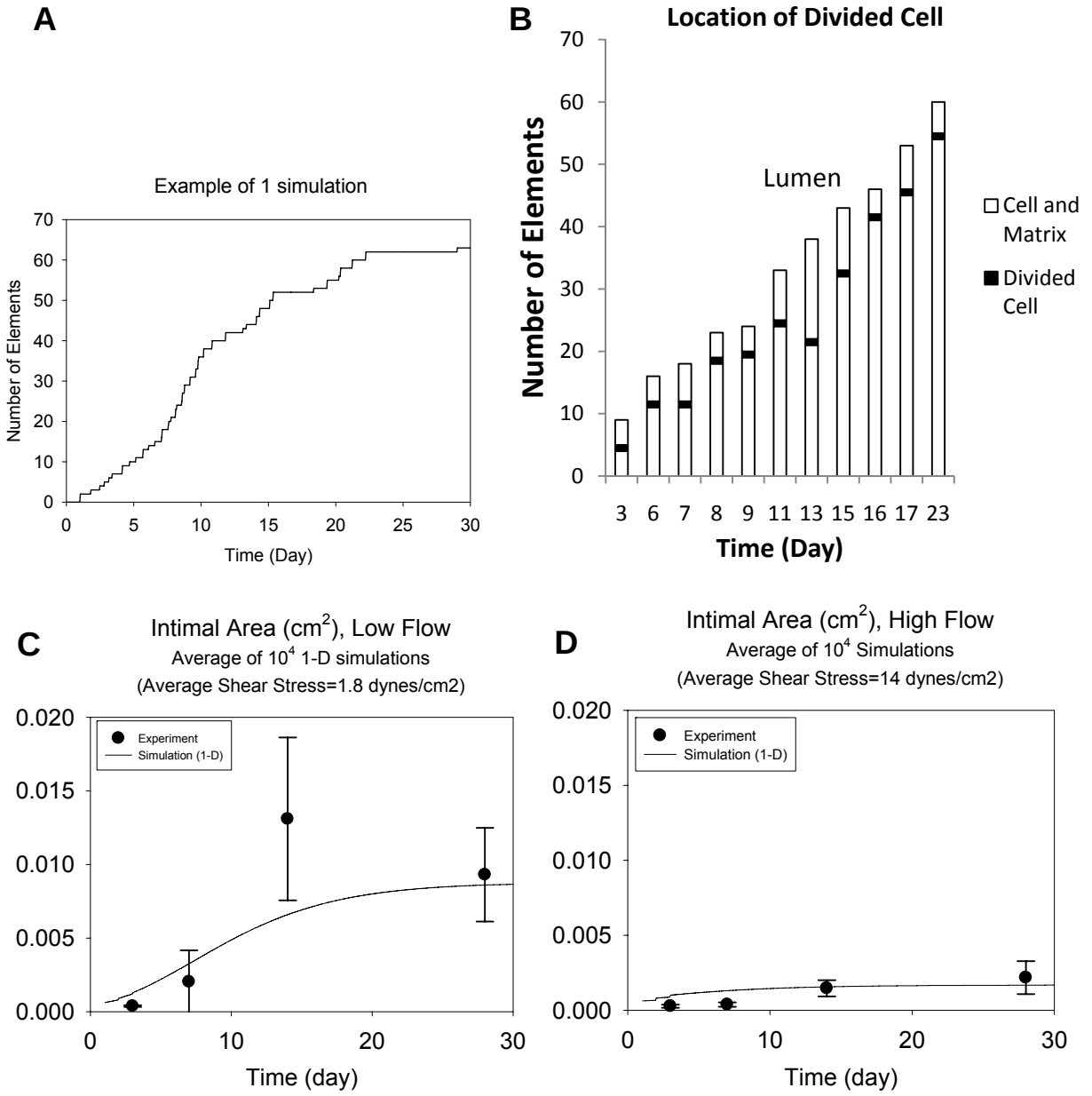

Figure 5-11. 1-D simulation results. A. Change of the number of elements with time. B. Location of cell division. C. Intimal area for low flow condition. D. Intimal area for high flow condition. Experimental data are from Jiang et al. (2004).

2-D Model Validation

Figure 5-12 shows an example of 2-D simulation. The simulation starts with one line of elements composed of SMC (25%) and ECM (75%) elements. The simulation is

run up to 28 days with time step of 1 hour. Most of the growth of the wall area occurs up to 2 weeks, and the wall area does not change much from 2 weeks to 4 weeks. More monocytes (grey cell) are located away from the lumen because monocyte migration is not taken into account in the simulation. According to Equation (5-11), more monocytes enter the wall at earlier time points. Due to the redistribution algorithm (Figure 5-9B), no two adjacent columns show the difference of the element number greater than 1.

Figure 5-13 shows 2-D simulation result of intimal area compared with experimental data. Among the simulation parameters, cell size and BrdU availability time are the ones that are uncertain and have significant impact on simulation results. As such, the two parameters were determined such that the simulated intimal area matches well with the experimental data.

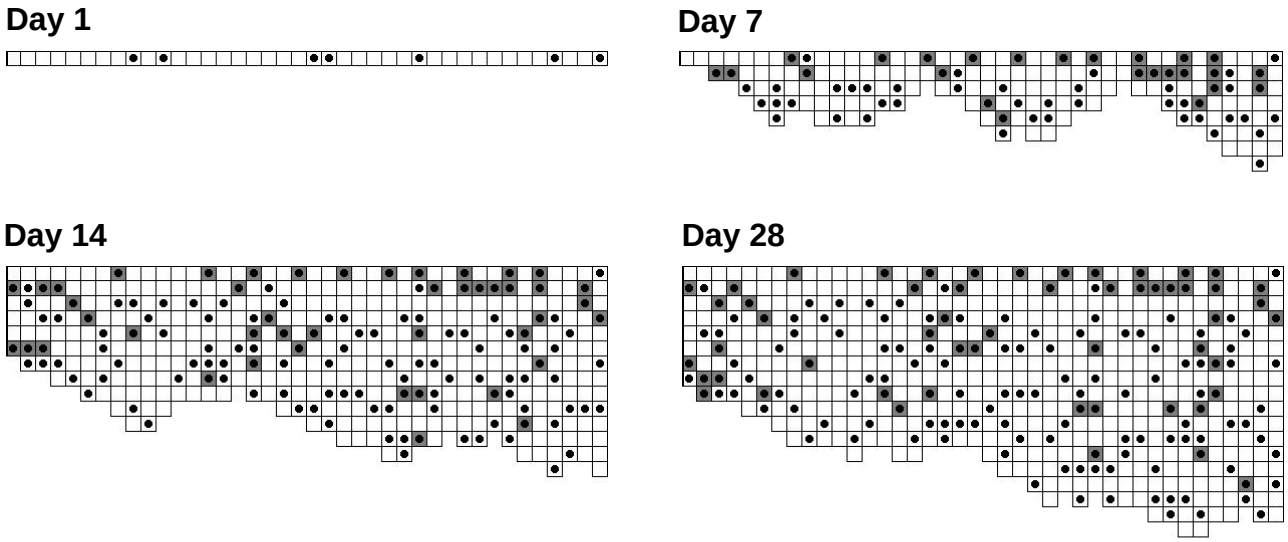

Figure 5-12. An example of 2-D simulation. Empty elements are ECM. The elements with a filled circle at the center are SMC. Grey elements are monocytes.

Figure 5-13 also compares intimal areas from 1-D and 2-D simulations. 1-D simulation predicts less wall area than 2-D simulation because the greater thickness in 1-D domain makes the cell proliferation concentrated near the lumen with higher probability which gives cells less time to produce matrix elements. The reason for the concentrated area of higher probability near the lumen for 1-D simulation is because the same coefficient E in Equation (5-3) is applied to both 1-D and 2-D simulation. Because the space averaged probability of cell division is the same for both 1-D and 2-D simulation, the probability at the surface of the lumen should be higher in 1-D case (thicker intima) to maintain the same coefficient E in Equation (5-3). The 2-D simulation curve in the low flow case is S-shaped because of the initial burst and later decrease of cell division.

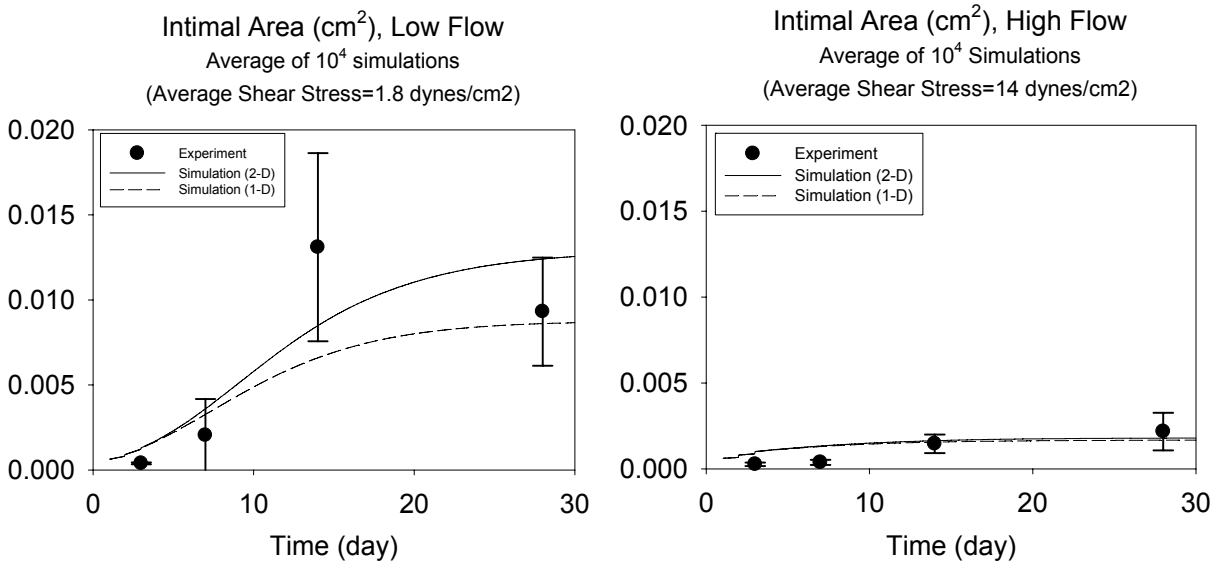

Figure 5-13. Simulation results and experimental data of intimal area and comparison of 1-D and 2-D simulations for low and high flow conditions. Experimental data are from Jiang et al. (2004).

Focal Stenosis Simulation

Figure 5-14 shows an example of focal stenosis simulation. The initial curve was reconstructed from experimental data (Figure 5-15) using smoothing spline algorithm as described in chapter 3. The initial curve is placed on a rectangular grid, and the elements through which the curve passes are assigned either cell (25%) of matrix (75%). Shear stress was calculated based on Poiseuille flow assumption. Greater intimal thickening is observed distal to the stenosis where shear stress is relatively low. In the figure, black elements are cells, and grey elements are matrix.

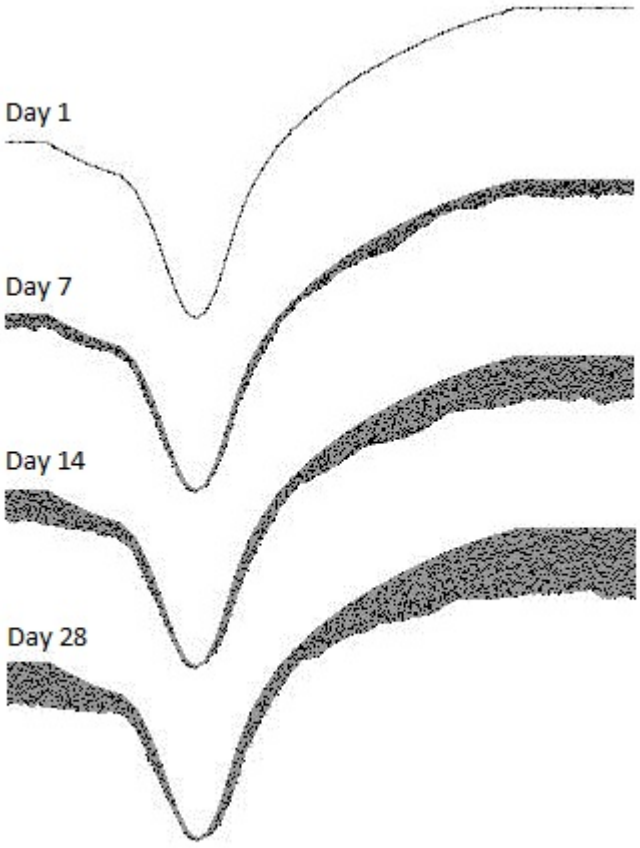

Figure 5-14. An example of focal stenosis simulation. Black dots are cells, and grey area is extracellular matrix.

Figure 5-15 shows the comparison between the simulation and experimental data. The simulation result over-predicts the intimal thickening distal to the stenosis at Day 28, which is consistent with the over-prediction observed in the 2-D validation at Day 28 (Figure 5-13). This suggests that the experimental data at Day 14 may contain significant amount of error.

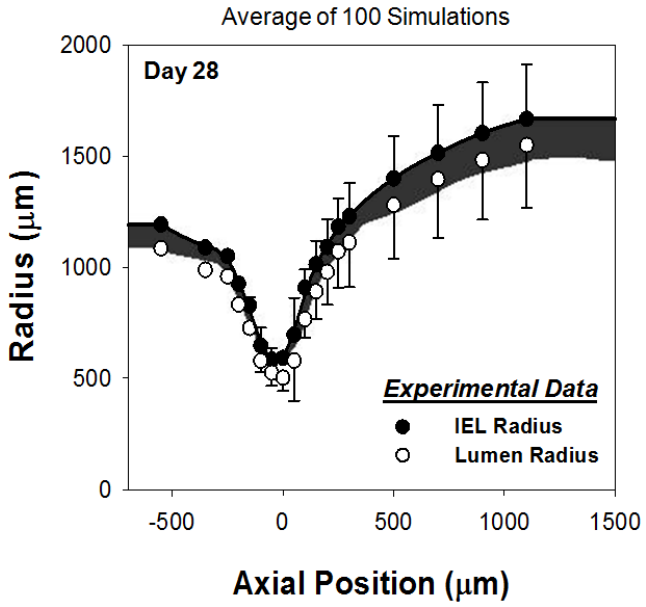

Figure 5-15. Comparison between simulation result and experimental data for intimal thickening around focal stenosis. Experimental data are from the vascular biology laboratory (Dr. Scott A. Berceli).

Discussion

Rule-based modeling method is appropriate for simulation of biological systems because biological systems are intrinsically multi-scale systems in which different scale components such as molecules, cells, tissue, and organs comprise the system. The behaviors of greater scale component result from the interactions among the smaller

scale components, and the rule-based method enables the observation of the greater behavior emerging from the interactions among the small scale components in the system. Vein graft wall consists of mostly smooth muscle cells and extracellular matrix, and the wall thickening is the result of the cell proliferation and matrix deposition, and the interactions among them. In this chapter, the wall thickening has been simulated by applying rules of behaviors to cell and matrix elements.

The rules were determined from the experimental data when they are available, and those rules that were not available experimentally were obtained either from the literature or by assuming appropriate values. Experimental data often contains uncertainties and needs to be analyzed more to be used as quantitative values for simulation. In this study, BrdU experimental data needed to be analyzed more to extract cell division probability from the data. The most uncertain thing about BrdU data is how many hours BrdU is available after it is injected into the body. Phuphanich and Levin (1985) found that the half-life of BrdU is on the order of hours, but it depended on whether it was administered intravenously or orally. In this study, the BrdU availability time together with other parameters were determined by fitting the simulation results to experimental data of wall area (global behavior). The BrdU availability time determined in this manner is 2 hours which is consistent with the observation by Phuphanich and Levin (1985). The other parameters determined together with the BrdU availability time were cell size and initial volume ratio of cell to matrix. The initial volume ratio of cell to matrix determines the initial number of cells which significantly affects the number of cells at later time points. The initial ratio of 1(cell):3(matrix) was tested based on the observation in the literature that the cells occupy 20% to 40% of wall volume (Kohler et

al., 1991; Kraiss et al., 1991; Zwolak et al., 1987) regardless of wall thickness, and this ratio together with cell size of 7μm×7μm resulted in simulation results that match experimental data very well (Figure 5-13).

When the rule-based approach was applied to the simulation of wall thickening around focal stenosis, it predicted thicker wall at the regions where wall shear stress is lower. Though this is consistent with experimental observation, Figure 5-15 shows that the model over-predicts the wall thickness compared to experimental data where wall shear stress is lower. This over-prediction is consistent with that observed in Figure 5-13 where the intimal area is over-predicted at Day 28 for low flow condition. As shown in the Figure 5-13, the experimental data at Day 14 shows a peak compared with the other data points, but there seems to be no physiological reason that the intimal area should decrease from Day 14 to Day 28. Nevertheless, the model parameters were determined such that the model prediction fits the experimental data including the data point at Day 14. As a result, the model over-predicts the experimental data at Day 28, and this is also shown in the focal stenosis simulation as shown in Figure 5-15. Considering that the two graphs (Figure 5-13 and Figure 5-15) show the same tendency to over-prediction at Day 28, it is very likely that the experimental data at Day 14 contains significant amount of variation.

CHAPTER 6
CONCLUSION

Vein graft remodeling is a complex process involving a large number of biological and hemodynamic factors. These factors act together affecting the outcomes of the other factors. The cells in the vascular system respond to hemodynamic forces, and collectively generate global phenomena such as wall thickening. Endothelial cells are in direct contact with blood flow, thus respond to wall shear stress imposed by blood flow, and release signaling molecules which modulate wall remodeling. On the other hand, wall tension acts on the whole wall, and thus smooth muscle cells, which are the primary cell type in the vascular system, respond to wall tension. In this dissertation, the effects of hemodynamic forces on vein graft remodeling have been examined through mathematical and computational modeling approach.

Vein graft experiences higher flow and pressure environment when implanted in the arterial system compared with the hemodynamic environment of the venous system. Vein graft adapts to the arterial hemodynamic environment by thickening its wall and expanding its diameter. Thickening wall reduces wall tension, and increasing diameter reduces wall shear stress. The size of the lumen is determined by these two remodeling processes. After this adaptation, some vein grafts proceed to become pathologically occlusive just like the blocked artery that the vein graft bypasses. The occlusion occurs at focal regions while the neighboring regions remain patent. The mechanism of occlusive adaptation seems to be different from that of early adaptation, and the focus of this dissertation has been modeling the early stage of the adaptation.

In the early stage of the vein graft adaptation, the most notable change occurs in the layer of intima. The thickness of the intimal layer become comparable to that of

medial layer in the time frame of weeks, while the intima in normal vein is just a single cell layer. The intima is composed of mostly SMC and ECM. SMC comes from medial layer and proliferate in the intimal layer, and ECM is produced by SMC. A mathematical model of this intimal layer remodeling has been developed in chapter 3. Experimental data show shear stress imposed by blood flow has significant impact on the intimal thickening, and the intimal thickening rate is dependent on time. Thus, the mathematical model is a function of wall shear stress and time. The mathematical form has been determined based the behavior of the experimental data. As simple model form as possible has been selected, while the experimental data has relatively large variations from individual animal to animal. When the model was applied to a focal stenosis simulation, the simulation results agreed well with the focal stenosis experimental data. Certainly, shear stress is not the only factor influencing the intimal layer, and all the other factors can be considered to be included in the time term. However, the model successfully describes the change of intimal layer, where most notable change occurs in the vein graft remodeling, using only two variables: shear stress and time.

Even though the intimal layer shows the most notable change, medial layer also thickens, and the diameter of EEL layer changes as well. The size of lumen can be considered to be determined by the geometrical relation among these three layers. Mathematical models of these three layers have been developed in chapter 4. The mathematical form is based on logistic model, and the experimental data at 3 months and 6 months were added to the one used in chapter 3. Wall tension has been added as a hemodynamic factor since experimental data showed that it is related to medial layer remodeling. Experimental data show that the diameter change of EEL layer is not

very related to shear stress. This is somewhat surprising because it has been believed that vein grafts dilate to reduce wall shear stress. However, at higher shear stress, the intimal layer thickening is reduced, which makes the size of the lumen greater. Experimental data of vein graft remodeling show S-shaped behavior which is typically observed in cell population growth, and the logistic model which is one of the simplest form that describes S-shaped behavior successfully modeled the behaviors of each layer of vein graft. When the model was coupled with a flow solver, and applied to the simulation of idealized stenosis and human vein graft, it predicted the remodeling of each layer of vein graft around stenosis region depending on the severity of the stenosis at different flow conditions.

Even though mathematical model of vein graft remodeling explicitly shows the relationship between the hemodynamic factors and the geometrical variables of each layer of vein graft, biologic mechanism behind the vein graft morphology change is not included in the model equation. To overcome this limitation, rule-based modeling approach has been applied to the simulation of vein graft remodeling in chapter 5. The components in the model are cells and matrix elements, and rule of behaviors were applied to the elements. The rules were selected based on experimental data. The model parameters were determined based on the evidences in the literature, but those that were hard to find in the literature were determined by comparing the simulation results with experimental data. Simulation results show intimal thickening (global behavior) around a focal stenosis, which resulted from the local interactions among the cell and matrix elements. The simulation results also show advanced intimal thickening distal to the throat where wall shear stress is lower, which is expected from the model,

and agrees with experimental observations. However, quantitative comparison shows that the model over-predicts the intimal thickness at the low shear region, presumably due to the variations in the experimental data the model is based on. It is consistent with 2-D model validation where the simulation results were compared with another set of experimental data.

The models developed in this dissertation are focused on predictive capability rather than explanatory one, though explanatory model usually precedes the predictive one (Engelberg et al., 2011). Despite significant advances in the understanding of the mechanism of vein graft failure and surgical techniques, vein graft failure rate is still significantly high as described in chapter 1, and if it can be predicted whether a vein graft will be successful or not after the surgery, healthcare cost would be significantly reduced. The models in this dissertation are closely linked to experimental data which were obtained within 6 months period, and the predictive capability beyond 6 months was not confirmed in this study. To make both the mathematical and rule-based models be able to predict longer time period than 6 months without experimental data, more fundamental biologic mechanisms would have to be incorporated into the models, and, because the complete biologic mechanism of vein graft failure is currently unknown, the investigation of biologic mechanism together with theoretical modeling work would be needed for the development of a successful predictor of vein graft failure.

LIST OF REFERENCES

Alber, M.S., Kiskowski, M.A. Glazier, J.A., Jiang. Y., 2003. On cellular automaton approaches to modeling biological cells. In: Rosenthal, J., Gilliam, D.S. (Eds.), Mathematical Systems Theory in Biology, Communications, Computation, and Finance. Springer-Verlag, New York, 1-40.

Alford, P.W., Humphrey, J.D., Taber, L.A., 2008. Growth and remodeling in a thick-walled artery model: effects of spatial variations in wall constituents. Biomechanics and Modeling in Mechanobiology 7, 245-262

Alon, R., Kassner, P.D., Carr, M.W., Finger, E.B., Hemler, M.E., Springer, T.A., 1995. The integrin VLA-4 supports tethering and rolling in flow on VCAM-1. Journal of Cell Biology 128, 1243-1253

Ausk, B.J., Gross, T.S., Srinivasan, S., 2006. An agent based model for real-time signaling induced in osteocytic networks by mechanical stimuli. Journal of Theoretical Biology 39, 2638-2646.

Bailey, A.M., Lawrence, M.B., Shang, H., Katz, A.j., Peirce. S.M., 2009. Agent-based model of therapeutic adipose-derived stromal cell trafficking during ischemia predicts ability to roll on P-selectin. PLoS Computational Biology 5, e1000294.

Bailey, A.M., Thorne, B.C., Peirce, S. M., 2007. Multi-cell agent-based simulation of the microvasculature to study the dynamics of circulating inflammatory cell trafficking. Annals of Biomedical Engineering 35, 916-936.

Bartha, K., Rieger, H., 2006. Vascular network remodeling via vessel cooption, regression and growth in tumors. Journal of Theoretical Biology 241, 903-918.

Berceli, S.A., Davies, M.G., Kenagy, R.D., Clowes, A.W., 2002. Flow-induced neointimal regression in baboon polytetrafluoroethylene grafts is associated with decreased cell proliferation and increased apoptosis. Journal of Vascular Surgery 36, 1248-1255.

Berceli, S.A., Tran-Son-Tay, R., Garbey, M., Jiang, Z., 2009. Hemodynamically driven vein graft remodelig: a systems biology approach. Vascular 17, (Suppl 1)S2-S9.

Berguer, R., Higgins, R.F., Reddy, D.J., 1980. Intimal hyperplasia. Archives of Surgery 115, 332-335.

Bhardwaj, S., Roy, H., Ylä-Herttuala, S., 2008. Gene therapy to prevent occlusion of venous bypass grafts. Expert Review of Cardiovascular Therapy 6, 641-652.

Bonabeau, E., 2002. Agent-based modeling: Methods and techniques for simulating human systems. Proceedings of the National Academy of Sciences U.S.A. 99, 7280-7287.

Bongrand, P., Bell, G.I., 1984. Cell-cell adhesion: parameters and possible mechanisms. In: Perelson, A.S., DeLisi, C., Wiegel, F.W. (Eds.), Cell surface dynamics, Concepts and models. Marcel Dekker, New York.

Boyle, C.J., Lennon, A.B., Early, M., Kelly, D.J., Lally, C., Predergast, P.J., 2010. Computational simulation methodologies for mechanobiological modeling: application of a cell-centered approach to neointima development around stents. Philosophical Transactions. Series A, Mathematical, Physical, and Engineering Sciences 368, 2919-2935.

Britton, N.F., 2003. Essential Mathematical Biology. Springer, London.

Bruehl, R.E., Springer, T.A., Bainton, D.F., 1996. Quantitation of L-selectin distribution on human leukocyte microvilli by immunogold labeling and electron microscopy. Journal of Histochemistry and Cytochemistry 44, 835-844.

Budu-Grajdeanu, P., Schugart, R.C., Friedman, A., Valentine, C., Agarwal, A.K., Rovin, B.H., 2008. A mathematical model of venous neointimal hyperplasia formation. Theoretical Biology and Medical Modeling 5, 2.

Byrne, H., Drasdo, D., 2009. Individual-based and continuum models of growing cell populations: a comparison. Journal of Mathematical Biololgy 58, 657-687.

Checa, S., Prendergast, P.j., 2009. A mechanobiological model for tissue differentiation that includes angiogenesis: A lattice-based modeling approach. Annals of Biomedical Engineering 37, 129-145.

Chen, S., Springer, T.A., 2001. Selectin receptor-ligand bonds: Formation limited by shear rate and dissociation governed by the Bell model. Proceedings of the National Acadamy of Sciences U S A 98, 950-955.

Cheng, G., Youssef, B.B., Markenscoff, P., Zygourakis. K., 2006. Cell population dynamics modulate the rates of tissue growth processes. Biophysical Journal 90, 713-724.

Chavali, A.K., Gianchandani, E.P., Tung, K.S., Lawrence, M.B., Peirce, S.M., Papin, J.A., 2008. Characterizing emergent properties of immunological systems with multi-cellular rule-based computatioanl modeling. Trends in Immunology 29, 589-599.

Conte, M.S., Bandyk, D.F., Clowes, A.W., Moneta, G.L., Seely, L., Lorenz, T.J., Namini, H., Hamdan, A.D., Roddy, S.P., Belkin, M., Berceli, S.A., DeMasi, R.J., Samson,

R.H., Berman, S.S., and P. I. Investigators, 2006. Results of PREVENT III: A multicenter, randomized trial of edifoligide for the prevention of vein graft failure in lower extremity bypass surgery. Journal of Vascular Surgery 43, 742-751.

Deutsch, A., Dormann, S., 2005. Cellular Automaton Modeling of Biological Pattern Formation. Birkhäuser, Boston.

Dewitt, S., Hallett, M., 2007. Leukocyte membrane "expansion": a central mechanism for leukocyte extravasation. Journal of Leukocyte Biology 81, 1160-1164.

Dobrin, P.B., Littooy, F.N., Endean, E.D., 1989. Mechanical factors predisposing to intimal hyperplasia and medial thickening in autogenous vein grafts. Surgery 105, 393-400.

Dong, C., Lei, X.X., 2000. Biomechanics of cell rolling: shear flow, cell-surface adhesion, and cell deformability. Journal of Biomechanics 33, 35-43.

Dormann, S., Deutsch, A., 2002. Modeling self-organized avascular tumor growth with a hybrid cellular automaton. In Silico Biology 2, 0035.

Dwir, O., Solomon, A., Mangan, S., Kansas, G.S., Schwarz, U.S., Alon, R., 2003. Avidity enhancement of L-selectin bonds by flow: shear-promoted rotation of leukocytes turn labile bonds into functional tethers. Journal of Cell Biology 163, 649-659.

Engelberg, J.A., Datta, A., Mostov, K.E., Hunt, C.A., 2011. MDCK Cystogenesis Driven by Cell Stabilization within Computational Analogues. PLoS Computational Biology 7(4), e1002030.

Engelberg, J.A., Ropella, G.E.P., Hunt, C.A., 2008. Essential operating principles for tumor spheroid growth. BMC Systems Biology 2, 110.

Ermentrout, G.B., Edelstein-Keshet, L., 1993. Cellular Automata Approaches to Biological Modeling. Journal of Theoretical Biology 160, 97-133.

Fernandez, C.M., Goldman, D.R., Jiang, Z., Ozaki, C.K., Tran-Son-Tay, R., Berceli, S.A., 2004. Impact of shear stress on early vein graft remodeling: A biomechanical analysis. Annals of Biomedical Engineering 32, 1484-1493.

Ferreira, Jr., S.C., Martins, M.L., Vilela, M.J., 2002. Reaction-diffusion model for the growth of avascular tumor. Physical Review E 65, 021907.

Figueroa, C.A., Baek, S., Taylor, C.A., Humphrey, J.D., 2009. A computational framework for fluid-solid-growth modeling in cardiovascular simulations. Computational Methods in Applied Mechanics and Engineering 198, 3583-3602.

Fillinger, M.F., Cronenwett, J.L., Besso, S., Walsh, D.B., Zwolak, R.M., 1994. Vein adaptation to the hemodynamic environment of infrainguinal grafts. Journal of Vascular Surgery 19, 970-979.

Finger, E.B., Purl, K.D., Alon, R., Lawrence, M.B., Von Andrian, U.H., Springer, T.A., 1996. Adhesion through L-selectin requires a threshold hydrodynamic shear. Nature 379, 266-269.

Fitzgibbon, G.M., Kafka, H.P., Leach, A.J., Keon, W.J., Hooper, G.D., Burton., J.R., 1996. Coronary bypass graft fate and patient outcome: Angiographic follow-up of 5,065 grafts related to survival and reoperation in 1,388 patients during 25 years. Journal of the American College of Cardiology 28, 616-626.

Friedman, M.H., Deters, O.J., Bargeron, C.B., Hutchins, G.M., Mark, F.F., 1986. Shear-dependent thickening of the human arterial intima. Atherosclerosis 60, 161-171.

Fujikawa, H., Kai, A., Morozumi, S., 2004. A new logistic model for *Escherichia coli* growth at constant and dynamic temperatures. Food Microbiology 21, 501-509.

Galle, J., Hoffmann, M., Aust, G., 2009. From single cells to tissue architecture-a bottom-up approach to modelling the spatio-temporal organisation of complex multi-cellular systems. Journal of Mathematical Biology 58, 261-283.

Galle, J., Loeffler, M., Drasdo, D., Modeling the effect of deregulated proliferation and apoptosis on the growth dynamics of epithelial cell populations in vitro. Biophysical Journal 88, 62-75.

Galt, S.W., Zwolak, R.M., Wagner, R.J., Gilbertson, J.J., 1993. Differential response of arteries and vein grafts to blood flow reduction. Journal of Vascular Surgery 17, 563-570.

Galvão, V., Miranda, J.G.V., Ribeiro-dos-Santos, R., 2008. Development of a two-dimensional agent-based model for chronic chagasic cardiomyopathy after stem cell transplantation. Bioinformatics 24, 2051-2056.

Gerlee, P., Anderson, A.R.A., 2007. An evolutionary hybrid cellular automaton model of solid tumour growth. Journal of Theoretical Biology 246, 583-603.

Gerlee, P., Anderson, A.R.A., 2008. A hybrid cellular automaton model of clonal evolution in cancer: The emergence of the glycolytic phenotype. Journal of Theoretical Biology 250, 705-722.

Gervertz, J.L., Torquato, S., 2006. Modeling the effects of vasculature evolution on early brain tumor growth. Journal of Theoretical Biology 243, 517-531.

Gilbert, N., 2008. Agent-Based Models. Sage Publications, Los Angeles.

Glagov, S., Weisenbeg, E., Zarins, C.K., Stankunavicius, R., Kolettis, G.J., 1987. Compensatory enlargement of human atherosclerotic coronary arteries. New England Journal of Medicine 316, 1371-1375.

Goetz, D.J., El-Sabban, M.E., Pauli, B.U., Hammer, D.A., 1994. Dynamics of neutrophil rolling over stimulated endothelium in vitro. Biophysical Journal 66, 2202-2209.

Goldman, A.J., Cox, R.G., Brenner, H., 1967. Slow viscous motion of a sphere parallel to a plane wall. I. Motion through a quiescent fluid. Chemical Engineering Science 22, 637-652.

Goldman, A.J., Cox, R.G., Brenner, H. 1967. Slow viscous motion of a sphere parallel to a plane wall. II. Couette Flow. Chemical Engineering Science 22, 653-659.

Goudar, C.T., Joeris, K., Konstantinov, K.B., Piret, J.M., 2005. Logistic Equations Effectively Model Mammalian Cell Batch and Fed-Batch Kinetics by Logically Constraining the Fit. Biotechnology Progress 21, 1109-1118.

Grabe, N., Neuber, K., 2005. A multicellular systems biology model predicts epidermal morphology, kinetics and Ca^{2+} flow. Bioinformatics 21, 3541-3547.

Grant, M.R., Mostov, K.E., Tisty, T.D., Hunt, C.A., 2006. Simulating properties of in vitro epithelial cell morphogenesis. PLoS Computational Biology 2, e129.

Grondin, C.M., Lepage, G., Castonguay, Y.R., Meere, C., Grondin, P., 1971. Aortocoronary bypass graft: Initial blood flow through the graft, and early postoperative patency. Circulation 44, 815-819.

Guo, Z., Sloot, P.M.A., Tay, J.C., 2008. A hybrid agent-based approach for modeling microbiological systems. Journal of Theoretical Biology 255, 163-175.

Haga, M., Yamashita, A., Paszkowiak, J., Sumpio, B.E., Dardik, A., 2003. Oscillatory shear stress increases smooth muscle cell proliferation and Akt phosphorylation. Journal of Vascular Surgery 37, 1277-1284.

Hammer, D.A., Apte, S.M., 1992. Simulation of cell rolling and adhesion on surfaces in shear flow: general results and analysis of selectin-mediated neutrophil adhesion. Biophysical Journal 63, 35-57.

Hoch, J.R., Stark, V.K., Rooijen, N., Kim, J.L., Nutt, M.P., Warner, T.F., 1999. Macrophage depletion alters vein graft intimal hyperplasia. Surgery 126, 428-437.

Hwang, M., Garbey, M., Berceli, S.A., Tran-Son-Tay, R., 2009. Rule-Based Simulation of Multi-Cellular Biological Systems-A Review of Modeling Techniques. Cellular and Molecular Bioengineering 2, 285-294.

Jacot, J.G., Abdullah, I., Belkin, M., Gerhard-Herman, M., Gaccione, P., Polak, J.F., Donaldson, M.C., Whittemore, A.D., Conte, M.S., 2004. Early adaptation of human lower extremity vein grafts: Wall stiffness changes accompany geometric remodeling. Journal of Vascular Surgery 39, 547-555.

Jadhav, S., Eggleton, C.D., Konstantopoulos, K., 2005. A 3-D computational model predicts that cell deformation affects selectin-mediated leukocyte rolling. Biophysical Journal 88, 96-104.

Jeremy, J.Y., Gadsdon, P., Shukla, N., Vijayan, V., Wyatt, M., Newby, A.C., Angelini, G.D., 2007. On the biology of saphenous vein grafts fitted with external synthetic sheaths and stents. Biomaterials 28, 895-908.

Jiang, Y., Pjesivac-Grbovic, J., Cantrell, C., Freyer, J.P., 2005. A multiscale model for avascular tumor growth. Biophysical Journal 89:3884-3894.

Jiang, Z., Tao, M., Omalley, K.A., Wang, D., Ozaki, C.K., Berceli, S.A., 2009. Established neointimal hyperplasia in vein grafts expands via TGF-b-mediated progressive fibrosis. American Journal of Physiology – Heart and Circulatory Physiology 297, H1200-H1207.

Jiang, Z., Wu, L., Miller, B.L., Goldman, D.R., Fernandez, C.M., Abouhamze, Z.S., Ozaki, C.K., Berceli, S.A., 2004. A novel vein graft model: Adaptation to differential flow environments. American Journal of Physiology - Heart and Circulatory Physiology 286, H240-H245.

Jiang, Z., Yu, P., Tao, M., Fernandez, C., Ifantides, C., Moloye, O., Schultz, G.S., Ozaki, C.K., Berceli, S.A., 2007. TGF-{beta}/CTGF mediated fibroblast recruitment influences early outward vein graft remodeling. American Journal of Physiology - Heart and Circulatory Physiology 293, H482-H488.

Jiang, Z., Yu, P., Tao, M., Ifantides, C., Ozaki, C.K., Berceli, S.A., 2009. Interplay of CCF2 signaling and local shear force determines vein graft neointimal hyperplasia in vivo. FEBS Letters 583(21), 3536-3540.

Jung, U., Bullard, D.C., Tedder, T.F., Ley, K., 1996. Velocity differences between L- and P-selectin-dependent neutrophil rolling in venules of mouse cremaster muscle in vivo. Americal Journal of Physiology - Heart and Circulatory Physiology 271, H2740-H2747.

Kansal, A.R., Torquato, S., Harsh IV, G.R., Chiocca, E.A., Deisboeck, T.S., 2000. Simulated brain tumor growth dynamics using a three-dimensional cellular automaton. Journal of Theoretical Biology 203, 367-382.

Kim, S.H.J., Park, S., Mostov, K., Debnath, J., Hunt, C.A., 2009. Computational Investigation of Epithelial Cell Dynamic Phenotype In Vitro. Theoretical Biology and Medical Modelling 6, 8.

Knutton, S., Sumner, M.C.B., Pasternak, C.A., 1975. Role of microvilli in surface changes of synchronized P815Y mastocytoma cells. Journal of Cell Biology 66, 568-576.

Kohler, T.R., Kirkman, T.R., Kraiss, L.W., Zierler, B.K., Clowes, A.W., 1991. Increased blood flow inhibits neointimal hyperplasia in endothelialized vascular grafts. Circulation Research 69, 1557-1565.

Korshunov, V. A., Berk, B.C., 2004. Strain-dependent vascular remodeling: The "Glagov phenomenon" is genetically determined. Circulation 110, 220-226.

Kraiss, L.W., Kirkman, T.R., Kohler, T.R., Zierler, B., Clowes, A.W., 1991. Shear stress regulates smooth muscle proliferation and neointimal thickening in porous polytetrafluoroethylene grafts. Arteriosclerosis and Thrombosis 11, 1844-1852.

Lao, B.J., Kamei, D.T., 2008. Investigation of cellular movement in the prostate epithelium using an agent-based model. Journal of Theoretical Biology 250, 642-654.

Lawrence, M.B., Kansas, G.S., Kunkel, E.J., Ley, K., 1997. Threshold levels of fluid shear promote leukocyte adhesion through selectin (CD62L, P, E). Journal of Cell Biology 136, 717-727.

Lawrence, M.B., Springer, T.A., 1991. Leukocytes roll on a selectin at physiologic flow rates: distinction from and prerequisite for adhesion through integrins. Cell 65, 859-873.

Lee, D., Chiu, J.J., 1992. A numerical simulation of intimal thickening under shear in arteries. Biorheology 29, 337-351.

Lemson, M.S., Tordoir, J.H.M., Daemen, M.J.A.P., Kitslaar, P.J.E.H.M., 2000. Intimal Hyperplasia in Vascular Grafts. Europena Journal of Vascular and Endovascular Surgery 19, 336-350.

Mai, J., Sameni, M., Mikkelsen, T., Sloane, B.F., 2002. Degradation of Extracellular Matrix Protein Tenascin-C by Cathepsin B: An Interaction Involved in the Progression of Gliomas. Biological Chemistry 383, 1407-1413.

Mallet, D.G., De Pillis, L.G., 2006. A cellular automata model of tumor-immune system interactions. Journal of Theoretical Biology 239, 334-350.

Mann, M.J., 2004. Novel Strategies for the Prevention of Bypass Graft Failure. BioDrugs 18, 1-8.

Mansury, Y., Deisboeck, T.S., 2003. The impact of "search precision" in an agent-based tumor model. Journal of Theoretical Biology 224, 325-337.

Meyerson, S.L., Skelly, C.L., Curi, M.A., Shakur, U.M., Vosicky, J.E., Glagov, S., Schwartz, L.B., 2001. The effects of extremely low shear stress on cellular proliferation and neointimal thickening in the failing bypass graft. Journal of Vascular Surgery 34, 90-97.

Mills, J.L., Bandyk, D.F., Gahtan, V., Esses, G.E., 1995. The origin of infrainguinal vein graft stenosis: A prospective study based on duplex surveillance. Journal of Vascular Surgery 21, 16-25.

Mitra, A.K., Gangahar, D.M., Agrawal, D,K., 2006. Cellular, molecular and immunological mechanisms in the pathophysiology of vein graft intimal hyperplasia. Immunology and Cell Biology 84, 115-124.

Morinaga, K., Eguchi, H., Miyazaki, T., Okadome, K., Sugimachi, K., 1987. Development and regression of intimal thickening of arterially transplanted autologous vein grafts in dogs. Journal of Vascular Surgery 5, 719-730.

N'Dri, N.A., Shyy, W., Tran-Son-Tay, R., 2003. Computational modeling of cell adhesion and movement using a continuum-kinetics approach. Biophysical Journal 85, 2273-2286.

Neumann, J. v., 1966. Theory of Self-Reproducing Automata. Edited and completed by Burks, A.W.. University of Illinois Press, Urbana.

O'Sullivan, D., 2001. Graph-cellular automata: a generalised discrete urban and regional model. Environment and Planning B 28, 687-705.

Owens, C.D., Wake, N., Jacot, J.G., Gerhard-Herman, M., Gaccione, P., Belkin, M., Creager, M.A., Conte, M.S., 2006. Early biomechanical changes in lower extremity vein grafts - Distinct temporal phases of remodeling and wall stiffness. Journal of Vascular Surgery 44, 740-746.

Palsson, E., 2008. A 3-D model used to explore how cell adhesion and stiffness affect cell sorting and movement in multicellular systems. Journal of Theoretical Biology 254, 1-13.

Pappu, V., Bagchi, P., 2008. 3D computational modeling and simulation of leukocyte rolling adhesion and deformation. Computers in Biology and Medicine 38, 738-753.

Park, E.Y.H., Smith, M.J., Stropp, E.S., Snapp, K.R., DiVietro, J.A., Walker, W.F., Schmidtke, D.W., Diamond, S.L., Lawrence, M.B., 2002. Comparison of PSGL-1 microbead and neutrophil rolling: Microvillus elongation stabilizes P-selectin bond clusters. Biophysical Journal 82, 1835-1847.

Pérez, M.A., Prendergast, P.J., 2007. Random-walk models of cell dispersal included in mechanobiological simulations of tissue differentiation. Journal of Biomechanics 40, 2244-2253.

Peskin, C.S., 1977. Numerical analysis of blood flow in the heart. Journal of Computational Physics 25, 220-252.

Phuphanich, S., Levin, V.A., 1985. Bioavailability of Bromodeoxyuridine in Dogs and Toxicity in Rats. Cancer Research 45, 2387-2389.

Piotrowska, M.J., Angus, S.D., 2009. A quantitative cellular automaton model of *in vitro* multicellular spheroid tumour growth. Journal of Theoretical Biology 258, 165-178.

Qutub, A.A., Popel, A.S., 2009. Elongation, proliferation & migration differentiate endothelial cell phenotypes and determine capillary sprouting. BMC Systems Biology 3, 13.

Richter, Y., Groothuis, A., Seifert, P., Edelman, E.R., 2004. Dynamic flow alterations dictate leukocyte adhesion and response to endovascular interventions. Journal of Clinical Investigation 113, 1607-1614.

Robertson, S.H., Smith, C.K., Langhans, A.L., McLinden, S.E., Oberhardt, M.A., Jakab, K.R., Dzamba, B., DeSimone, D.W., Papin, J.A., Peirce, S.M., 2007. Multiscale computational analysis of *Xenopus laevis* morphogenesis reveals key insights of systems-level behavior. BMC Systems Biology 1, 46.

Roger et al., 2011. Heart Disease and Stroke Statistics - 2011 Update. Circulation 123, e18-e209

Rosamond et al., 2007. Heart Disease and Stroke Statistics - 2007 Update. Circulation 115, e69-e171.

.

Schaller, G., Meyer-Hermann, M., 2007. A modelling approach towards epidermal homoeostasis control. Journal of Theoretical Biology 247, 554-573.

Schwartz, L.B., O'Donohoe, M.K., Purut, C.M., Mikat, E.M., Hagen, P.O., McCann, R.L., 1992. Myointimal thickening in experimental vein grafts is dependent on wall tension. Journal of Vascular Surgery 15, 176-186.

Schwartz, S.M., 1999. The Intima: A New Soil. Circulation Research 85, 877-879.

Shao, J.-Y., Ting-Beall, H.P., Hochmuth, R.M., 1998. Static and dynamic lengths of neutrophil microvilli. Proceedings of the National Academy of Sciences U S A 95, 6797-6802.

Shuhaiber, J.H., Evans, A.N., Massad, M.G., Geha, A.S., 2002. Mechanism and future directions for prevention of vein graft failure in coronary bypass surgery. European Journal of Cardio-thoracic Surgery 22, 387-396.

Shyy, W., Francois, M., Udaykumar, H.S., 2001. Moving boundaries in micro-scale biofluid dynamics. Applied Mechanics Review 5, 405-453.

Shyy, W., Kan, H.-C., Udaykumar, H.S., 1999. Interaction between fluid flows and flexible structures. In: Shyy, W., Narayanan, R. (Eds.), Fluid dynamics at interfaces. Cambridge University Press, Cambridge, UK.

Silverthorn, D.U., Ober, W.C., Garrison, C.W., 2001. Human physiology an integrated approach. Prentice Hall, Upper Saddle River.

Simpson, M.J., Merrifield, A., Landman, K.A., Hughes, B.D., 2007. Simulating invasion with cellular automata: Connecting cell-scale and population-scale properties. Physical Review E 76, 021918.

Smith, M.J., Berg, E.L., Lawrence, M.B., 1999. A direct comparison of selectin-mediated transient, adhesive events using high temporal resolution. Biophysical Journal 77, 3371-3383.

Sumpio, B.E., Banes, A.J., 1988. Response of porcine aortic smooth muscle cells to cyclic tensional deformation in culture. Journal of Surgical Research 44, 696-701.

Sumpio, B.E., Banes, A.J., Link, W.G., Johnson, Jr., G., 1988. Enhanced collagen production by smooth muscle cells during repetitive mechanical stretching. Archives of Surgery 123, 1233-1236.

Tang, J., Ley, K.F., Hunt, C.A., 2007. Dynamics of in silico leukocyte rolling, activation, and adhesion. BMC Systems Biology 1, 14.

Thorne, B.C., Bailey, A.M., DeSimone, D.W., Peirce, S.M., 2007. Agent-based modeling of multicell morphogenic processes during development. Birth Defects Research C Embryo Today 81, 344-353.

Thorne, B.C., Bailey, A.M., Peirce, S.M., 2007. Combining experiments with multi-cell agent-based modeling to study biological tissue patterning. Briefings in Bioinformatics 8, 245-257.

Tran-Son-Tay, R., Hwang, M., Garbey, M., Jiang, Z., Ozaki, C.K., Berceli, S.A., 2008. An Experiment-Based Model of Vein Graft Remodeling Induced by Shear Stress. Annals of Biomedical Engineering 36, 1083-1091.

Valentín, A., Humphrey, J.D., 2009. Evaluation of fundamental hypotheses underlying constrained mixture models of arterial growth and remodeling. Philosophical Transacionts of the Royal Society A 367, 3585-3606.

Varty, K., Allen, K.E., Bell, P.R.F., London, N.J.M., 1993. Infrainguinal vein graft stenosis. British Journal of Surgery 80, 825-833.

Walker, D.C., Southgate, J., Hill, G., Holcombe, M., Hose, D.R., Wood, S.M., Mac Neil, S., Smallwood, R.H., 2004. The epitheliome: agent-based modelling of the social behaviour of cells. BioSystems 76, 89-100.

Walpola, P.L., Gotlieb, A.I., Cybulsky, M.I., Langille, B.L., 1995. Expression of ICAM-1 and VCAM-1 and monocyte adherence in arteries exposed to altered shear stress. Arteriosclerosis, Thrombosis, and Vascular Biology 15, 2-10.

Wentzel, J.J., Kloet, J., Andhyiswara, I., Oomen, J.A.F., Schuurbiers, J.C.H., de Smet, B.J.G.L., Post, M.J., de Kleijn, D., Pasterkamp, G., Borst, C., Slager, C.J., Krams, R., 2001. Shear-stress and wall-stress regulation of vascular remodeling after balloon angioplasty : Effect of matrix metalloproteinase inhibition. Circulation 104, 91-96.

Westerband, A., Crouse, D., Richter, L.C., Aguirre, M.L., Wixon, C.C., James, D.C., Mills, J.L., Hunter, G.C., Heimark, R.L., 2001. Vein adaptation to arterialization in an experimental model. Journal of Vascular Surgery 33, 561-569.

Wolfram, S., 2002. A New Kind of Science. Wolfram Media, Champaign.

Yamamoto, M., Acevedo-Duncan, M., Chalfant, C.E., Patel, N.A., Watson, J.E., Cooper, D.R., 2000. Acute glucose-induced downregulation of PKC-beta II accelerates cultured VSMC proliferation. American Journal of Physiology - Cell Physiology 279, 587-595.

Yang, C., Tang, D., Liu, S.Q., 2003. A multi-physics growth model with fluid-structure interactions for blood flow and re-stenosis in rat vein grafts A growth model for blood flow and re-stenosis in grafts. Computers and Structures 81, 1041-1058.

Zhang, L., Athale, C.A., Deisboeck, T.S., 2007. Development of a three-dimensional multiscale agent-based tumor model: Simulating gene-protein interaction profiles, cell phenotypes and multicellular patterns in brain cancer. Journal of Theoretical Biology 244, 96-107.

Zhang, L., Hagen, P.-O., Kisslo, J., Peppel, K., Freedman, N.J., 2002. Neointimal hyperplasia rapidly reaches steady state in a novel murine vein graft model. Journal of Vascular Surgery 36, 824-832.

Zhang, L., Wang, Z., Sagotsky, Z.A., Deisboeck, T.S., 2009. Multiscale agent-based cancer modeling. Journal of Mathematical Biology 58, 545-559.

Zohdi, T. I., 2005. A simple model for shear stress mediated lumen reduction in blood vessels. Biomechanics and Modeling in Mechanobiology 4, 57-61.

Zou, Y., Dietrich, H., Hu, Y., Metzler, B., Wick, G., Xu, Q., 1998. Mouse Model of Venous Bypass Graft Arteriosclerosis. American Journal of Pathology 153, 1301-1310.

Zwolak, R.M., Adams, M.C., Clowes, A.W., 1987. Kinetics of vein graft hyperplasia: Association with tangential stress. Journal of Vascular Surgery 5, 126-136.

BIOGRAPHICAL SKETCH

Minki Hwang received his bachelor's and master's degrees in aerospace engineering from the Korea Advanced Institute of Science and Technology (KAIST) in 1995 and 1997, respectively. He worked as a research and development engineer for Samsung Techwin Corporation from 1997 to 2002. He received a master's degree in bioengineering from Penn State University in 2004.